UNDERSTANDING THE IMPACT OF CELLULOSE AND CHITIN-BASED NANOMATERIALS IN VARIOUS POLYMER MATRIX CONSTRUCTS

A Dissertation
Presented to
The Academic Faculty

by

Cameron William Irvin

In Partial Fulfillment
of the Requirements for the Degree
Doctor of Philosophy in the
School of Materials Science and Engineering

Georgia Institute of Technology
May 2020

UNDERSTANDING THE IMPACT OF CELLULOSE AND CHITIN-BASED NANOMATERIALS IN VARIOUS POLYMER MATRIX CONSTRUCTS

Approved by:

Dr. Meisha L. Shofner, Advisor
School of Materials Science
and Engineering
Georgia Institute of Technology

Dr. Donggang Yao
School of Materials Science
and Engineering
Georgia Institute of Technology

Dr. J. Carson Meredith
School of Chemical and
Biomolecular Engineering
Georgia Institute of Technology

Dr. Yulin Deng
School of Chemical and
Biomolecular Engineering
Georgia Institute of Technology

Dr. Blair K. Brettmann
School of Chemical and
Biomolecular Engineering,
School of Materials Science
and Engineering
Georgia Institute of Technology

Date Approved: March 13th, 2020

This work is dedicated to my family.

ACKNOWLEDGEMENTS

Firstly, I would like to express my gratitude to my advisor, Dr. Meisha Shofner, for her mentorship and advice throughout my doctoral research. She taught me how to think critically about polymer science and she always made her office a welcoming environment for thoughtful discussion. I entered graduate school with a limited background in MSE, but Dr. Shofner's endless patience and guidance was invaluable in my development as a materials researcher. I would also like to thank the rest of my committee members, Dr. Carson Meredith, Dr. Yulin Deng, Dr. Blair Brettmann, and Dr. Donggang Yao for giving suggestions on how to better my research. Their insights throughout the last few years provided me with new, exciting directions to pursue.

I would especially like to thank the members of the Shofner Lab: Dr. Matthew Orr, Dr. Emily Ftizharris, and Dr. Prateek Verma. I cherish the friendships I was able to form with each member and I greatly appreciate the countless times they would fulfill my requests for help. Emily first taught me how to prepare my PVA composite solutions, while Matt educated and trained me on nearly every instrument I used throughout my career. Prateek provided me with valuable SEM images of my samples and was always open to hearing about my research. I would also like to thank my undergrad, Nicole Arroyo, for her help with my aerogel samples. Together we all shared meals, stories, and companionship that I will be forever thankful for.

Additionally, I would like to thank the IGER collaboration team of Dr. Shofner, Dr. Meredith, Dr. Deng, Wei Liu, and Chinmay Satam for providing a space to share and discuss our work. The feedback I received from our meetings was incredibly valuable in

the development of my research. I also want to give a special thanks to Chinmay, as none of my work would have been possible without his contribution. I thank him for providing a consistent supply of chitin to me throughout the years and for serving as a great friend that I could discuss various topics with, both professional and personal.

I would like to thank Dr. Paul Russo for introducing me to the field of light scattering and for helping me prepare, test, and analyze samples. His limitless curiosity and willingness to share his time for discussions were greatly appreciated. Additionally, I would like to thank Jianshan Liao and Dr. Victor Breedveld for their help with the rheological analysis of my samples. The data collected from these techniques was critically important to developing a greater understanding of my composite system.

I must also thank the Renewable Bioproducts Institute for their generous funding through my Paper Science and Engineering Fellowship. I thoroughly enjoyed my time as a part of this institute and I valued having access to many other cellulose researchers for insightful discussions. I would also like to thank the GAANN Fellowship and Jewell Family Fellowship for their financial support along the way, in addition to providing funding for materials in my research. I would also like to thank the Polymer Characterization Facility, STAMI, and OPALL for providing equipment that was used to analyze my samples thermally and chemically.

Finally, I would like to thank the members of my family. I am eternally grateful to my mom and dad for encouraging me to be curious, to always work hard, and to follow my passions. Their love and support throughout my life has allowed me to pursue the path I am on now. I would like to thank my brother and sister, Chris and Clair, for their friendship

and for giving me countless wonderful memories. You two have always been able to easily take my mind off things during stressful times. I want to thank Tyler Stowell for always being an amazing friend throughout the years and for being a great source of support in all matters of my life. Lastly, I would like to thank Kaitlyn Kolesaire. She has been my biggest supporter, a constant source of encouragement, and she never fails to make me laugh. She could always help me decompress after a bad day. I appreciate the continued interest she took in my work and everyday life, as well as the affectionate names she called my hydrogel samples. I would not have been able to accomplish this goal without my family and friends' endless support and I am thankful to be surrounded by so many great people.

TABLE OF CONTENTS

LIST OF TABLES

LIST OF FIGURES

LIST OF SYMBOLS AND ABBREVIATIONS

AF	Annulus Fibrosus
AF4	Asymmetric Field Flow Field Fractionation
AFM	Atomic Force Microscopy
ASTM	American Society for Testing and Materials
ATR	Attenuated Total Reflectance
C=O	Carbonyl Chemical Group
CdS	Cadmium Sulfide
C-H	Methylidyne Chemical Group
CH_2	Methylene Chemical Group
CH_3	Methyl Group
ChNC	Chitin Nanocrystal
ChNF	Chitin Nanofibers
ChNW	Chitin Nanowhisker
CNC	Cellulose Nanocrystals
CNW	Cellulose Nanowhiskers
C-O	Carbon-Oxygen Chemical Group
CO_2	Carbon Dioxide
d	Diameter
DA	Degree of Acetylation
DA	Degree of Acetylation
DSC	Differential Scanning Calorimetry
E^*	Modulus

E_s	Solids Modulus
FT	Freeze-Thaw
FTIR	Fourier Transform Infrared Spectroscopy
G’	Shear Storage Modulus
G”	Shear Loss Modulus
GO	Graphene Oxide
h	Height
HChNF	High Acetylated Chitin Nanofibers
HPVA	High Molecular Weight Poly(vinyl alcohol)
HTMECH	High-Throughput Mechanical Characterization
IGER	Integrated Graduate Education and Research
IVD	Intervertebral Disc
l	Length
LChNF	Low Acetylated Chitin Nanofibers
LPVA	Low Molecular Weight Poly(vinyl alcohol)
m	Mass
M(0)	Initial Stress
M(t)	Stress Value as a Function of Time
MADLS	Multiangle Dynamic Light Scattering
MCC	Microcrystalline Cellulose
MDSC	Modulated Differential Scanning Calorimetry
m_f	Filler Mass Fraction
MFC	Microfibrillated Cellulose
MW	Molecular Weight
n	Refractive Index

NP	Nucleus Pulposus
-OH	Hydroxyl Chemical Group
OP	Oxygen Permeability
PCL	Polycaprolactone
PE	Polyethylene
PEO	Poly(Ethylene Oxide)
PET	Poly(Ethylene Terephthalate)
PLA	Poly(lactic acid)
PMMA	Poly(methyl methacrylate)
POM	Polarized Optical Microscopy
PU	Polyurethane
PVA	Poly(vinyl alcohol)
PVAc	Poly(vinyl acetate)
PVC	Poly(vinyl chloride)
q	Scattering Vector Amplitude
R_h	Hydrodynamic Radius
RH	Relative Humidity
SEM	Scanning Electron Microscopy
TEMPO	2,2,6,6-tetramethyl-piperidinyl-l-oxyl
TGA	Thermogravimetric Analysis
TiO_2	Titanium Oxide
UTS	Ultimate Tensile Strength
V_c	Volume Fraction Percolation Threshold
V_f	Volume Fraction
w	Polymer Weight Fraction

WVTR	Water Vapor Transmission
X_c	Sample Crystallinity
β	Temperature Dependent Exponent
ΔH_m	Sample Enthalpy of Fusion
ΔH_m^o	Enthalpy of Fusion of Theoretically 100% Crystalline Polymer
θ	Angle
λ_o	Wavelength
ρ	Density
ρ^*	Aerogel Density
ρ_f	Filler Density
ρ_m	Matrix Density
ρ_s	Solids Density
σ^*_{pl}	Aerogel Yield Stress
σ_{ys}	Solids Yield Stress
τ	Relaxation Time
Γ	Decay Rate

SUMMARY

Cellulose nanocrystals (CNCs) and chitin nanofibers (ChNFs) are two emerging nanomaterials that are garnering significant interest recently. CNCs and ChNFs can be derived from trees and crab shells, respectively, and possess remarkable mechanical properties that make them ideal for use as reinforcement materials in polymer composites. When processed through sulfuric acid hydrolysis, CNCs are left with a negative charge along the surface of the nanocrystals. In contrast, ChNFs produced through high-pressure homogenization possess a positive charge due to chemical side groups along the nanofiber. These opposite charges allow for electrostatic interactions between the particles that can be tuned to allow for certain nanoscale structure formation. When incorporated into a water soluble, commercially available polymer such as poly(vinyl alcohol) (PVA), there is potential for understanding the impact of these nanofillers in a variety of polymer constructs. PVA offers the unique ability to be formed into films, hydrogels, and aerogels without the aid of additional chemicals, which expands the range of commercial applications that CNCs and ChNFs can be applied. Additionally, there are certain characterization techniques that can be applied to one construct that cannot be applied to another, resulting in a large range of studies that can be performed in order to uncover individual characteristics about how the nanofillers are interacting with the each other and the polymer matrix.

Results of this study indicate that charge-matched ratios between the nanofillers results in a reduction in properties relative to other composites, likely due to a mass aggregation between particles destabilizing the particles and, thus, the reinforcement

mechanisms. However, other ratios between CNCs and ChNFs enhance the mechanical properties beyond that of what is capable with singular nanofillers. In addition to the improved capabilities as a result of their interactions, the combination of these two nanofillers also allows for certain characteristics of each nanofiller type to influence the properties of the overall structure that cannot be achieved with the other. For instance, while CNCs were shown to increase the elasticity of composite hydrogels, ChNFs were shown to increase the polymer structure's water absorption and retention capabilities. The combination of these two materials into a tricomponent composite could then possess several desirable qualities that are applicable in biomedical or membrane technologies.

The purpose of this research is to more fully understand the impact of these renewable, abundant nanomaterials when used in these three PVA constructs both as individual nanofillers and when used in conjunction. This study aims to better understand the electrostatic interactions between different nanofillers and how these can affect the polymer matrix to optimize customizable, high-performance polymeric composite materials.

CHAPTER 1. INTRODUCTION

A composite is generated from the combination of two or more distinct components with the intent of imparting positive qualities of one constituent material onto the other(s). The inclusion of filler materials into a larger matrix can result in improved biocompatibility, improved thermal stability, and greater mechanical reinforcement, in addition to other enhancements such as greater liquid absorption or barrier properties. While the fillers can encompass a large range of different materials with different shapes and sizes, nanofillers are materials specifically containing at least one dimension under 100 nm that can be incorporated into a binding material matrix in order to improve the overall properties. Additionally, polymers provide the ability to incorporate these nanofillers into multiple constructs to expand on their range of applications. In a world where there is a growing need for customizable materials to fit consumer needs, the generation of polymer composites utilizing these nanofillers becomes increasingly more important.

Furthermore, there has been increased interest in the development of composites utilizing renewable materials in an effort to reduce dependence on petroleum-based goods. Two such renewable nanomaterials are cellulose nanocrystals (CNCs) and chitin nanofibers (ChNFs). Derived from trees and crabs, respectively, they possess similar chemical structures and nano-scale properties, but they possess opposite surface charges as a result of their processing conditions. The negatively charged CNCs and positively charged ChNFs offer potential for controlled aggregation, leading to greater capabilities through structure formation than what is available with a singular nanofiller. In order to assess the impact of these nanofillers' structure formation within composite materials, a

polymer was chosen as the binding matrix. Poly(vinyl alcohol) (PVA) is a versatile, non-toxic, biodegradable, and water-soluble polymer that offers the ability to be formed into a variety of different polymer constructs, particularly films, hydrogels, and aerogels. Each of these three constructs require the same two basic components, water and PVA, but changes to the processing steps result in very different structures that do not require the aid of additional chemicals or cross-linkers. Additionally, each of these polymer forms can be characterized in a variety of ways unique to each construct, thus providing an opportunity to measure CNC and ChNF interactions with each other and the polymer matrix under different conditions. Therefore, this research is dedicated to applying these CNCs and ChNFs to PVA films, hydrogels, and aerogels and characterizing each system in an effort to more fully understand how the nanofillers are interacting with themselves, each other, and the polymer matrix in order to allow for the design of customizable, high-performance tricomponent composites. To analyze these effects, the objectives of this research were the following:

1. Assess the impact of CNCs and ChNFs when incorporated both individually and in conjunction in polymer composite films
2. Assess the impact of CNCs and ChNFs when incorporated both individually and in conjunction in porous-cross-linked polymer composite hydrogels
3. Assess the impact of CNCs and ChNFs when incorporated both individually and in conjunction in porous-cross-linked polymer composite aerogels
4. Valorization of cellulose and chitin nanomaterials for biomedical and packaging applications

These objectives outline four distinct, yet interconnected studies that are presented in chapters 3-6, with relevant background for this research in chapter 2. Chapter 2 will review the current state of renewable materials, as well as the history and usage of CNCs, ChNFs, and the chosen polymer matrix, PVA, in addition to some preliminary information on the different polymer constructs assessed. Chapter 3 examines the combination of CNCs, ChNFs, and low and high molecular weight PVA into bi- and tricomponent composite films and delves into the thermomechanical properties of these materials. Chapter 4 expands these bi- and tricomponent composites to PVA hydrogels, focusing on the mechanical performance and water absorption behavior, in addition to studies of rheological properties in solution and light scattering properties between CNCs and ChNFs. Chapter 5 looks at CNC/ChNF/PVA composites in PVA aerogels, providing insight into the thermomechanical and porosity properties with the introduction of nanofillers. Chapter 6 then analyses the utilization of these composite materials studied in chapters 3-5 in both biomedical and packaging applications. Conclusions for each individual chapter in addition and suggestions for future work are included in chapter 7.

CHAPTER 2. BACKGROUND

In this chapter, relevant information on renewable bioproducts, polymer nanocomposites, different methods of processing polymer nanocomposites, and tricomponent and coacervate systems are reviewed. In particular, this chapter reviews the current state of research on cellulose and chitin, their applications to nanocomposites, and their influence on various polymer matrices both singularly and together. Additional background on the polymer matrix, poly(vinyl alcohol) (PVA), and its various constructs are also discussed. Discussion of existing tricomponent composites, as well as a review of cellulose and chitin nanomaterial mixed films, is covered at the end. Lastly, some background of the valorization of these materials is included throughout the chapter under the various sub-sections.

2.1 Need for Renewable Materials

Nanofillers are a type of material possessing at least one dimension under 100 nm, which can be incorporated into a larger matrix in an attempt to impart its properties on the overall structure. Their inclusion can improve the conductive properties,[1] mechanical properties,[2-4] and/or thermal stability,[5-6] among many other properties of whatever matrix they are embedded within. Among the most commonly used nanofillers are carbon black,[1, 7] graphene,[8-9] silica,[6] and clay.[10-12] A major driving factor for this shift to these nanomaterials is the mechanical properties that they offer. These nanomaterials allow for strengthening of polymers and, therefore, a customization of their mechanical properties for a variety of applications. However, there are some concerns about the environmental impact of some of these nanomaterials.[4] Therefore, there has been a growing interest in

renewable materials to take advantage of an abundant source for nanofillers and to improve ecological safety of the resulting high-performance materials.[13]

Renewable materials are a class of materials that are derived from natural resources and have continued to garner popularity and development into a large field of study under materials science.[4, 14-18] In a sense, "nanocomposites" are common in nature, where materials such as nacre and bone are made up of multiscale structures that rely on ordered microstructures and interface interactions to impart strength and stiffness on a larger matrix.[19] Scientists have tried to mimic these natural structures in part by utilizing nanomaterials derived from natural resources and repurposing them for the same reinforcement role in polymer matrices. These resulting nanocomposites are often called "green materials" and they have been working to replace non-renewable nanomaterials to improve sustainability and thermomechanical properties in multiple markets including the automotive[4, 13] and packaging industries,[14, 20-21] as well as improving biocompatibility in biomedical applications.[22-23] "Green materials" also encompass polymeric materials aiming to replace petroleum-based materials, as oil availability is continually declining and its impact on the environment has received much scrutiny in the last few decades.[4] These replacements for petroleum-based materials encompass biobased polymers that are biodegradable or compostable, thus reducing their overall negative impact on the world's ecosystem.[4, 13, 16, 24]

In the biomedical field, polymers and polymer composites have been a growing material of study in the use of implants, drug delivery, and tissue engineering.[25-27] Titanium is one of the most commonly used materials for hard implants, but it is difficult to machine, is radiopaque, and possesses strength much greater than that of human bone/tissue.[28] It is

a common rule within biomedical device design that the utilized materials in implants should only be as strong as the material they are replacing (i.e. bone, cartilage, etc.), otherwise they may absorb too much of the load from the surrounding tissue, thus leading to early failure and potential damage to the patient. Polymers, such as poly(ether ether ketone) (PEEK), poly(lactic acid) (PLA), and PVA, have gained greater development into a wide variety of biomedical applications because they have a closeness in mechanical properties to natural human tissue in addition to ease of machinability and customizability, as well as radiolucency.[25, 29] Provided that renewable materials are extracted from biological sources, their introduction into biomedical products may also allow for an enhancement in biocompatibility and mechanical customizability without risk of inducing a negative response from the surrounding tissue. Patient specific devices have grown increasingly popular and the modular nature of renewable bioproduct polymer composites allows for the ability to tune the materials to the needs of the recipient.

2.2 Cellulose

2.2.1 Cellulose Nanomaterials Structure and Production

Cellulose is the most abundant biopolymer on the planet and can be derived from trees, other plants, and even bacteria. The cellulose molecule contains repeat units of two anhydroglucose rings[30] arranged in a linear chain that form a flat ribbon-like conformation. Figure 2.1 shows a diagram outlining a progressive breakdown of a tree into smaller and smaller components, which each can be utilized in different ways depending on application size and property needs. While the whole tree is on the scale of meters, the structure

contains cells and fibers on the order of tens of micrometers, fibrils are on the order of tens of nanometers, and the molecular structure is on the order of Ångstroms.[31]

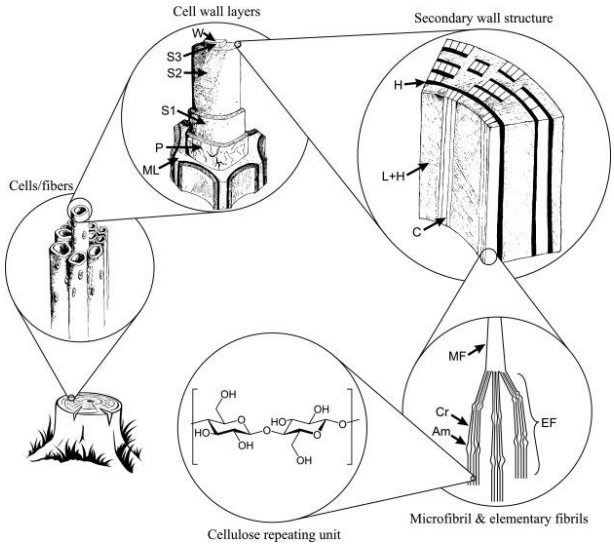

Figure 2.1 Hierarchical arrangement of cellulose nanocrystals from trees to the molecular level.[32] (f1)

Cellulosic materials have been used for millennia, specifically in the form of paper. However, more recently, it has become much more studied due to its potential applications in its nano and micro forms. Individual cellulose molecules are able to come together and form cellulose microfibrils due to hydrogen bonding between the hydroxyl side groups, which can then be broken down into cellulose nanofibers (CNFs) and cellulose nanocrystals (CNCs).[30] Cellulose nanomaterials can be produced in two primary ways: (1) mechanically and (2) chemically, in addition to methods combining both forms of

(f1) Reprinted from Industrial Crops and Products, 93, Nechyporchuk, O.; Belgacem, M. N.; Bras, J., "Production of cellulose nanofibrils: A review of recent advances." pp. 2-25. Copyright (2016), with permission from Elsevier.

processing. Mechanical separation of cellulose can be performed with grinders/refiners, sonication, microfluidization, and homogenization, which shears off long cellulose fibrils from the longitudinal axis of the cellulose, resulting in microfibrilated cellulose (MFC) and CNFs. The mechanical processing to produce these MFCs and CNFs is repeated in order to create finer and more homogeneous nanomaterials, often finishing with a filtration step to remove any unfibrillated sections from the suspension.[30] One method of facilitating the mechanical separation of these fibrils includes treating the stock suspension with a 2,2,6,6-tetramethyl-piperidinyl-l-oxyl radical (TEMPO) oxidation step, resulting in a charge being imparted onto the surface of the cellulose, thus lowering the overall energy required for the mechanical methods to separate the fibers from the surface.[30, 33]

In order to generate CNCs, an additional chemical treatment is necessary to dissolve away the disordered regions of the cellulose chain. CNCs are separated into their individual ordered forms either through an acid hydrolysis step or enzymatic step,[34] though the former is a more commonly used option performed by utilizing either hydrochloric or sulfuric acid.[30, 35] For instance, the CNCs utilized in this study were derived from wood pulp, which was mixed with a 64 wt.% solution of sulfuric acid and heated to 45 °C for 60 minutes. Additional processing steps can be applied to remove unwanted byproducts of the acid hydrolysis method, which can include sonication, centrifugation, and water filtration. However, while this is the most common way of producing the CNCs, one side effect of the sulfuric acid hydrolysis methodology is that it leaves negative surface charges on the CNCs as a result of hydroxyl groups being replaced with sulfate ester groups.[36] These negative charges provide a level of stabilization that allows for dispersion in water,[33, 37] in addition to the capability of interacting with other charged particles in aqueous suspension.

An additional side effect is the thermal stability properties are also influenced by the level of acid hydrolysis the cellulose suspension experiences, as it has a degradation temperature range of 200-300 °C that depends on factors such as the heating rate, surface modification, and particle type.[30] For instance, an increasing number of sulfate groups on the surface of CNCs has been previously shown to significantly decrease the degradation temperature.[38] The resulting CNCs or CNFs are often freeze-dried in order to generate a more compact product that can be more readily transported. The appearance of these freeze-dried materials is of a white, flaky material, though they can begin to clump into low-density blocks if allowed to sit for extended periods of time.

2.2.2 Cellulose Properties and Nanocomposite Usage

These nanomaterials can be utilized in a variety of ways to generate materials with specific properties for new and expanding applications. Cellulose has been used as a reinforcement material in many polymers including polyethylene (PE),[39-40] poly(vinyl chloride) (PVC),[41-42] polyurethane (PU),[43-45] poly(methyl methacrylate) (PMMA),[46-48] polycaprolactone (PCL),[49-50] and PVA.[51-54] CNCs and CNFs are stiff, have oxygen barrier properties,[55] low density, and are relatively inexpensive.[56] Depending on the polymer matrix, CNC-based composites have previously been demonstrated to be melt processed,[3, 57] and CNCs also work well being dispersed in aqueous environments.[33, 49] CNCs can vary in size depending on the source, but they have been previously cited to have lengths on the order of a few hundred nanometers and widths of only a couple nanometers.[31, 58] Optically, CNCs have exhibited a chiral nematic or cholestreric liquid crystalline behavior in both

suspensions and in dried films, which is indicative of a liquid crystalline type structure that is either translucent or slightly iridescent.[30, 33, 59] CNCs also have good barrier applications, as neat CNC films have demonstrated low oxygen permeability rates. Petersson and Oksman[60] demonstrated that the barrier properties of PLA increased by over three times with the addition of 5 wt.% microcrystalline cellulose (MCC), while Li et al. demonstrated that a 1.5 μm thick CNC coating on top of various polymer films can significantly decrease the oxygen permeability while maintaining high transparency.[61] The translates into applications in the packaging industry, which is continually moving away from petroleum-based materials as a result of societal concerns of their impact on the environment and general sustainability.

Cellulosic materials can also be modified to enhance particular properties. Surface functionalization is an expanding field of study for cellulosic materials, as the hydroxyl groups on the surface can be modified to adapt the material to certain conditions. Specifically, they can be changed to be more compatible with hydrophobic polymers that allow for increased dispersion and integration.[39] CNC functionalization can occur through many processes and a variety of functional groups can be attached to the cellulose backbone including acetate, nitrate, and xanthate groups.[62] This can be done to improve certain chemical properties; one study influenced urethane linkages, *silylation*, and esterification in CNCs in order to reduce hornification, increase re-dispersibility after drying, and tune to the adsorption of different molecules.[63] In addition to allowing for additional surface functionalization, another positive aspect of the hydroxyl groups that extend from the cellulose chain is that they allow for a higher amount of biocompatibility. This

biocompatibility allows for use in tissue engineering, drug delivery, wound dressing, and other biomedical applications.[64]

However, in addition to the optical, chemical, and barrier properties of CNCs, the primary interest in these nanomaterials for this work is due to their extensive use as mechanical reinforcement in polymer matrices. These materials have a high modulus and specific strength, which has led to cellulose being used as a reinforcing agent in polymers since Favier began studies with the material in 1995.[65] CNCs have been previously described to be similar in strength to Kevlar, with potential to surpass even steel.[31, 66] Specifically, a review by Moon et al. (2011) cites that the cellulose crystalline structure has a theoretical axial elastic modulus of 110-220 GPa and transverse elastic modulus of 10-50 GPa, with a tensile strength of 7.5-7.7 GPa[30] that makes them well-suited for use in polymer matrices for imparting strength to the overall structure. However, the difficulties in producing consistent batches of CNCs is one of the main obstacles facing the scale up potential of the material in markets moving forward. The variance in the size and strength of the cellulosic materials depends on a variety of factors including source, level of refinement, and processing conditions. Differences in cellulose source can have a dramatic impact on length of the particles as well as the mechanical properties, though chemical processing can be used to produce a more consistent product.[30, 67]

2.3 Chitin

2.3.1 Chitin Nanomaterials Structure and Production

Chitin is another one of the most abundant biopolymers on the planet alongside cellulose and lignin, and it shares many of the same mechanical properties. Chitin is produced by insects, fungi, and yeast, though it is found primarily in the exoskeleton/shells of arthropods such as crabs.[68-69] The molecular structure of chitin consists of repeat units of N-acetyl-D-glucosamine, which can be arranged to generate chitin nanowhiskers (ChNWs) or chitin nanofibers (ChNFs).[70] Figure 2.2 shows a diagram of the breakdown of chitin from the source of a crustacean at the tens of millimeters scale to individual molecules on the order of Ångstroms.

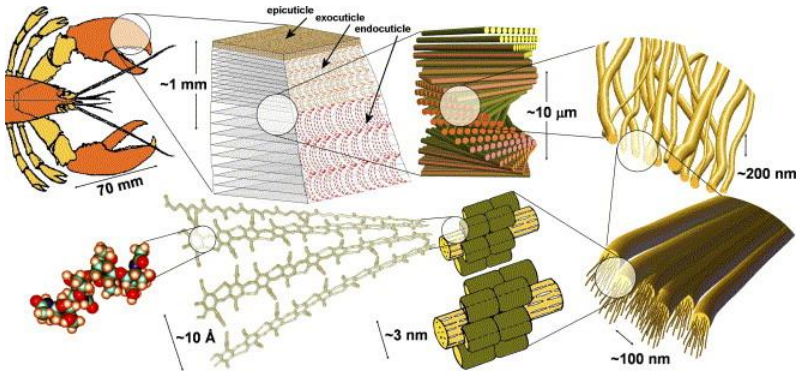

Figure 2.2 Hierarchal arrangement of chitin nanofibers from crustacean shell to the molecular level.[71] (f2)

(f2) Reprinted from Acta Materialia, 53, Raabe, D.; Sachs, C.; Romano, P., "The crustacean exoskeleton as an example of a structurally and mechanically graded biological nanocomposite material." Pp. 4281-4292, Copyright (2005), with permission from Elsevier.

Chitin has three polymeric forms: α, β, and γ, which can vary depending on where the material is sourced. α-chitin is the most abundant variant with a highly ordered crystalline structure, which can be found in crab and shrimp shells, as well as fungus cell walls. The less abundant β-chitin can be found in squid ink and tubeworms and possesses a different crystal structure to α-chitin. Lastly, γ-chitin exists as a combination between the α and β forms.[72-75] Often sourced from food industry waste, chitin can be obtained by grinding crab shells to a powder that can then be cleaned and processed into ChNWs or ChNFs. Due to the ease of access to source material for generation, α-chitin was chosen as the form of study for this thesis.

As previously discussed with CNCs and CNFs, chitin nanomaterials can be produced through chemical methods as well, resulting in a variety of different surface chemistries. For instance, the deacylated form of chitin is called chitosan, though it is important to note that nearly all naturally-sourced chitin is at least partially deacylated. Therefore, chitosan is characterized by a chitin nanomaterial with a degree of acetylation greater than 50%, which makes it soluble in aqueous acidic media.[74] Polymeric chitosan has previously been blended with PVA with lignin nanoparticles for the potential use in packaging materials,[21] as well as incorporated with gelatin for use as a potential nerve regeneration material.[76] However, one advantage that chitin has over chitosan, is that it is more naturally occurring and can be sourced more readily. Additionally, there is less variance and defects as it lacks the additional processing steps, and there is a removal of any risk of introducing chemical agents that may not be compatible with certain applications.

2.3.2 Chitin Properties and Nanocomposite Usage

Given chitin's ability to be formed into nanofibers, it has recently become a topic of interest to include in polymers as a potential reinforcement material like that of cellulose and carbon nanofibers. The crystalline regions of chitin are slightly weaker than that of cellulose, with a reported theoretical modulus of about 41 GPa,[77] though this is still strong enough to be effectively used as reinforcement material in polymer composites. Chitin has been used as a nanofiller embedded into various polymer matrices including unvulcanized and prevulcanized natural rubber,[78] PVA,[68, 73, 75] and poly(ethylene oxide) (PEO).[79] Ifuku et al.[80] demonstrated a significant increase in the Young's modulus and tensile strength of various nanocomposite resins utilizing ChNFs. Chitin has also shown to have useful barrier properties, as Wu et al.[81] previously produced films that exhibited oxygen and carbon dioxide (CO_2) permeabilities of 0.006 and 0.018 barrer, respectively, performing on par or better than one of the most commonly used packaging materials, poly(ethylene terephthalate) (PET).[82] Biologically, chitin is biodegradable, biocompatible, non-toxic, and possesses hydrating features, and it has a history of use due to its antibacterial and antimicrobial properties.[79, 83] However, despite properties that are comparable or better to some of the most commonly used nanofillers, the history of chitin's use in polymer composites is less than that of its peer materials, though commercial interest in it is growing.[68-69] Despite some processing difficulties, chitin has still found development for packaging applications,[20-21] as well as biomedical applications such as sutures, wound dressings, and in a hydrogel form for use in tissue engineering.[22]

2.4 Poly(vinyl alcohol)

PVA was first synthesized in 1924 by Hermann and Haehnel[84] and it has since been applied to a variety of industries due to many desirable properties including little to no toxicity, the ability to be dissolved in water, and biodegradability. PVA consists of a carbon backbone with hydroxyl group branches that allows it to react to many kinds of functional groups.[25, 68, 85-87] PVA's chemical structure is depicted in Figure 2.3 below.

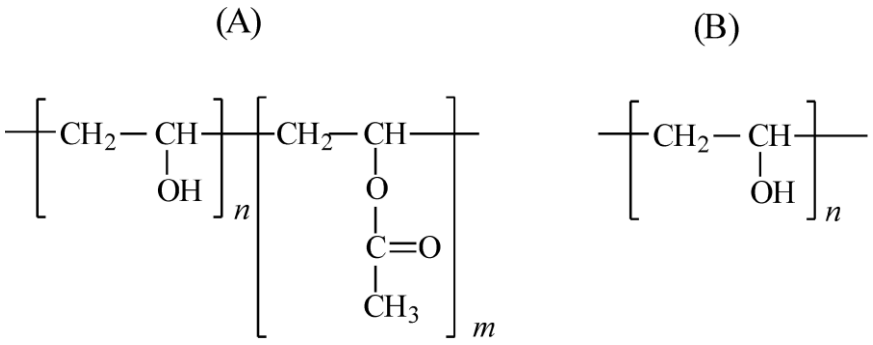

Figure 2.3 Chemical structure of (a) partially hydrolyzed PVA and (b) fully hydrolyzed PVA.[88] (f3)

PVA is unique from other vinyl polymers in that it is not produced through the polymerization of a single monomer, instead it is generated from the hydrolysis of poly(vinyl acetate) (PVAc).[18] Polymerized PVA is processed through the partial replacement of ester branch groups on PVAc with a hydroxyl group. However, since PVA is not capable of achieving 100% hydrolysis, it is effectively a co-polymer of PVAc and

(f3) Reprinted from Food and Chemical Toxicology, 41, DeMerlis, C. C.; Schoneker, D. R., "Review of the oral toxicity of polyvinyl alcohol (PVA)." pp. 319-326, Copyright (2003), with permission from Elsevier.

PVA and the degree of hydrolysis plays a role in the chemical and crystallization properties of PVA.[89] For instance, depending on the water temperature, a higher degree of hydrolysis is associated with a lower solubility in water as shown in Figure 2.4.

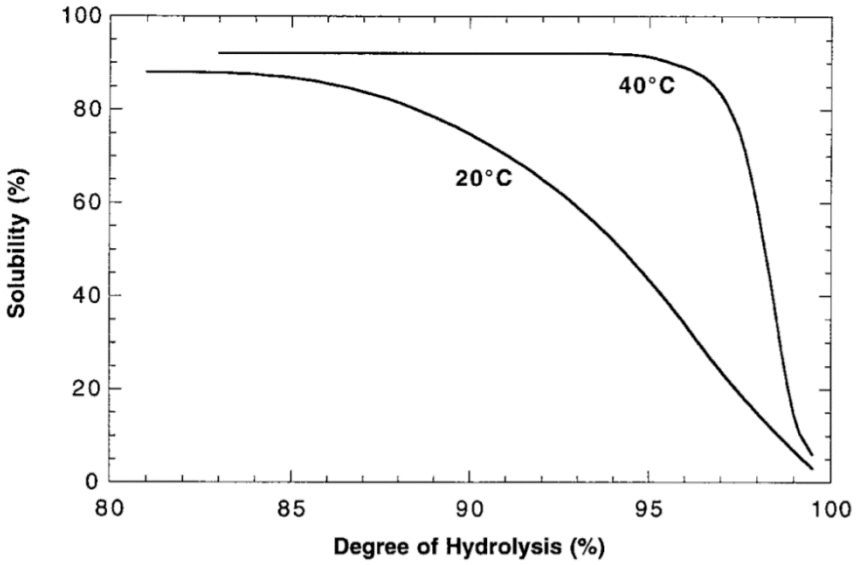

Figure 2.4. Impact of degree of hydrolysis on the solubility of PVA in water.[90] (f4)

PVA exists in isotactic, syndiotactic, and atactic forms, and depending on its stereoregularity it will possess certain properties. For instance, syndiotactic PVA will not dissolve in water, while isotactic PVA will dissolve even in cold water.[89] Furthermore, in addition to the stereoregularity and degree of hydrolysis playing a role in the overall properties of PVA, a third molecular characteristic also impacts the properties: molecular weight. With a polydispersity index of roughly 2 to 2.5, the molecular weight of PVA can

(f4) Reprinted by permission from Springer: Springer, Advances in Polymer Science,153, Hassan, C. M.; Peppas, N. A., "Structure and applications of poly(vinyl alcohol) hydrogels produced by conventional crosslinking or by freezing/thawing methods." pp. 37-65, Copyright (2000), advance online publication, March 1st, 2020 (doi: 10.1038/sj.APS)

impact the crystallinity, adhesion, mechanical properties, and diffusivity of PVA. [90-92] Additionally, the level of PVA crystallinity can influence the density of the PVA, as well as the mechanical properties with stiffer PVA at higher levels of crystallinity. The crystallinity also can be influenced by the molecular weight (MW) of the PVA, as a minimum chain length is usually necessary to achieve the folded structure of the crystallites. Additionally, a higher MW is associated with an increase in size of the crystallites, as the longer chains are able to form more layers.[90]

In commercial applications, PVA has been continually growing in usage and projects to continue growth as there is an increase in need for biodegradable products.[21, 84] PVA is mostly found in the packaging industry,[15, 21] but it is also used in papermaking, construction, and electronics. For construction purposes, it can be used as an additive for better water solubility, adsorption capacity, and particle size. In the biomedical field, PVA has often been looked at as a replacement for fibrocartilage such as the nucleus pulposus in an intervertebral disc.[93-94]

2.4.1 Polyvinyl Alcohol Composite Constructs

For composite studies with the nanomaterials of interest, PVA has previously been successfully integrated with both chitin[68, 95] and cellulose[24, 96-97] independently, however, the use of a CNC/ChNF tricomponent composite at similar weight loadings and how they influence the overall thermomechanical properties is currently understudied. This project aims to process and characterize three different types of PVA-based nanocomposites using

CNCs, ChNFs, or CNC/ChNF mixtures. These three PVA forms include: (1) PVA films, (2) PVA hydrogels, and (3) PVA aerogels.

Certain PVA constructs can be characterized in unique ways, allowing for a more complete understanding of how the nanofillers are interacting with the polymer matrix. The primary reason to choose PVA as the polymer matrix for this study is the similarity in processing steps that each of the three constructs share. The preparation of the CNC/ChNF/PVA suspension utilizes the same five materials: CNCs, ChNFs, PVA, acetic acid, and water; and PVA's physical crosslinking eliminates the need for additional chemicals to transition from one construct to another. A schematic of the three polymer constructs and how they are generated is displayed in Figure 2.5 below.

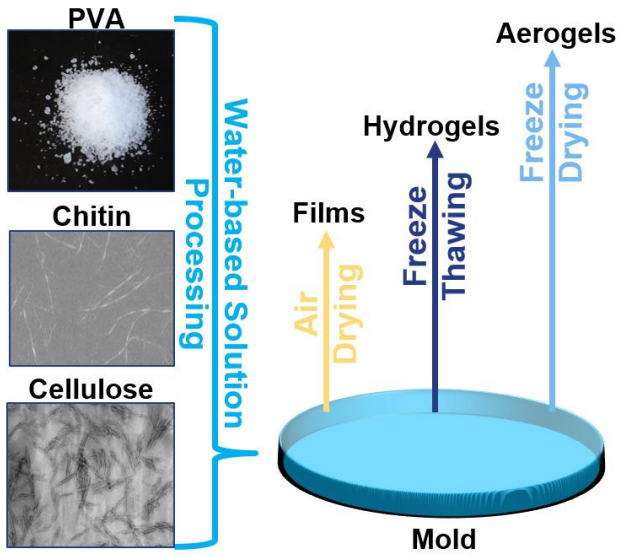

Figure 2.5 Schematic of the generation of the different PVA constructs.

As mentioned previously, the CNC/ChNF/PVA solutions for all of the tested samples can be produced through the same steps with only minor processing steps added to generate films, hydrogels, or aerogels. The tricomponent composite solution processing utilized in this study begins by dissolving PVA powder of a specific MW into deionized water. This is performed by heating a water bath on a hot plate until the thermometer reads 100 °C, adding the PVA powder to deionized water in a beaker suspended in the water bath by a clamp, then mixing with a magnetic stir bar at 300 RPM for approximately 8 hours. Throughout this process, additional water will likely be needed to be added periodically to the water bath to account for evaporation. After the PVA powder has completely dissolved and is no longer visible, the hot plate heat is turned off and the PVA solution is cooled (while still mixing at 300 RPM) until the water bath temperature reads below 50 °C, after which acetic acid is added to achieve 1 vol.% acetic acid concentration and mixed for an additional 30 – 60 minutes. Acetic acid addition is used to protonate the suspension. Then a desired quantity of a 0.5 wt.% suspension of ChNFs is added followed by an additional 30 – 60 minutes of mixing with the magnetic stir bar. Finally, a desired quantity of a 0.5 – 5.5 wt.% suspension of CNCs was added to the mixture and stirred once more for an additional 30 – 60 minutes with a magnetic stir bar. Mixing of the final CNC/ChNF/PVA suspension may require higher RPM than 300 if the surface of the suspension in the beaker is not perturbed. If bubbles are present, the final suspension can be sonicated in a bath sonicator for 5 minutes at 80W to remove the bubbles. The sample suspensions can then be cast into different molds based on the desired final construct which are described in more detail below, as well as in chapters 3-5.

Polymer films are thin, flexible materials that are typically translucent and are generally designed for packaging applications. PVA has excellent film forming properties and offers many attributes including flexibility, barrier properties, and tensile strength.[98] PVA films are typically generated by casting the CNC/ChNF/PVA solution into a mold and allowing them to dry under heat or ambient conditions. The resulting films are transparent and flexible, and they can redissolve in water if submerged. PVA nanocomposite films have been made from a variety of different blends including starch,[99] CNCs,[100] ChNFs,[75] and carbon nanotubes.[101] The introduction of nanofillers have also previously shown to delay the thermal degradation of PVA within the film construct.[6, 75, 100] From a characterization standpoint, they offer the advantage of being easily generated and tested to obtain qualities such as the elastic modulus, tensile strength, strain at break, thermal degradation, and barrier properties. In comparison to lower MW films, high MW PVA has been previously shown to possess higher thermal stability, higher levels of crystallinity, and increased mechanical properties.[102]

The second form of PVA generated in this project is a hydrogel. This form is highly utilized in the tissue engineering applications given its closeness in structure to natural human soft tissues. Hydrogels are three-dimensional structures primarily made up of water, though they display solid-like properties due to the structure of the dispersed component.[103-105] Traditionally, polymer hydrogels are generated through the addition of chemical agents to form crosslinks, but this methodology often leads to a decrease in biocompatibility[103] or the necessity of a chemical leaching step.[90] Therefore, while PVA can be crosslinked with chemicals such as glutaraldehyde,[106] a common way of generating PVA hydrogels was developed by Peppas et al. in 1975 and consists of consecutive freezing

and thawing cycles that encourage the formation of physical crosslinks.[107] This method of physical crosslinking is the result of the freezing process driving polymer-water phase separation from the formation of water ice crystals, which promotes a molecular mesh entanglement between PVA chains held together by crystalline regions and yields a solid structure containing pockets of trapped water within the hydrogel.[90, 103, 108-109] Repeating this freeze-thaw (FT) process increases the level of crosslinking, density, and modulus of the hydrogels, resulting in progressively stiffer materials.[90, 103] The properties of FT PVA hydrogels can be influenced by water percentage, degree of hydrolysis, and preparation methodology (i.e. freezing and thawing rates/duration), which results in a high level of customizability.[91] Solids content of PVA can be controlled through initial solutions processing followed by subsequent drying and/or water absorption to achieve a specific concentration. The resulting hydrogels are solid, highly elastic, and relatively insoluble in water. These properties combined with their low protein absorption and biocompatibility[110] have allowed PVA polymer hydrogels to be used in several biomedical devices including artificial cartilage,[25] contact lenses,[111] and wound-dressings.[12] For tissue engineering applications, the necessity for material customizability leads to the introduction of nanofillers as a means of providing reinforcement and tuning to the properties of patient needs.

The third and final form of PVA addressed in this research is PVA aerogels. Aerogels are porous materials that are extremely lightweight and thus have been applied to insulating, barrier, and reinforcement applications aiming to reduce weight of the overall structure. The initial steps for generating aerogels is very similar to PVA hydrogels, as a PVA solution is placed in the freezer and allowed to cross-link for several hours. However,

when the freezing is complete, the sample is placed in a freeze-dryer at low temperature and low pressure where the water is sublimated out of the structure to leave behind a porous, low-density material with high specific surface area.[112] The resulting material takes the shape of its freeze-drying container is compressible with a tunable elastic modulus based on the PVA molecular weight, concentration, and content of nanofillers. Similar to the other two PVA constructs, the processing method for generating PVA aerogels is environmentally friendly and does not require the usage of any other chemicals or materials outside of water and PVA. PVA aerogels have been previously studied with the introduction of CNCs,[108, 112] with the CNC/PVA aerogel material construct previously developed for use as artificial meniscus replacement given its closeness to cartilaginous tissue.[113]

2.5 Tricomponent Composites and Charge-Driven Complexes

Tricomponent composites are materials that utilize three different materials in an effort to generate an overall higher performance composite structure that exhibits increases in properties beyond that of what is possible with a single filler. These improved properties could be mechanical, chemical, or specific to a certain application and may be the result of enhancements afforded by the unique constituents or an interaction between the nanofillers or matrix. For instance, in photoelectrode research, cadmium sulfide (CdS) and titanium oxide (TiO_2) devices experienced a 6-fold increase in quantum efficiency with the addition of reduced graphene oxide (GO), which was theorized to facilitate electron transfer between the two layers.[114] Another case is the tricomponent composites may also be used

to mimic existing natural structures, such as bone, which incorporate nanofibers into a larger tissue matrix.[115] PVA aerogels even include some tricomponent composites with CNC/clay[116] and CNC/carbon nanotubes,[117] both of which exhibited drastic increases in mechanical properties in the tricomponent composites relative to single nanofillers. One study by Bian (2018) assessed CNF, lignin, and PVA tricomponent hydrogel composites and found that mechanical properties increased with the addition of a small amount of lignin to the CNF/PVA composites. The author theorized that this was the result of lignin binding the CNF chains, which allowed for greater entanglement within the PVA matrix and an overall increase in reinforcement.[118]

As discussed previously, CNCs hold a negative charge on their surface and ChNFs hold a positive charge on their surface, which opens avenues for studies into their electrostatic interactions. To reiterate, the negative charge on the CNCs is the result of the sulfuric acid hydrolysis processing method that is commonly used to dissolve away the disordered regions of the cellulose chain, which leaves anionic sulfate ester groups on the surface in place of some of the hydroxyl groups.[119] For chitin, the N-acetyl groups on the surface of the ChNFs provide a positive charge that allows for opportunities of generating electrostatically influenced microstructures in combination with CNCs. In colloidal science, these combination of oppositely-charged particles are called a coacervate. Some animals, such as snails, produce these liquid-liquid coacervates for adhesion, and researchers have looked into replicating this natural phenomenon for applications as encapsulants, additives, emulsifiers, and viscosity modifiers within the food science and personal care product marketplaces. Furthermore, they have been analyzed for use in drug delivery or biosensing, specifically for the encapsulation of proteins, RNA, DNA.[120] In this

thesis, the study of coacervates is motivated by a desire of manipulating these electrostatic differences between oppositely-charged particles for generating structures otherwise not possible with a single nanomaterial.

Several previous studies have assessed cellulose and chitin nanomaterials blended together with a variety of processing methods in order to analyze the potential of their synergistic interactions. Takegawa et al. (2010) prepared chitin and cellulose-based hydrogels and films with ionic liquids, which had previously been shown to effectively dissolve the nanomaterials. The results of this study showed an increase in modulus and strength with increased loadings of cellulose measured through compression testing of the gels and tensile testing of the films.[121] Similarly, Duan et al. (2018) also used ionic liquids to prepare chitin-cellulose films along with a solvent sourced from lignocellulosic biomass, γ-Valerolactone, which demonstrated that a 4:1 ratio of chtin:cellulose produced the highest tensile stress, elastic modulus, and breaking elongation, in addition to the highest water absorption, compared to neat and mixed films.[122] Zhang et. al (2002) analyzed the mechanical properties of cellulose and chitin films produced from dissolving in NaOH/thiourea and NaOH, respectively. The results of this study reported that the tensile strength and strain at break were improved with certain ratios of cellulose to chitin and the authors attributed the improvement to increased intermolecular hydrogen bonds between the two nanomaterials.[123] A study by Robles et al. (2016) assessed hot-pressed antifungal films generated from CNFs produced through high pressure homogenization and ChNCs produced through acid hydrolysis. The authors found that the addition of ChNCs up to 10 wt.% decreased the growth of fungus and decreased the water vapor permeability (WVP) of the CNF films.[124] Additional research has been performed with chitosan as well.

Khan et al. (2000) generated chitosan films reinforced with up to 10 wt.% CNCs and showed that increased CNC loadings reduced WVP of the films.[125]

Overall, the study of cellulose and chitin nanomaterials together in polymer nanocomposites is limited. One study by Mok et al. analyzes nanocellulose, polymeric chitin, and PVA nanocomposites with chitin loadings up to 30% and cellulose loadings up to 1.5%.[73] Mechanically, this study found that the highest tensile strength and Young's modulus values belonged to the 1 wt.% CNC composites regardless of chitin loading. These enhancements were explained by potential electrostatic and hydrogen bonding between the cellulose and chitin components. Nakagaito et al. (2018) prepared hot-pressed PLA films reinforced with 50 wt.% ChNFs and CNFs at different ratios to each other, in which they reported greater mechanical properties in cellulose/chitin tricomponent films relative to chitin or cellulose reinforcement alone. These results were attributed to the formation of a nanoscale network made up of the CNFs where the connected ChNFs were able to act as a bridge between the hydrophobic PLA and hydrophilic CNFs, thus allowing for greater interaction and reinforcement between all combined components.[126] However, this study concluded that the reinforcing mechanisms for cellulose and chitin were not fully understood and require additional study. Through the incorporation of negatively-charged CNCs and positively-charged ChNFs into PVA, the current work aims to contribute to the field of composite science by furthering understanding of network formation between bio-derived nanomaterials and how these can influence the overall properties of a polymer matrix, particularly mechanically. Furthermore, the utilization of PVA will allow for the generation of tricomponent composites in a variety of polymer constructs, thus allowing for an analysis of how nanofiller influence on the polymer matrix translates between films,

hydrogels, and aerogels, in addition to expanding the realm of potential applications for these customizable, high-performance materials.

CHAPTER 3. CELLULOSE- AND CHITIN-BASED NANOMATERIALS INCORPORATED INTO POLYMER FILMS

This chapter was adapted from a publication in *Composites Part A.*

Irvin, C. W.; Satam, C. C.; Carson Meredith, J.; Shofner, M. L., Mechanical Reinforcement and Thermal Properties of PVA Tricomponent Nanocomposites with Chitin Nanofibers and Cellulose Nanocrystals. *Composites, Part A* **2019**.

In this chapter, PVA films were generated and reinforced with two nanofillers, CNCs and ChNFs, in order to analyze enhancements in the polymer composite structure. The goal of this chapter was to analyze the effects that the nanofillers had on the thermomechanical properties and crystallinity of the PVA polymer matrix and whether these loadings could be tuned to allow for greater overall properties. In addition to comparisons of composites containing only CNCs or ChNFs, composites containing varying ratios of the two nanofillers were compared to assess the impact that differences in aspect ratio, chemical makeup, and surface charge have on properties. Lastly, the effects of polymer molecular weight on developing microstructures in these composites was assessed by comparing composites prepared by using high and low molecular weight PVA. This construct was chosen as the initial form to be studied due to the wealth of information available on the effects of nanomaterials on the structure of PVA films. Trends observed in this study could then be applied to the analysis of the hydrogel and aerogel systems in later studies.

3.1 MATERIALS AND METHODS

3.1.1 Polyvinyl Alcohol

Two different variants of PVA were used in this study: one with a weight average molecular weight of 31,000 – 50,000 g/mol and 98-99% and was hydrolysed, and one with a weight average molecular weight of 146,000-186,000 g/mol and was 99+% hydrolysed. The polymer with the higher molecular weight is denoted in this study as HPVA, and the polymer with the lower molecular weight is denoted as LPVA. These polymers were purchased from Sigma-Aldrich (St. Louis, Missouri) and used as received.

3.1.2 Cellulose Nanocrystals

CNCs were purchased from the USDA Forest Service Forest Products Laboratory (Madison, Wisconsin) and used as received. CNCs produced at this facility were derived from dissolving pulp that was hydrolysed with 64% sulfuric acid, with the crystalline regions then separated out and through a series of dilutions, filtrations, centrifugations, and settling.[127] The resulting material was freeze-dried and stored in opaque bags prior to shipment. These freeze-dried CNCs were then redispersed in water at 5.5 wt.% solids content using a Talboys model 134-1 overhead mixer set at 2000 RPM for at least 90 minutes.

3.1.3 Chitin Nanofibers

For this work, ChNFs were produced mechanically through high-pressure homogenization as previously described,[81] which subjects the chitin fibrils to forces that can strip ChNFs off the surface of a larger chitin structure. This process used crab shells sourced from bio-waste, where different types of crabs can yield chitin of different degrees of acetylation (DA). These shells were first thoroughly washed several times in deionized (DI) water and then ground into a fine powder with a commercial grinder. The ground crab shell powder was then refluxed at a temperature of 110 °C with 5 wt. % NaOH for 6 hours. The resulting solids were passed through a filter and washed with DI water until the pH of the water was 7. These solids were then held in a 7 wt.% HCl bath for 6 hours at lab conditions, filtered again, and washed with DI water until the pH of the wash water was 7. These acid-treated chitin solids were then refluxed with 5 wt.% NaOH for 48 hours at a temperature of 110 °C, then again filtered and washed with DI water until the wash water pH was 7. The final product of these steps was a fine, white powder of purified chitin, which was then dried in an oven at 60 °C for 24 hours to remove any residual water. In order to extract the ChNFs from the chitin powder, the powder was redispersed in DI water at 0.5 wt.% and passed through a high-pressure homogenizer. Prior to the first pass, the pH of the suspension was adjusted to 3.0 using glacial acetic acid to encourage dispersion of the positively charged chitin molecules. Glacial acetic acid was purchased from Sigma-Aldrich and used as received. The homogenizer used in this thesis was a Mini DeBEE Homogenizer (BEE International, South Easton, MA). The first 20 passes of the chitin suspension were carried out at a pressure of 1034 bar and with a 0.2 mm nozzle. The final 10 passes were carried out at a pressure of 1516 bar and with a smaller 0.13 nozzle for a

total of 30 passes. A water-cooled heat exchanger was utilized throughout the homogenization process in order to cool the shear-heated nozzle and resulting ChNF suspension to below 35 °C.

3.1.4 Nanocomposite Solution Processing Procedure

PVA powder of one molecular weight (HPVA or LPVA) was mixed with deionized water at 300 RPM with a stir bar in a water bath at 100 °C until no visible PVA particles were present. The amount of PVA powder mixed was consistent at 4.75 g, but the amount of initial water it was dissolved into varied depending on the amount of nanofillers needed, which always resulted in a final loading of 5 wt.% in suspension. If containing CNCs and/or ChNFs, the solution was cooled to below 50 °C and 1 mL glacial acetic acid for every 100 mL of solution was added to reduce the solution's pH and encourage dispersion of the ChNFs. The desired amount of ChNFs suspended in water at 0.5 wt.% were then added to the PVA solution, and the components were mixed at 300 RPM with a stir bar for at least 30 minutes. Finally, the desired amount of CNCs suspended in water at 5.5 wt.% was added and mixed at 300 RPM with a stir bar for at least 30 minutes. The resulting nanocomposite suspension was cast into a polystyrene Petri dish and covered with aluminum foil to prevent contamination during drying. For neat PVA polymer samples containing no nanofillers, PVA was dissolved in deionized water with a stir bar at 300 RPM in a 100 °C water bath. The resulting solution was cast in a polystyrene Petri dish and allowed to dry in the same fashion as the nanocomposite samples. Drying to a solid film took between 7-12 days depending on the water content and PVA type. In all cases studied here, the filler loading

in the nanocomposites was kept constant at 5 wt.%. This filler loading consisted of either only CNCs, only ChNFs, or different mixtures of CNCs and ChNFs at weight ratios of 1:4, 1:1, and 4:1. The naming convention for samples in this study follows the template: [wt.%]CNC/[wt.%]ChNF/[L or H]PVA. For example, a sample containing 1 wt.% CNC and 4 wt.% ChNF in high molecular weight PVA is denoted as 1CNC/4ChNF/HPVA.

3.1.5 Polarized Optical Microscopy

Polarized optical microscopy (POM) was performed utilizing an Olympus BX51 microscope in bright field mode with images captured by an Olympus UC30 camera. A polarizer was applied below the sample stage at an angle 90° to the analyzer so that no light was able to propagate through the two cross polarizers. Samples were then placed on the stage and analyzed to assess nanofiller aggregation.

3.1.6 Titration Testing and Zeta-Potential Testing

To more fully understand the nature of nanofiller interactions in suspension and the resulting nanocomposite films, titration and zeta-potential testing was performed. For the titration testing, a 5.5 wt.% aqueous suspension of CNCs was diluted with DI water to approximately 1 wt.%. The resulting suspension was ion exchanged with Merck Ion Exchanger I, a strongly acidic cation exchange resin, to remove any cations. The resin was then washed with DI water to wash out entrapped CNCs and the resulting suspension was titrated against a 1.5 N NaOH solution by potentiometric titration with a Mettler Toledo

Seven Excellence S400 pH meter. A 0.5 wt.% aqueous ChNF suspension was ion exchanged with Alfa Aesar Amberlite IRN-78, a strongly basic anion exchange resin, to remove acetate anions. This resin was then washed with DI water to wash out entrapped ChNFs. A volume of 20 ml of 0.25 N HCl was added to the resulting suspension which was then titrated against a 0.5 N NaOH solution by potentiometric titration. Both titrations were repeated three times, and the results were reported as an average ± standard deviation.

For zeta-potential testing, a series of aqueous CNC/ChNF suspensions were prepared by mixing the 0.5 wt.% ChNF and 5.5 wt.% CNC aqueous suspensions to obtain different ratios of ChNF to CNC by weight. The suspensions were diluted with acidified water that consisted of 1 mL acetic acid in 100 mL water to mimic the nanocomposite preparation conditions. Each suspension's zeta-potential was then measured using a Malvern Nano-ZS90 Zetasizer with an equilibration time of three minutes. Each reading was repeated three times, and the count averaged zeta-potential of distribution was used with the maximum-observed standard deviation of the three readings being used as the uncertainty.

3.1.7 FTIR Characterization

Chemical structure changes were assessed using Fourier Transform Infrared Spectroscopy with an Attenuated Total Reflectance fixture (ATR-FTIR). A Thermo Fisher Scientific Nicolet iS50 FTIR spectrometer was utilized for this testing. Spectra were generated based on the average of 64 scans with a resolution of 4 cm^{-1}, then normalized to

a C-H stretching peak around 2910 cm^{-1} that did not appear to shift with the introduction of nanofillers.

3.1.8 Thermogravimetric Analysis

Thermogravimetric analysis (TGA) was conducted on the neat PVA and nanocomposite samples. A single witness sample for each of the neat PVA and nanocomposite samples with a mass ranging from 8-12 mg was punched from the films and dried for one hour at 110 °C, held at lab conditions for 40-48 hours, and then tested with a TA Instruments TGA Q50 with platinum pans in a flowing nitrogen gas environment. The TGA protocol heated the samples from 30 to 110 °C, held them isothermally for one hour to remove residual water, then heated them at 10 °C/min up to 600 °C. Testing was performed to evaluate any effects the nanofillers might have on sample degradation and to measure sample water content.

3.1.9 Modulated Differential Scanning Calorimetry

To assess the crystallinity of samples, modulated differential scanning calorimetry (MDSC) was performed utilizing a TA Instruments Discovery DSC with standard aluminum pans in a flowing nitrogen gas environment. Two of each of the neat PVA and nanocomposite samples were tested. Sample masses used were 5 mg (± 0.5 mg). These samples were dried in an oven for one hour at 110 °C prior to testing. Samples were heated from 30 °C to 250 °C at a rate of 10 °C/min., held for five minutes at 250 °C, then cooled

to 30 °C at a rate of 10°C/min, per ASTM D3418. The modulation rate was set to 1 °C every 30 seconds. Enthalpy of fusion was calculated from the reversible heat flow melting peaks and compared to a 100% crystalline PVA value of 161 J/g, to obtain the percent crystallinity of the sample [128]. In order to account for nanofiller weight percentage, sample mass for this % crystallinity calculation was adjusted to consider the PVA mass only. An equation outlining this calculation is shown below, where X_c represents the sample crystallinity, ΔH_m represents the enthalpy of fusion for the sample, ΔH_m^o represents the 100% crystalline sample value, and w is the PVA weight fraction:

$$X_c = \frac{\Delta H_m}{w \Delta H_m^o}$$

3.1.10 Mechanical Testing

Samples were cut from the films with an ASTM D-1708 die cutter and dried for one hour in an oven at 110 °C to remove water. Samples were held on the ends with the center bridge suspended in air to optimize water removal uniformly from the testing region of the sample. Samples were then kept at laboratory conditions for 40-48 hours, and humidity levels in the laboratory were monitored. Humidity levels were observed to stay between 35% and 52% depending on the day of measurement.

Samples were tested following the ASTM D-1708 standard for polymer microtensile testing. An Instron 5566 Materials Testing Frame and a 1000 N load cell were used for testing tensile properties. After drying and conditioning, each sample was placed in the grips at a gage length of 22 mm. Samples' thicknesses were 0.3 mm ± 0.09 mm. The tests

were conducted at a displacement rate of 0.1 mm/minute until fracture. While the microtensile testing standard is not designed to obtain quantitative Young's modulus values, the testing data were used to obtain relative modulus data. The relative modulus of the samples was calculated by taking the slope of the stress-strain curve from 5 MPa to 30 MPa for each sample. Tensile strength was indicated as the maximum stress experienced by the sample during testing. Strain at break values were calculated from the initiation point of 40% drop off in recorded force within the software. All data reported in this study is represented as an average ± standard deviation**.** For statistical analysis between sets, a two-tailed Student's T-Test assuming unequal variances and an alpha value of 0.05 was performed. Statistical significance was determined by having a sample set average with a p value of less than 0.05. Sample set averages that were statistically significantly greater than the neat PVA film were indicated with an * in figures, while a ^ indicates a sample set average that is statistically significantly greater than all other values. Complete statistical maps for modulus, tensile strength, and strain at break are included in the Appendix (Figures A.1, A.2 and A.3, respectively).

3.2 RESULTS AND DISCUSSION

3.2.1 Polarized Optical Microscopy

Neat PVA and nanocomposite films were imaged with POM to qualitatively assess the levels of aggregation between nanofillers in each sample, and the images are displayed in Figure 3.1. In the images, neat PVA films (Figures 3.1a and 3.1g) possessed a consistent coloring throughout. In comparison, the 5CNC samples (Figures 3.1b and 3.1h) showed

white features that could be birefringence from CNCs aggregates. In contrast, the 5ChNF samples (Figures 3.1f and 3.1l) showed fewer white areas and resembled the neat polymer films more closely, possibly indicating that there was less aggregation of ChNFs. The tricomponent composites (Figures 3.1c-e and 3.1i-k) showed white features as well, and the features generally were smaller and more homogeneously distributed over the area in the images. Overall, these images indicated that some degree of nanofiller agglomeration was present in all of the nanocomposites containing CNCs. Despite the appearance of nanofiller aggregation in POM images, the neat PVA and nanocomposite films appeared transparent to the naked eye (Figure A.4).

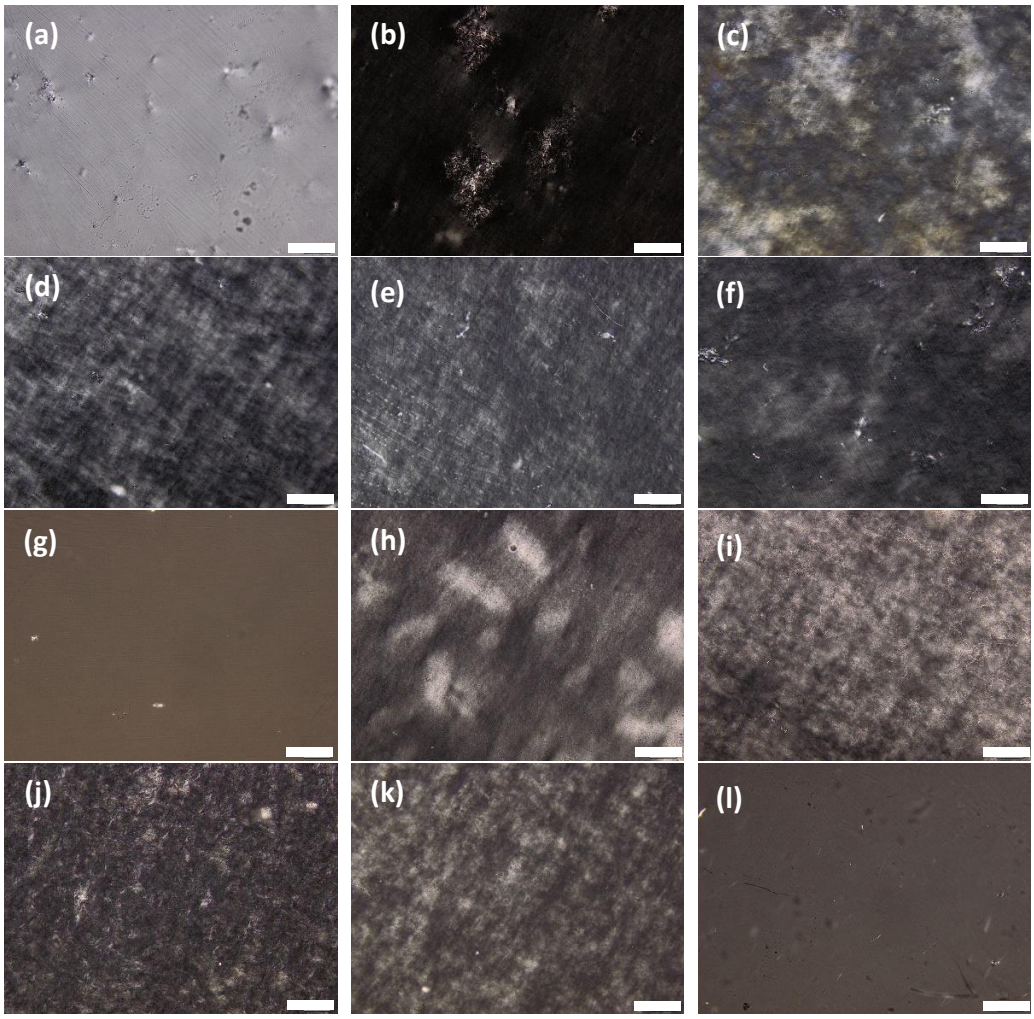

Figure 3.1. Polarized optical microscopy images of (a) Neat HPVA, (b) 5CNC/HPVA, (c) 4CNC/1ChNF/HPVA, (d) 2.5CNC/2.5ChNF/HPVA, (e) 1CNC/4ChNF/HPVA, (f) 5ChNF/HPVA, (g) Neat LPVA, (h) 5CNC/LPVA, (i) 4CNC/1ChNF/LPVA, (j) 2.5CNC/2.5ChNF/LPVA, (k) 1CNC/4ChNF/LPVA, and (l) 5ChNF/LPVA.

3.2.2 Interactions between CNCs and ChNFs

To characterize the interactions between CNCs and ChNFs in suspension, titration and zeta-potential testing were performed. The titration tests provided surface charge values for CNC and ChNF in aqueous suspension, while the zeta-potential tests investigated how these surface charges changed when CNC and ChNF suspensions were

combined. The titration experiments yielded surface charge values of 1.4 ± 0.1 meq/g and 0.49 ± 0.09 meq/g for the ChNFs and CNCs, respectively.

The resulting equivalents for ChNFs and CNCs from these tests represented the maximum number of cationic groups, primarily free amine groups for ChNFs, and, anionic groups, primarily sulfate groups for CNCs that could participate in any neutralization reactions. When CNCs and ChNFs were mixed together in suspension, the oppositely charged surface groups could interact, leading to the formation of a ChNF-CNC complex or aggregate. However, this assembly process would be dependent on the total number of free groups present, which in turn would depend on the pH of the surrounding medium and presence of ions, as governed by the screening effect. The actual aggregate formation could be inferred from zeta potential measurements of various ChNF/CNC mixtures. The resulting data for these tests is shown in Figure 3.2.

In CNC/ChNF mixtures, the suspensions were stabilized by strong electrostatic repulsions between oppositely charged particles. In suspensions containing CNCs and ChNFs, the zeta potential values were intermediate between those obtained for the suspensions containing only one type of nanofiller. Interpolating the data in Figure 3.2 suggests that the CNCs and ChNFs neutralize one another at a CNC:ChNF mass ratio of approximately 3:1. This ratio, while approximate, is comparable to the ratio present in the 4CNC/1ChNF nanocomposites.

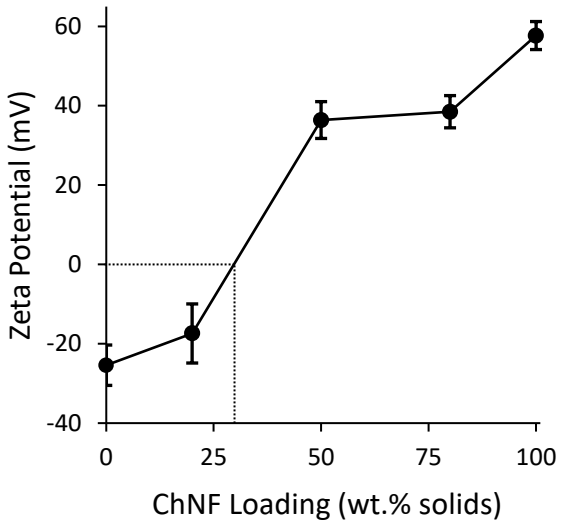

Figure 3.2. Zeta Potential of CNC and ChNF suspensions at various ratios.

3.2.3 FTIR

ATR-FTIR analysis was performed on both HPVA and LPVA for each of the five nanofiller loaded samples and neat polymer with the aim of understanding the changes in chemical structure as a result of the introduction of CNCs and ChNFs into the system. From the spectra for HPVA represented in Figure 3.3 (staggered for clarity), the large peak in the 3500-3000 cm^{-1} range was attributed to stretching of hydrogen–bonded hydroxyl groups. Hydroxyl groups are present on PVA, CNC and ChNF, as well as any absorbed water that is present. The highest intensity peak in this range belonged to 2.5CNC/2.5ChNF/HPVA, followed by 1CNC/4ChNF/HPVA, with progressively smaller intensity peaks from 5ChNF/HPVA, 5CNC/HPVA, neat HPVA, and 4CNC/1ChNF/HPVA. Two peaks at 1720 and 1660 cm^{-1} could be attributed to C=O and C-O stretching of acetyl groups, which appeared to grow in intensity with ChNF

composition, as expected. The medium sized peak at 1410 cm^{-1} was assigned to CH_2 and CH_3 bending deformation. The peaks around 1380, 1327, and 1235 cm^{-1} were attributed to the bending of C-H, CH_2, and -OH, while the peak around 1086 cm^{-1} was considered to be C-O stretching.[5] There is an additional peak at 1065 cm^{-1} that was only present in samples containing at least 2.5 wt. % CNCs, indicating that it may be the result of alkoxy C-O-C group stretching or primary aliphatic alcohol stretching in CNCs.[129] However, despite the presence of alkoxy groups in ChNFs, this peak does not appear in the samples containing higher amounts of ChNFs. Skeletal signals appeared around the 915 and 845 cm^{-1} bands.

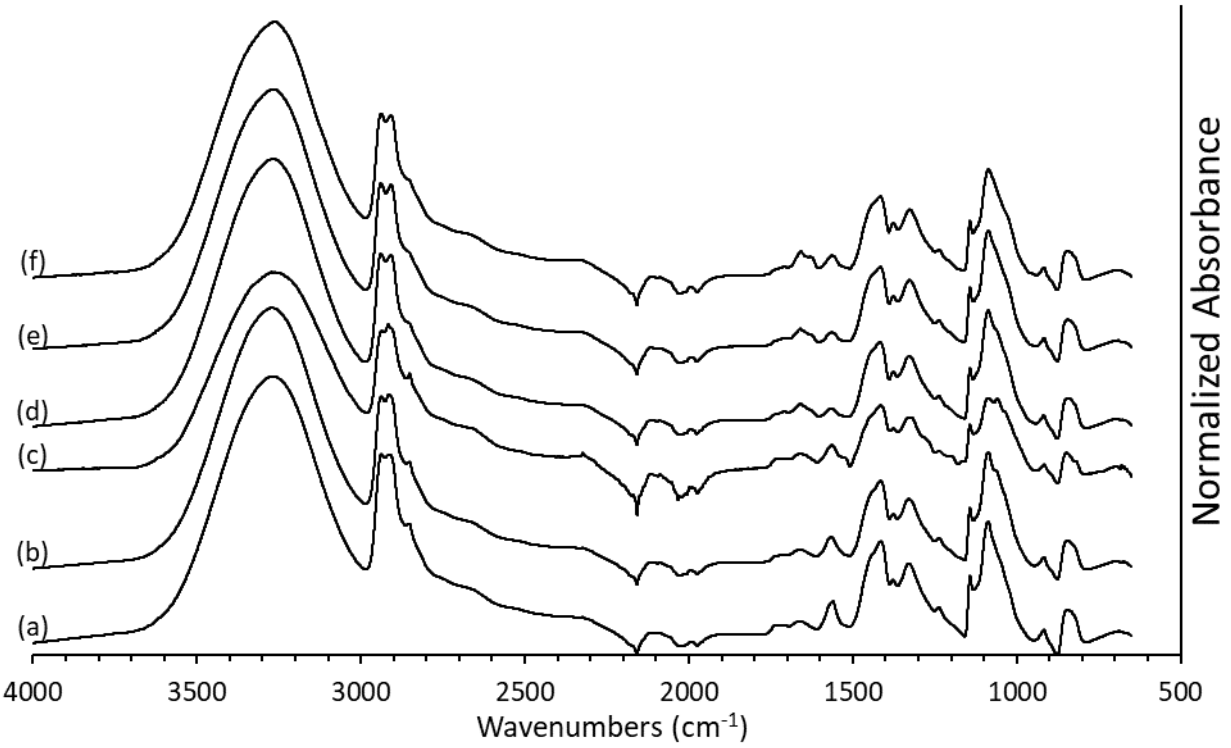

Figure 3.3. FTIR analysis of (a) Neat HPVA, (b) 5CNC/HPVA, (c) 4CNC/1ChNF/HPVA, (d) 2.5CNC/2.5ChNF/HPVA, (e) 1CNC/4ChNF/HPVA, and (f) 5ChNF/HPVA.

The spectra of LPVA represented in Figure 3.4 displayed the same structural peaks discussed previously for HPVA. In regard to the differences in intensities of the hydrogen bonding peak between 3500-3000 cm^{-1}, the highest intensity peak belonged to 2.5CNC/2.5ChNF/LPVA, followed by 5CNC/LPVA, 5ChNF/LPVA, 1CNC/4ChNF/LPVA, 4CNC/1ChNF/LPVA, and neat LPVA. Additionally, while only 4CNC/1ChNF/HPVA and 5ChNF/HPVA experienced a small shift at this peak to higher wavenumbers compared to neat HPVA, the entirety of the LPVA sample set experienced a 10-20 cm^{-1} shift to higher wavenumbers in comparison to neat LPVA. While the peaks were broad, a shift to lower wavenumbers is often attributed to the presence of hydrogen bonds,[130-131] which suggested the addition of CNCs/ChNFs to the LPVA caused a decrease in the amount of hydrogen bonding within the system.[72] A main difference between the HPVA and LPVA sets was in regards to the 1720 cm^{-1} peak, which was much more pronounced in the LPVA sample sets. As a peak belonging to the C=O stretching of acetyl groups, the higher intensities of the LPVA analysis may have been the result of the higher amount of acetyl groups present in the slightly less hydrolyzed LPVA.

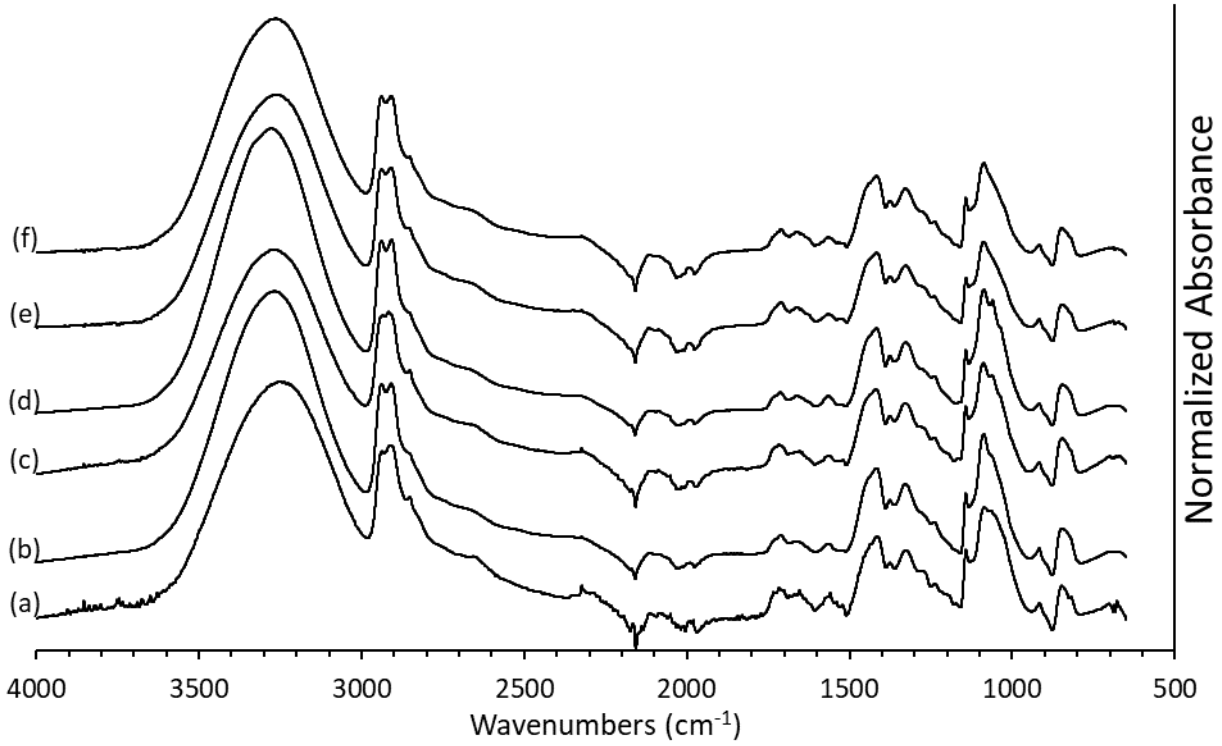

Figure 3.4. FTIR analysis of (a) Neat LPVA, (b) 5CNC/LPVA, (c) 4CNC/1ChNF/LPVA, (d) 2.5CNC/2.5ChNF/LPVA, (e) 1CNC/4ChNF/LPVA, and (f) 5ChNF/LPVA.

3.2.4 Thermal Degradation

TGA was used to assess the thermal degradation patterns of the neat PVA and the nanocomposites. The analysis was used to help understand the impact that the nanofillers had on thermal stability and whether they formed structures that were more resistant to degradation at higher temperatures. Table 3.1 outlines the onset of the two degradation events in addition to the residual weight percentage left in the pan at the conclusion of the test.

Table 3.1. TGA data that provides the first and second degradation onsets and the final residual weight percentage.

Sample Name	Onset Degradation Temperature 1 (°C)	Onset Degradation Temperature 2 (°C)	Residual Weight (%)
Neat HPVA	241	406	7.1
5CNC/HPVA	253	400	10.3
4CNC/1ChNF/HPVA	257	400	8.5
2.5CNC/2.5ChNF/HPVA	262	429	8.9
1CNC/4ChNF/HPVA	256	423	9.4
5ChNF/HPVA	242	421	11.7
Neat LPVA	252	429	9.1
5CNC/LPVA	256	412	8.2
4CNC/1ChNF/LPVA	263	411	8.5
2.5CNC/2.5ChNF/LPVA	248	414	9.5
1CNC/4ChNF/LPVA	246	419	10.5
5ChNF/LPVA	254	423	10.5

The samples experienced the same general thermal degradation pattern, which consisted of three weight loss steps (Figure A.5 and A.6). The first weight loss occurred below 110 °C and was attributed to the loss of water in the sample. HPVA- and LPVA-based samples showed a consistent water content of approximately 3%, indicating that the drying and conditioning steps affected the samples relatively uniformly. The second weight loss step indicated the beginning of PVA degradation, and it occurred among all samples in the temperature range of 240 – 265 °C. It was also likely that CNC and ChNF degradation was occurring simultaneously at different rates within this weight loss step based on the degradation patterns for the nanofillers when not contained in a composite. CNCs utilized in this study had a degradation temperature around 189°C and ChNFs were measured to degrade at 285 °C (Figure A.7).

In comparison to the neat PVA, most of the nanocomposite samples, except the 2.5CNC/2.5ChNF/LPVA and 1CNC/4ChNF/LPVA samples, exhibited a higher onset

degradation temperature for this step. This data is supported by a study performed by Sriupayo et al. (2005).[75] This work also showed that the introduction of α-chitin whiskers caused an overall delay in thermal degradation in PVA nanocomposites compared to neat PVA. For higher weight percentages up to 25% CNCs, thermal degradation has been shown to be delayed by up to 80 °C for PVA nanocomposites compared to neat PVA.[100] In another study for PVA and silica nanocomposites, the initial onset of degradation temperature was higher in the nanocomposites than in neat PVA. Additionally, using mass spectrometry, they were able to identify that polyene structures are formed during the first degradation step through dehydration.[6] However, this behavior is not general and depends on component interactions and the degradation temperature of the neat polymer. In a study regarding poly(lactic acid) (PLA) composites with cellulose whiskers, the nanocomposites were shown to degrade at a lower temperature compared to the neat PLA.[132] Lastly, Pracella et al. (2014) showed similar results of earlier degradation in non-PVA systems in a study with PLA, PVAc, and CNCs with neat PVAc beginning degradation first, followed by pure CNCs, 1 wt.% CNC/PLA, 1 wt.% CNC/PVAc/PLA, and neat PLA.[133]

The second major weight loss step, which occurred in the range of 400-430 °C. This has been previously attributed to chain-scission reactions and resulted in products of acetaldehyde, low-molecular-weight polyenes, benzenoid derivatives, furan, acetone and acetic acid [6]. LPVA-based samples showed that there was a progressively increased delay in this degradation step as the amount of CNCs was reduced in the composite, but all composites exhibited this degradation step at a lower onset temperature than the neat LPVA. The HPVA samples did not show the same trend, but the two lowest onset degradation temperatures for this process belonged to witness samples cut from the 5CNC

and 4CNC/1ChNF films. This result could be related to the lower degradation temperature of CNCs in comparison to ChNFs. Outside of these two similarities, no trend related the behaviors of the HPVA- and LPVA-based samples. In regards to the residual solids found at the conclusion of each test, the values were not greatly different from one another (Table 3.1). and did not show any clear trends.

3.2.5 Matrix Crystallinity

MDSC was used to assess the relative crystallinity values of each of the films in order to more completely understand the effects of filler addition on matrix crystallinity. The use of MDSC allowed the total heat flow to be split into its reversible and non-reversible parts. Given PVA's propensity for thermally degrading near its melting point due to the production of volatile products and overall dehydration above 200 °C,[134] this calorimetry method allowed for the degradation and melting to be separated,[135] likely leading to a more accurate measurement of crystallinity. Additionally, only data obtained during the first heating ramp were analyzed since the data obtained from a second heating step would likely be affected more strongly by polymer degradation (example heat flow curves are given in Figures A.8 and A.9). Table 3.2 displays the melting temperature, enthalpy of fusion, and % crystallinity values taken from the reversible heat flow signal during melting.

Table 3.2 MDSC data for HPVA- and LPVA- based samples.

Sample Name	Melting Temperature (°C)	Enthalpy of Fusion (J/g)	Crystallinity (%)
Neat HPVA	211 ± 3	61 ± 0	38 ± 0
5CNC/HPVA	200 ± 0	68 ± 0	44 ± 0
4CNC/1ChNF/HPVA	199 ± 8	39 ± 9	25 ± 5
2.5CNC/2.5ChNF/HPVA	198 ± 0	49 ± 1	32 ± 1
1CNC/4ChNF/HPVA	200 ± 3	45 ± 7	29 ± 5
5ChNF/HPVA	200 ± 0	40 ± 10	27 ± 6
Neat LPVA	200 ± 8	41 ± 3	25 ± 2
5CNC/LPVA	200 ± 2	52 ± 8	34 ± 5
4CNC/1ChNF/LPVA	187 ± 1	48 ± 4	31 ± 3
2.5CNC/2.5ChNF/LPVA	188 ± 2	51 ± 2	33 ± 1
1CNC/4ChNF/LPVA	190 ± 3	38 ± 4	25 ± 2
5ChNF/LPVA	184 ± 1	49 ± 6	32 ± 3

The addition of CNCs and ChNFs affected the crystal structure and crystallinity of both PVA matrices. The crystal structure was assessed qualitatively through measuring the melting temperature. If there is no change to the crystal form, changes in melting temperature can be used to qualitatively understand the size of crystalline domains and/or the level of crystal perfection. Lower melting temperatures, such as those observed here, are associated with smaller, less perfect crystalline domains. The majority of the composites showed lower melting temperatures than the neat polymer, and that decrease in melting temperature was up to 10 °C. The one notable exception to this behavior was the 5CNC/LPVA composite, which had an average melting temperature that was equal to that of the neat LPVA. A lowered melting temperature with nanocellulose addition has been observed previously for nanocellulose/PVA composites, and this trend was more likely to be observed in PVA polymers with very high levels of hydrolysis, though the melting temperature depression observed in that work was lower than that seen here.[96] Melting temperature depression of PVA with a high level of hydrolysis was also observed for montmorillonite/PVA composites with similar filler loadings. Montmorillonite

platelets should have the ability to form hydrogen bonds with PVA. Additionally, as loadings increased, the composites with montmorillonite had progressively lower melting temperatures.[136]

For the composites made with HPVA, the crystallinity was increased in the 5CNC composite, but the other composite samples showed lower values of crystallinity. This trend suggested that the CNCs and ChNFs interacted differently with the HPVA. Both types of nanofillers had hydroxyl groups on their surfaces which could form hydrogen bonds with PVA; however, they each had different surface charges associated with other features than the hydroxyl groups. The ChNFs contained protonated amine groups, leading to a net positive surface charge, and the CNCs had sulfate ester groups. These groups, which were produced during hydrolysis with sulfuric acid, result in a net negative CNC surface charge. The presence of these different groups, hydroxyls and charged groups, could affect the crystallization of PVA.

Hydrogen bonding between ChNFs and PVA [72-73, 75] as well as between CNCs and PVA [5, 24, 86] has been reported in previous studies with nanocomposites and may be present in this study as well. Results for polymer blends containing PVA and polymeric chitin, i.e. not in nanofiber form, have shown that the polymers interact strongly through hydrogen bonding, leading to reductions in crystallinity of both components.[72] While polymeric chitin could interact differently with PVA than ChNFs, this reported behavior in addition to the observation that all the HPVA composites containing ChNFs had lowered matrix crystallinity, it is likely that interactions between ChNFs and HPVA reduced crystallinity.

Though PVA is largely an uncharged and nonionic polymer, it has previously been used in metal ion removal through electrostatic interactions with cations, including Ag^{+},[137] $Fe(III)^{3+}$,[138] and Cu^{2+}.[139] The ionic bonding required for removal occurs as cations bind to the -OH groups of the PVA, which may also be interacting with the protonated amine groups on the ChNF in our system. Additionally, while sulfate groups have previously been shown to bind to PVA,[110] the low amount of sulfate groups present on the CNC's (approximately 1 wt. %) would suggest they do not experience as much electrostatic binding as the ChNF that possesses much more amine binding sites. Therefore, while the amount of hydrogen bonding was found to be relatively the same between 5CNC/PVA and 5ChNF/PVA, the presence of greater electrostatic bonding for bi- and tricomponent composites containing ChNF could be a differentiating factor in greater overall filler/matrix interactions and, thus, a decrease in polymer crystallinity.[96]

The LPVA-based samples showed a different trend in crystallinity with the addition of nanofibers. With the exception of the 1CNC/4ChNF/LPVA composite, all LPVA composites possessed higher levels of crystallinity than the neat LPVA. The crystallinity values for these composites were not distinct due to the experimental error. The melting temperatures for the composites containing ChNFs were lower than those for the neat LPVA and 5CNC composite, this trend suggested that the crystals were smaller and/or less perfectly structured in composites containing ChNFs. The 5CNC composite is a notable exception since it also showed higher crystallinity than the neat LPVA but a similar melting temperature. Ultimately, the difference in molecular weight for LPVA and HPVA appeared to have an important effect on the matrix crystallinity.

While not necessary for improving dispersion of CNCs, acetic acid was still added to the 5 wt. % CNC PVA solutions in order to maintain uniformity across samples. In order to test the potential impact of the acetic acid on crystallinity, an additional test performed on 1 vol.% acetic acid in neat HPVA sample showed a similar crystallinity of 38% in comparison to neat HPVA.

3.2.6 Mechanical Testing

Mechanical testing data consisting of modulus, tensile strength, and strain at break were collected from the neat PVA and nanocomposite samples that contained various ratios of CNCs and ChNFs. These data are shown in Figure 3.5 and Table 3.3. Bar graphs and box and whisker plots for the mechanical data are shown in Figures A.10 and A.11. These figures also denote which sample sets had property differences that were statistically significant, as well as any outliers.

Table 3.3. Mechanical testing data for HPVA- and LPVA-based samples.

Sample Name	Number of Specimens	Modulus (MPa)	Tensile Strength (MPa)	Strain at Break (%)
Neat HPVA	7	5210 ± 1040	112 ± 15	17.9 ± 9.2
5CNC/HPVA	7	6540 ± 458	128 ± 11	14.3 ± 10.5
4CNC/1ChNF/HPVA	5	6420 ± 710	116 ± 13	18.6 ± 25.4
2.5CNC/2.5ChNF/HPVA	6	6570 ± 427	121 ± 31	3.3 ± 1.6
1CNC/4ChNF/HPVA	8	7430 ± 532	138 ± 7	7.0 ± 3.3
5ChNF/HPVA	9	6320 ± 763	130 ± 16	15.8 ± 9.6
Neat LPVA	4	5200 ± 428	115 ± 11	3.3 ± 1.3
5CNC/LPVA	6	6550 ± 487	107 ± 12	2.1 ± 0.4
4CNC/1ChNF/LPVA	4	5670 ± 235	80 ± 11	1.6 ± 0.3
2.5CNC/2.5ChNF/LPVA	6	7470 ± 258	120 ± 7	1.9 ± 0.1
1CNC/4ChNF/LPVA	6	6600 ± 557	108 ± 11	2.0 ± 0.3
5ChNF/LPVA	6	6510 ± 383	117 ± 4	2.4 ± 0.1

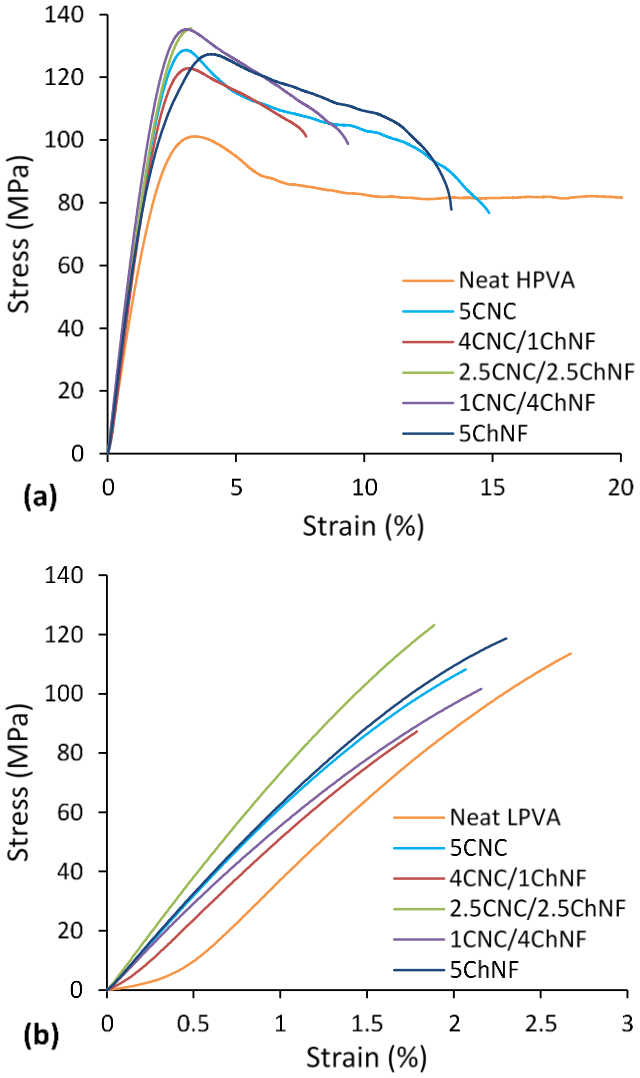

Figure 3.5. Representative stress-strain curves of (a) HPVA-based samples and (b) LPVA-based samples.

Figure 3.5a displays representative stress-strain curves of each of the HPVA-based samples. The samples selected for inclusion in this figure most closely approximated the average and/or median values for modulus, tensile strength, and strain at break for each sample set. All the nanocomposite samples were found to have statistically greater average

values of modulus than that of the neat HPVA (Figure A.1), suggesting that the addition of cellulose- and/or chitin-based nanofillers at a 5 wt.% loading caused an increase in resistance to deformation. Within this sample set, the highest modulus was observed for the 1CNC/4ChNF/HPVA nanocomposite. Additionally, the 5CNC and 5ChNF nanocomposite samples were shown to have statistically similar modulus values. This result appeared logical provided that CNCs have a reported elastic modulus around 50 GPa[140] compared to the slightly lower 41 GPa of crystalline regions of chitin.[77] The short length of the CNCs suggested there might not be a complete load transfer, possibly explaining the similar values between the two different nanofiller types despite the slightly higher modulus of CNCs.

The tensile strength data did not show that all of the composites had a higher tensile strength than the neat HPVA. Three composite samples were found to have tensile strength values that were greater than that of the neat HPVA by statistically significant amounts: 5CNC/HPVA, 1CNC/4ChNF/HPVA, and 5ChNF/HPVA, though these values were not statistically different from one another (Figure A.2). Furthermore, a previous study by Mok et al. (2017) compared tricomponent PVA composites containing cellulose and chitin in nanofiber form. Results showed certain ratios between cellulose and chitin had the largest moduli and tensile strength. The authors suggested this is the result of chitin nanofibers binding to themselves through hydrogen bonding, creating a high strength network, with the CNCs potentially enhancing interaction among chitin molecules and increasing the mechanical capabilities. The authors also suggested that above certain CNC loadings (particularly 1 wt. %) agglomeration occurs between particles which generates weak points in the material, which could explain the relative decrease in mechanical properties with

particular loadings.[73] Additionally, it is worth noting that while the 2.5CNC/2.5ChNF/HPVA data set overall performed similarly to the other nanofiller data sets, one sample experienced brittle failure without yield and is represented in Figure A.10 as an outlier.

Overall, the strain at break data showed that the composites had less ductility than the neat HPVA**.** Some samples experienced wide ranges of breaking strain values, which complicated the data analysis. The 4CNC/1ChNF/HPVA sample specifically experienced relatively uniform strain at break values except for one sample that extended up to 65% of its original length, thus skewing its distribution. Furthermore, statistical analysis showed that all samples except for this 4CNC/1ChNF/HPVA data set were statistically greater than the 2.5CNC/2.5ChNF/HPVA data set (Figure A.3). Generally, the mechanical property data indicated that the addition of nanofillers caused an increase in modulus and tensile strength with a simultaneous decrease in strain at break properties. This type of behavior has been found previously in other polymer nanocomposites [7, 41, 141] and was not unexpected at this nanoparticle loading.

For the LPVA-based materials, some similarities and some differences in the mechanical properties were observed relative to the corresponding HPVA-based materials. Representative stress-strain curves for the LPVA-based materials are shown in Figure 3.5b. The stress-strain curves used in this figure were chosen in the same way as those used in Figure 3.5a. All of the composites except the 4CNC/1ChNF/LPVA composite showed a statistically significant increase in modulus in comparison to the neat LPVA control, indicating that a 5 wt.% loading of nanofillers caused an overall increase in resistance to deformation (Figures A.1 and A.11). Neat HPVA and neat LPVA average modulus values

were statistically similar with values of approximately 5200 MPa, and composites containing only one nanofiber (i.e. 5CNC or 5ChNF) were statistically similar to one another within the LPVA sample set and to the corresponding HPVA-based samples. However, the composites from the two different PVA sample sets with the highest modulus value did not have the same composition. The 2.5CNC/2.5ChNF/LPVA sample displayed a statistically significantly greater modulus average than the other LPVA samples. This sample had a different CNC/ChNF ratio than the HPVA-based composite with the highest modulus, which was 1CNC/4ChNF/HPVA. It was not clear why different combinations of nanofillers achieved the highest modulus value in different PVA polymers, while the composites containing only one type of nanofiber were more similar. This difference suggested that the molecular weight of polymer chains and entanglement density is a factor in the dispersion and interaction between CNCs and ChNFs.

While modulus was enhanced by the addition of nanofibers, the addition of CNCs, ChNFs, or combinations of these nanofibers did not improve the tensile stress. None of the composites had a statistically greater tensile strength than the neat LPVA. Additionally, the HPVA tensile strength values were higher than their corresponding LPVA values for all five of the nanofiller loadings by an average of approximately 20 MPa, with all but the 2.5CNC/2.5ChNF sample being statistically greater (Figure A.2).

For strain at break, the neat LPVA had the highest value, similar to the HPVA-based materials. The strain at break values for the LPVA nanocomposites appeared to have smaller distributions and standard deviations in comparison to the HPVA nanocomposites, though most were not statistically different from one another. One explanation could be related to how the LPVA samples tended to break at their tensile strength value, while the

HPVA tended to yield and break after the yield point. Therefore, differences in their mechanical properties in this regard could be related to characteristics in the matrix polymer such as the length of the polymer chains, entanglement density, and the ease of generating fracture points in the shorter chains as they are pulled apart. Four of six HPVA-based samples had a statistically greater strain at break value in comparison to their LPVA counterpart: 5CNC, 1CNC/4ChNF, 5ChNF, and neat PVA. Only the 4CNC/1ChNF/HPVA and 2.5CNC/2.5ChNF/HPVA data sets did not provide a statistically greater value than those given in the LPVA samples.

As a comparison to these mechanical property results, a previous study examined cellulose/chitin composite gels and films generated by combining the two biomaterials dissolved in ionic liquids and analyzed various properties of the bicomponent films.[121] Even though these results were for gels and films produced with cellulose and chitin solutions as opposed to the nanoscale fibers discussed here, they provide some context for the types of interactions that could occur. The mechanical properties determined by this previous study showed a progressive increase in relative modulus as the ratio of chitin to cellulose increased, which agreed with the trends observed here for HPVA-based samples. In addition, this trend agreed somewhat with the LPVA data (there was an increase in modulus as ChNF was added with exception to the 1CNC/4ChNF/LPVA sample). Lastly, it is worth noting that the sample with the lowest modulus average for combined nanofillers was the same for each molecular weight at weight loadings of 4% CNC and 1% ChNF (4CNC/1ChNF/HPVA and 4CNC/1ChNF/LPVA). While approximate, the 4CNC/1ChNF ratio is similar to that of the charge neutral ratio presented in the zeta-potential of Figure 3.2. From this correlation, it is possible that charge-driven association of CNCs and ChNFs

leads to less effective mechanical reinforcement through reduced nanofiber-polymer interactions. In contrast, composites containing CNC/ChNF ratios with unbalanced surface charges, specifically those with excess positive charge from excess ChNF content, were shown to have better mechanical properties than singular nanofiller composites containing only CNCs or only ChNFs.

This potential for charge-driven association was also alluded to in the FTIR results. While it was difficult to separate different contributions to the -OH stretching peak, the 1CNC/4ChNF/HPVA and 4CNC/1ChNF/HPVA samples possessed the highest and lowest mechanical properties of the HPVA-based composites, respectively, which correlated roughly to their -OH peak intensities. Similarly, the LPVA-based material with the largest modulus and tensile strength, 2.5CNC/2.5ChNF/LPVA, corresponded to the highest intensity –OH stretching peak, while the nanocomposite material with the lowest mechanical performance, 4CNC/1ChNF/LPVA, corresponded to the lowest intensity peak for a nanocomposite.

Aside from component interactions, the influence of matrix crystallinity on mechanical properties was also examined. Overall, the trends in matrix crystallinity did not correlate to the measured modulus and tensile strength values. For both molecular weights, the CNC/ChNF ratios that possessed the highest moduli and tensile strength did not correlate to the largest crystallinity value, so the crystallinity did not appear to be the most important factor influencing mechanical performance. However, while experimental error in the crystallinity values was larger for HPVA composites containing ChNFs than the 5CNC composite and neat HPVA, the 4CNC/1ChNF/HPVA sample had the lowest reported crystallinity of the HPVA-based composites, which corresponded to its relatively

low mechanical performance, so the matrix crystallinity could not be completely discounted as a contributing factor in this composite's mechanical properties. Considering the mechanical testing, FTIR, and MDSC data together, the results consistently suggested a lower performance for the composites containing the nanofillers at the CNC/ChNF ratio that was closest to a balanced charge ratio as shown by the zeta potential measurements. The improved mechanical performance for composites containing other CNC/ChNF ratios was not as easily deduced from these results and was likely a result of differences in nanofiller distribution and dispersion, which were influenced by the amounts of each nanofiller in the composite as well as the molecular weight of the polymer matrix.

While the amount of research available on tricomponent composites utilizing cellulose- and chitin-based nanomaterials is limited, the enhancement in properties presented in this study compare favorably to results from recent literature utilizing one of the nanomaterials. Roohani et al. (2008) demonstrated that roughly a 25% increase in modulus and a 18% increase in tensile strength can be achieved with 6 wt.% loadings of CNCs in HPVA, which agrees with the 26% and 14% increase in those respective properties found for 5CNC/HPVA in the current study. Additionally, the highest achieved properties from this earlier study from 12 wt.% CNCs experienced roughly a 50% increase in modulus and 23% increase in tensile strength, which is comparable to the 1CNC/4ChNF/HPVA sample set that possessed an average increase of 43% for modulus and 23% for tensile strength while utilizing less than half of the nanofillers.[96] For comparisons to LPVA, a study by Fortunati et al. (2013) found a decrease in modulus for 1, 3, and 5 wt.% CNC loadings, with an increase of 46% for 10 wt.% CNCs. Our study found a 26% increase in modulus for the 5CNC/LVPA samples compared to neat LPVA,

while the 43% increase in modulus measured for 2.5CNC/2.5ChNF/LPVA is comparable to the 10 wt.% loadings of Fortunati's study.[5] For comparing to chitin-based nanofillers, the more common acid hydrolysis of chitin to produce chitin nanowhiskers (ChNWs) has previously shown approximately a 36% and 28% increase in modulus and tensile strength, respectively, compared to neat PVA for 5 wt.% ChNWs.[95] These increases are greater than that achieved by 5ChNF/HPVA (21% and 16% increase in modulus and tensile strength, respectively) and 5ChNF/LPVA (25% and 2% increase in modulus and tensile strength, respectively), though this discrepancy may be the result of the shorter, more crystalline chitin nanomaterials. However, the same study reported a 46% increase in modulus for 10 wt.% ChNWs that is consistent with the modulus increases provided by 1CNC/4ChNF/HPVA and 2.5CNC/2.5ChNF/LPVA, in addition to a tensile strength increase of 22% consistent with the 23% increase provided by 1CNC/4ChNF/HPVA. Overall, composites containing certain CNC/ChNF ratios possessed greater values of modulus and tensile strength than composites containing only one type of nanofiller. Many of these differences were statistically significant, providing evidence of synergistic interactions between CNCs and ChNFs.

3.3 CONCLUSIONS

The ability to modulate properties of water-soluble polymers like PVA by creating nanocomposites with mixtures of cellulosic and chitinous nanomaterials is relatively underexplored. Traditionally nanocomposites are constructed utilizing one nanomaterial as a filler. However, this study draws attention to the possibility of allowing for further tuning

of the mechanical properties through the introduction of a second nanofiller. Materials generated in this study showed an overall increase in stiffness, tensile strength, and thermal degradation in both HPVA and LPVA systems. Furthermore, CNC/ChNF mixtures at certain ratios were able to more effectively reinforce PVA than CNCs or ChNFs alone. Films containing nanofillers also experienced a small shift in delay of polymer degradation. Properties appeared to be somewhat correlated to the PVA crystallinity, but with different trends observed in the different molecular weight samples containing ChNFs. While previous studies have shown that lower nanofiller loadings within polymers tended to correlate with higher strain at break values compared to high nanofiller loadings,[54, 142] the reduction in strain at break for 5 wt.% nanofiller samples compared to the neat PVA samples in this study provides a point to be improved in future work. Zeta-potential and titration testing suggested that this behavior could be linked to charge-driven association of ChNFs and CNCs near ratios of ChNF and CNC that achieve neutrality. This study provides evidence that there are some physical and/or chemical interactions the nanofillers and polymer matrix that are generating properties that extend beyond that of what can be achieved with a single nanofiller when nanofiller ratios are chosen to avoid complex formation. The combination of stiff, renewable biomaterials with the barrier properties of PVA could potentially be applied to industries looking to utilize a biodegradable packaging material that provides resistance to tear and air permeation.

This study opens questions about how polymer nanocomposites might be further altered to allow for additional customizability through the addition of a second nanofiller. How these materials behave when utilizing higher weight percent additions of CNCs, ChNFs, or any other nanocomposite are additional avenues for study. Furthermore, the

effects these fillers may have on other polymers and in other composite forms, such as hydrogels and aerogels, may provide additional information on their interactions with one another and surrounding polymer matrix. The materials generated in this study demonstrated that three-component polymer nanocomposites utilizing renewable nanofillers at relatively low loadings showed enhanced capabilities in modulus, tensile strength, and thermal degradation, and this general methodology has the potential to be used in applications necessitating a level of customizability.

CHAPTER 4. CELLULOSE- AND CHITIN-BASED NANOMATERIALS INCORPORATED INTO POLYMER HYDROGELS

The interactions between CNCs and ChNFs have been studied previously in a polymer film[73] and in the absence of a polymer matrix,[121] but the use of cellulose and chitin together in a tricomponent composite hydrogel has not yet been studied. Previous work on this topic has shown that certain ratios of cellulose to chitin result in higher performance compared to single nanofillers in mechanical and barrier properties,[2, 73, 82] which provides evidence of synergistic interactions that may be replicated in a polymer hydrogel. The aim of this study was to incorporate CNCs and ChNFs into a PVA tricomponent composite hydrogel and compare its properties to that of neat PVA and composite hydrogels containing only one type of nanofiller. The surface-charge differences between these two nanofillers lends itself to the development of polymer composites that may be able to optimize the interactions between CNCs, ChNFs, and the PVA matrix for high-performance materials. Provided that PVA hydrogel formation is the result of phase separation between the individual materials, the freeze-thaw process could result in greater interactions between these components as they are pushed into contact.

4.1 EXPERIMENTAL SECTION

4.1.1 Materials

Nanocomposite hydrogels containing PVA with CNCs and/or ChNFs were prepared and characterized to assess the impact of nanofillers on the polymer hydrogel. The average molecular weight (MW) of the PVA was 146,000-186,000 g/mol and it was 99+% hydrolyzed. Freeze-dried CNCs were provided by the USDA Forest Service Forest Product Laboratory (Madison, Wisconsin) and were produced via sulfuric acid digestion as previously described.[143] CNCs had a sulfur content of around 1 wt.% and were redispersed in water using a Talboys model 134-1 overhead mixer set at 2000 RPM for at least 90 minutes. Suspension were produced at solids loading of 5.5 wt.% for hydrogel production or 0.5 wt.% for characterization experiments. The chitin precursor material was Crabshell Fertilizer from Neptune's Harvest (Gloucester, Massachusetts), and ChNFs were produced by the authors using high-pressure homogenization as previously described[81] to produce an aqueous suspension with a solids loading of 0.5 wt. %. The length of CNCs and ChNFs used in this study were previously measured with atomic force microscopy (AFM): CNC length is 154 ± 59 nm and width is 6 ± 3 nm, while ChNF length is 675 ± 384 nm and width is 5 ± 3 nm. Densities of these materials were 1.600 g/cm^3 for CNCs[30] and 1.425 g/cm^3 for ChNFs.[144] Glacial acetic acid was purchased from Sigma-Aldrich and used as received.

4.1.2 Nanocomposite Hydrogel Processing Procedure

The nanocomposite hydrogel samples were produced through a series of steps. Firstly, PVA was dissolved in deionized water in a water bath at 100 °C while stirring at 300 RPM with a stir bar until no visible PVA particles were present, typically 6 to 8 hours. The PVA solution was covered with aluminum foil during the duration of the mixing process to minimize evaporation and contamination. The initial content of water that the PVA was dissolved into varied depending on the weight loadings of CNCs and/or ChNFs to be added. The PVA solution was then cooled to below 50 °C, and 1 mL glacial acetic acid for every 99 mL of polymer solution was added to encourage dispersion of the ChNFs.[82] Then, the desired amount of ChNF suspension was added to the PVA solution, and the components were mixed at 300 RPM with a stir bar for at least 30 minutes. Finally, the desired amount of CNC suspension was added, and the nanocomposite suspension was mixed at 300 RPM with a stir bar for at least 30 additional minutes. Suspension volume was approximately 120 mL in all cases. After suspensions were prepared, they were sonicated in a Misonix Sonicator 3000 for five minutes at 80W in order to improve dispersion of the nanofiller particles. For neat PVA solutions prepared for comparison, only the first mixing step was used.

Sample names in this document follow the following structure: [wt.%]CNC/[wt.%]ChNF. The weight percentages correspond to the loading in the solid phase of the suspension. This naming convention was also used previously for nanocomposite film samples produced by the authors. To demonstrate this naming convention, a sample containing 1 wt.% CNC and 4 wt.% ChNF is denoted as 1CNC/4ChNF, while a sample containing only 1 wt.% CNC is denoted as 1CNC.

Nanofiller loadings of 1 wt.% and 5 wt.% were prepared to test differences between loadings of CNCs (i.e. 1CNC and 5CNC) and ChNFs (i.e. 1ChNF and 5ChNF) in addition to two tricomponent samples of 1CNC/4ChNF and 4CNC/1ChNF chosen based on their performance from a previous study.[2] Additionally, using the sizes and densities of the nanomaterials, it was approximated that a 1:1 number ratio between CNCs and ChNFs would require 27% more ChNFs than CNCs. For a composite containing 5% total nanofillers, a 1.4CNC/3.6ChNF/PVA composite would have approximately one CNC for every ChNF. Therefore, the 1CNC/4ChNF sample would containing more ChNFs than CNCs, and vice versa for the 4CNC/1ChNF sample.

The resulting polymer solution or nanocomposite suspension was poured into an aluminum mold containing 20 cylindrical wells with a height of 12 mm and a diameter of 24 mm. The aqueous solution/suspension in the aluminum mold was then placed in a freezer at -10 °C to freeze the samples and allow for the formation of physical crosslinks. Throughout this document, any mention of crosslinks are physical in nature. Samples remained in the freezer for approximately 16 hours before being removed and allowed to thaw for approximately eight hours at ambient laboratory conditions. This 24-hour process constitutes one complete FT cycle and was repeated up to seven times.

4.1.3 Water Absorption Analysis

Cylindrical hydrogel samples were divided into four parts and submerged in 50 mL deionized water and weighed over the course of a six-hour period with timepoints at 0, 10, 20, 30, 45, 60, 75, 90, 105, 120, 180, 240, 300, and 360 minutes. At the specified time

points, the samples were vigorously shaken for three seconds when removed from the water bath to remove surface water then weighed. After each measurement, samples were placed back into the water for subsequent measurements. These experiments aimed to develop understanding of how these materials behave in specific environments and elucidate the water retention properties of the hydrogels after various FT cycles. Statistical analysis of comparisons between sets for this and all other analyses in this study were performed with two-tailed Student's T-Tests assuming unequal variances and an alpha value of 0.05. Complete statistical maps comparing all data sets are displayed in Figure A.12 in the Supporting Information.

4.1.4 Mechanical Testing

Mechanical properties were assessed through compression testing of the samples at a constant displacement rate. These results were used to understand the effects of the nanofillers, their mixtures, and the number of FT cycles on the hydrogels' properties. While not specific for hydrogel samples, ASTM D1621-16: Standard Test Method for Compressive Properties of Rigid Cellular Plastics was used to specify a sample geometry. The standard recommends a maximum height to diameter ratio of 1:1, so a height of 10 mm and diameter of 24 mm were chosen for these tests.[145] Freezing would cause greater expansion in some samples compared to others, so sample heights were slightly varied (i.e. ± 1 mm). Additionally, the cross sections of the 7FT samples were distorted to an irregular oval shape, so diameters were reported as an average of four measurements around the sample. Prior to testing, a preload of 0.01 N was applied to the 1FT sample, and a preload

of 0.1 N was applied for the remaining samples. The testing speed used was 1.2 millimeters per minute. Compression tests were run with n = 4 or 5 to 50% compression, and the average stress achieved at 50% strain was reported with standard deviations. Average modulus was calculated as the slope of the stress-strain curve over a strain range of 0 to 3% and reported with standard deviation. Complete statistical maps for modulus and compression stress values can be found in the Supporting Information as Figures A.13 and A.14, respectively.

4.1.5 Rheological Analysis

Rheology tests were performed on two types of samples. To probe nanofiber interactions, three aqueous suspensions of the nanofibers without polymer were tested. The first contained 0.125 wt.% CNC. The second contained 0.25 wt.% ChNF, and the third contained a nanofiber mixture with 0.125 wt.% CNCs and 0.25 wt.% ChNFs for an overall solids loading of 0.375 wt.%. These three samples are named CNC, ChNF, and CNC/ChNF, respectively, within the text. In addition, to composite suspensions of 5CNC/PVA, 5ChNF/PVA, and neat PVA were tested. The neat polymer suspension had a solids loading of 4.75 wt.%, while the composite suspensions had a total solids loading of 5 wt.%. For the composite suspensions, this solids loading was the same as that used to produce the 5CNC and 5ChNF hydrogels. These tests were performed with an Anton Paar MCR302 rheometer with a cone and plate geometry, both of which had smooth surfaces. The cone was 50 mm in diameter with a 1.01° cone angle and a 0.053 mm truncation, while the plate had a diameter of 60 mm. For all measurements, the set temperature was 25 °C

and an evaporation blocker was applied to reduce water evaporation during testing. Steady shear experiments were performed over a shear rate range of 0.1 to 100 s^{-1}. Frequency sweep measurements were performed from 0.1 to 100 rad/s, and the strains used were as follows: 20% for 0.25% ChNF, 100% for 0.125% CNC, 20% for 0.125CNC/0.25ChNF, 10% for neat PVA, 10% for 5CNC/PVA, and 3% for 5ChNF/PVA. All strains used were within the linear viscoelastic region based on the results of amplitude sweeps that were performed over a range of 1 to 1000% Figure A.15). Jianshan Liao of Dr. Victor Breedveld's group tested the prepared samples.

4.1.6 Light Scattering Analysis

Multi Angle Dynamic Light Scattering (MADLS) experiments were performed in order to analyze the sizes and aggregation behavior of the CNCs and ChNFs both individually and when mixed together at different ratios. The instrument used in these experiments was a Wyatt DAWN DSP equipped with a 685 nm gallium arsenide laser. The device was modified so that the signal from certain angles was carried by single-mode fiber optics to an ALV-7000 series multichannel autocorrelator. Correlation functions were measured simultaneously at 8 angles (50°, 57°, 64°, 81°, 99°, 117°, 134°, and 147°). A polarized optic was applied to the sample vial as a beamstop to eliminate back-reflected light from the exit window of the standard 20-mL scintillation vials used to hold the samples. Sample preparation for these experiments involved preparing 0.5 wt.% suspensions of the CNCs and ChNFs and transferring approximately 20 mL of each into a centrifuge tube. The two tubes were then placed into a centrifuge and spun at 5000 RPM (5250 g) for 24 hours at 25

°C to remove larger particles such as dust. Sample tubes were then removed without disturbing the contents, and approximately 10 mL of the suspension was extracted from the center of the centrifuge tube with a syringe in order to avoid use of the larger particles at the bottom of the tube or the smaller particles at the top. Then, using a 0.45 μm filter, the CNC or ChNF suspension was filtered into a scintillation vial and stored in ambient laboratory conditions for at least 30 minutes. Thermogravimetric analysis was performed on the CNC and ChNF suspensions in order to evaluate the concentrations before mixing. In these concentration measurements, the suspensions were held isothermally at 110 °C for one hour, and the final mass value was used as the concentration of the suspensions for mixing. Based on four replicate experiments, the final concentration value of the CNC suspension was approximately 0.16 ± 0.02 wt.%, while the ChNF suspension was approximately 0.10 ± 0.3 wt.%.

Collection of the MADLS data included taking initial measurements on the CNC-only and ChNF-only suspensions to establish the size of the individual nanofillers. Then the suspensions were mixed at various ratios including: 1CNC:9CHNF, 1CNC:3ChNF, 1CNC:1ChNF, and 3CNC:1ChNF. The 3CNC:1ChNF mixture correlated closely to a charge-matched ratio between the CNCs and ChNFs previously measured through titration of these materials.[2] In this previous study, the charge per mass of the CNCs was determined to be 0.49 ± 0.09 meq/g, while the ChNFs were 1.40 ± 0.10 meq/g. These ratios indicated that a CNC:ChNF weight ratio of 3:1 would approximately correspond to a 0 meq charge, which was supported by additional zeta-potential measurements. The mixed ratios were tested with MADLS for an experiment time of 30 minutes. The scattering vector amplitude

q was calculated with the following equation where n is the refractive index (1.33), θ is the measured angle, and λ_o is the wavelength of the laser (685 nm):

$$q = \frac{4\pi n}{\lambda_0} sin\left(\frac{\theta}{2}\right)$$

Diffusion coefficients were calculated as Γ/q^2 where Γ is the average decay rate from third-order cumulants analysis. Hydrodynamic radius (R_h) values were then obtained from the Stokes-Einstein equation,

$$R_h = \frac{kT}{6\pi\eta D}$$

where k is Boltzmann's constant (1.38×10^{-16} erg/Kelvin), T is the Kelvin temperature (298.15 K), and η is the viscosity of the solvent (0.008904 centipoise). Graphs of q^2 vs. Γ and q^2 vs. R_h for CNCs and ChNFs are shown in the Supporting Information in Figure A.16. Due to signs of polydispersity in the mixed CNC/ChNF suspensions, the cumulant method could not be utilized, so R_h values were obtained with an intensity weighted average methodology. Specifically, for each sample angle, the average of the products of the y-axis intensity values and x-axis radius values were obtained, then averaged across all eight angles.

The Kirkwood-Riseman equation was used to calculate the length of the CNCs from the resulting R_h values. A simplified form of this equation is shown below, where L is the length and d is the diameter of the particles.

$$L = 2R_h \ln\left(\frac{L}{d}\right)$$

4.2 RESULTS AND DISCUSSION

Neat and composite hydrogels were prepared and characterized to observe the visual appearance, measure the swelling behavior, and measure the mechanical properties. The appearance of the hydrogels was altered by repeated FT cycling, but remained similar for neat and composite samples. After 1FT cycle, the hydrogels were gelatinous and somewhat translucent. After 3FT cycles, the hydrogel samples became more opaque and whiter in color and were observed to be more rigid during handling. The appearance after 5FT cycles was similar to that observed after 3FT cycles. After 7FT cycles, the hydrogel samples began to shrink slightly in the aluminum mold, likely due to increased and/or more robust network junctions. To represent this change in appearance, Figure 4.1 shows the 1CNC/4ChNF hydrogels after 1FT, 3FT, 5FT, and 7FT cycles.

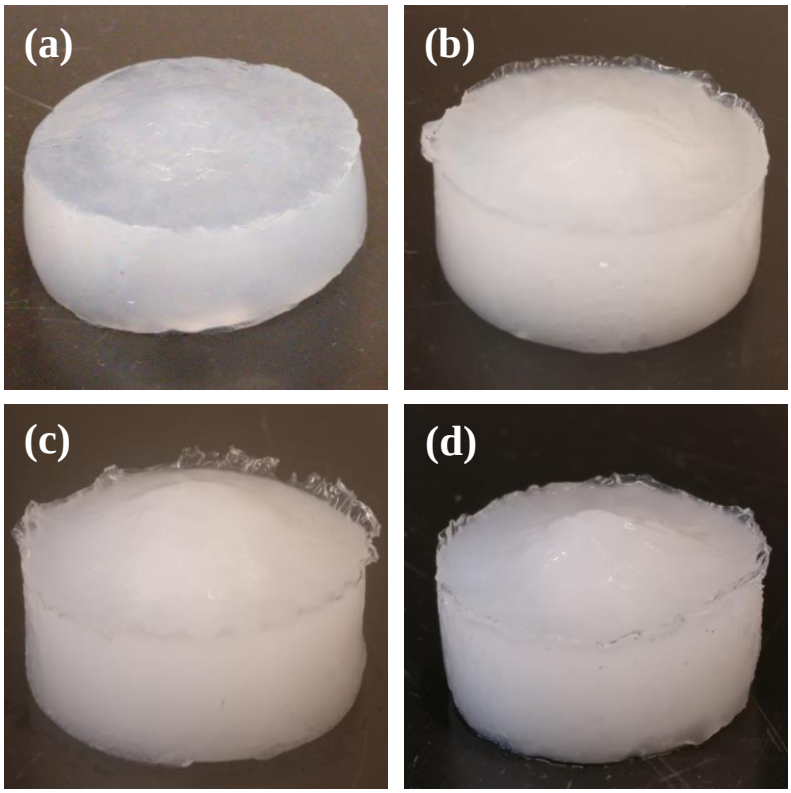

Figure 4.1 1CNC/4ChNF hydrogels after (a) 1FT, (b) 3FT, (c) 5FT, and (d) 7FT cycles. Each hydrogel sample had a nominal diameter of 24 mm.

Water absorption studies were performed to qualitatively assess the level of crosslinking within the polymer matrix and the potential influence of CNCs and/or ChNFs on the pore structure and swelling behavior. Figure 4.2 shows the water absorption curves for the neat PVA and 5ChNF hydrogels over the six-hour measurement as well as the final mass change values for the hydrogels as a function of FT cycles.

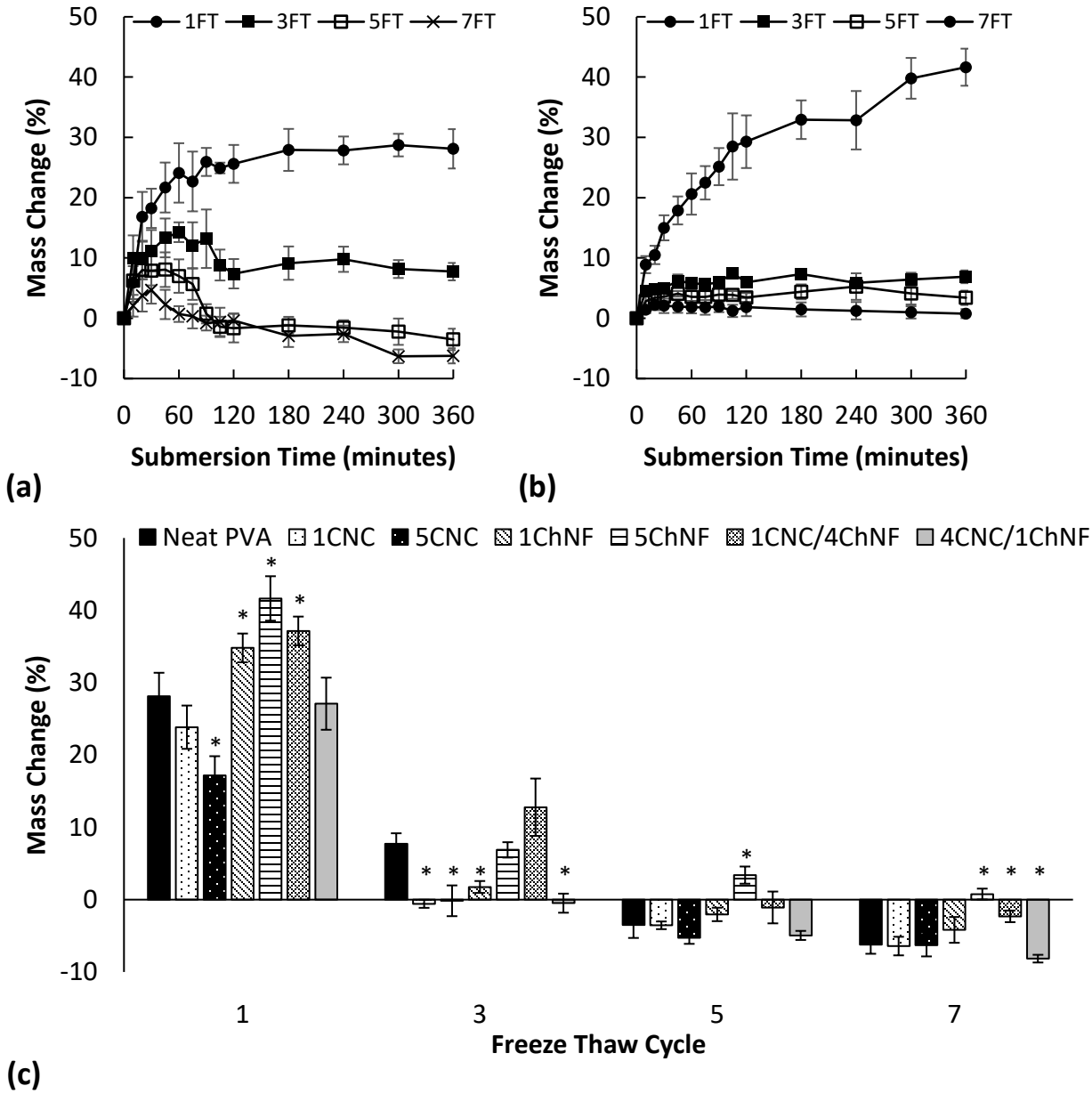

Figure 4.2 Water absorption change for (a) neat PVA and (b) 5ChNF over 360 minutes for 1, 3, 5, and 7FT cycles; (c) water absorption in neat PVA and nanocomposite hydrogels over 1, 3, 5, and 7 freeze-thaw cycles after six hours. * indicates statistical difference from the neat PVA hydrogel sample set.

The water absorption values were affected by hydrogel composition and number of FT cycles. Overall, the amount of mass change decreased or became negative as the number

of FT cycles increased, consistent with a more rigid structure. Many of the hydrogels exposed to higher numbers of FT cycles experienced some increase in mass at short submersion times, even if the mass change value recorded after six hours was negative. The hydrogels shown in Figure 4.2a and 4.2b show the range of behaviors observed. Comparatively, the 5ChNF hydrogel (Figure 4.2b) absorbed more water after 1FT and retained more water after 5FT and 7FT compared to the neat PVA hydrogel (Figure 4.2a). However, the 5ChNF hydrogel did not experience as large of an initial mass change as the neat PVA.

Figure 4.2c shows the final mass change values for the hydrogels as a function of number of FT cycles. After 1FT cycle, all hydrogels increased in mass. It was considered likely that the level of crosslinking would be relatively low; therefore, expansion of the molecular network upon exposure to water was expected. The sample composition for the 1FT hydrogels affected the magnitude of water absorption, with the 5CNC hydrogel having the smallest increase in mass and the 5ChNF hydrogel having the largest increase in mass. The neat PVA had a mass increase value between these two extremes. The increased level of crosslinking in the 3FT hydrogels was expected to generate a more rigid structure, impeding their ability to absorb water and resulting in a lower maximum water absorption compared to 1FT hydrogels. Four 3FT hydrogels had minimal or slightly negative mass changes: 1CNC, 5CNC, 1ChNF, and 4CNC/1ChNF. For 5FT and 7FT hydrogels, mass changes after six hours for all hydrogels except 5ChNF were negative.

The FT process for producing PVA hydrogels generated a network structure made up of polymer chains interconnected through hydrogen bonding and polymer crystallites along the perimeter of pores. The distance between network junction points, or mesh size,

can be influenced by adjusting the processing parameters or adding fillers to the PVA matrix. While it can be challenging to confirm the pore size/structure of a hydrogel, particularly when fillers are introduced, aerogels produced through freeze-drying of PVA hydrogels have previously demonstrated that nanofillers can lead to the pore shrinkage.[112, 117, 146] Due to this, it is possible that within the hydrogel structure there is a similar shrinkage of pores with varied levels of junction reinforcement as a result of the interactions between nanofillers and the matrix.

The different response of the 5ChNF hydrogel in comparison to the other samples suggested that the component interactions were different in this hydrogel. Additionally, the similarity in behavior between neat PVA hydrogels and hydrogels containing CNCs could indicate that intermolecular interactions were similar and stronger than those seen between ChNFs and PVA. The expected hydrogen bonding interactions between CNCs and the PVA molecules could result in a more rigid pore structure that would constrict and expel water in response to changes in external pressure experience when submersed. Conversely, the increased absorption/retention of water in ChNF-loaded hydrogels suggested that the degree of hydrogen bonding could be less in comparison to CNC-loaded hydrogels, which would likely result in a less rigid structure.

Regarding the cause of the mass loss over time observed for some hydrogel samples, various studies have assessed the behavior of hydrogels produced from PVA polymer with different molecular weights. Specifically, studies of FT hydrogels produced with 25 kg/mol,[91] 35 kg/mol,[90, 92] 75 kg/mol,[12, 92] and 92 kg/mol PVA[8] have observed that an increase in molecular weight generally results in a decrease in the water absorption capability of PVA hydrogels. Additionally, hydrogels prepared through a FT method have

previously been found to be relatively insoluble in water at lab conditions,[12] suggesting that polymer dissolution during submersion was not a significant factor in the mass change values obtained. While it is possible that weaker sections of the hydrogels could be dissolved in water, an increase in the number of FT cycles has been shown to reinforce PVA crystalline regions, not weaken them.[90] Therefore, it was likely that the loss in mass at higher FT cycles resulted from an expulsion of water from the hydrogel caused by changes to the pore structure in these samples. To test this assumption, the 7FT 4CNC/1ChNF hydrogel was dried and weighed, and the dry mass was not significantly different (216 mg) than the expected solids mass from calculation (213 mg); therefore, dissolution was not expected to play a significant role in mass loss during the swelling studies.

In comparison to other studies, differences in PVA molecular weight, PVA hydrolysis level, hydrogel water content, temperature, number of FT cycles, and FT parameters can influence the overall density and crosslinking of the polymer structure.[91-92, 103] Other studies have shown that CNC/PVA hydrogels absorb water when exposed to a similar number of FT cycles; however, the number of material and processing variables is large, as indicated above. Results for composite hydrogels produced under the same conditions were not available to assess if the results seen here would be expected.

In order to assess the influence of the nanofillers on the reinforcement of the pore structure both individually and in tricomponent composites, compression tests were performed up to a maximum strain of 50%. Figure 4.3 displays representative stress-strain curves for each of the seven sample sets, while Table 4.1 displays the modulus and maximum stress values obtained. The representative curves shown had the median

maximum compressive stress value of the five samples tested for a given sample set or for the case of a sample set with four samples, the representative curve was one of the two samples with an intermediate value for the maximum compressive stress. Data are shown for 1FT, 3FT, and 7FT hydrogels at each material composition. An incomplete data set was obtained for the 5FT hydrogels, so those data are not shown here.

Elastic modulus was found to vary with the number of FT cycles and with hydrogel composition. For each hydrogel composition, the modulus increased as the number of FT cycles increased from 1FT to 3FT. Going from 3FT to 7FT, the modulus of 5ChNF, 1CNC/4ChNF, and 4CNC/1ChNF increased. Other compositions did not display statistically significant increases when comparing 7FT samples to 3FT samples (Table A.1). Comparing the modulus values of different compositions for a given number of FT cycles, only the 1CNC/4ChNF was found to have a statistically larger modulus than the neat PVA after 1 FT cycle. Additionally, the modulus of this hydrogel was larger than all of the other hydrogels tested, demonstrating that tricomponent composite hydrogel can have higher stiffness than composite hydrogels containing only one of the filler types at the same overall filler loading. This result for 1CNC/4ChNF was qualitatively consistent with the reinforcement observed for tricomponent film samples.[2] However for the films, other composites also had higher moduli than the neat PVA films, suggesting some differences in the mechanical reinforcement between the film construct and hydrogel construct. For 3FT cycles, all of the hydrogels had statistically similar modulus values in comparison to the neat PVA hydrogel. This result showed that the increased phase separation and network development had a larger impact than composition at 3FT cycles. Considering the modulus values obtained for 7FT hydrogels, the 3FT hydrogels

represented a transitional state in the structure development because some composite hydrogels prepared with 7FT cycles did have higher moduli values than the neat PVA. Specifically, 4CNC/1ChNF, 1CNC/4ChNF, and 5ChNF hydrogels had higher moduli than the neat PVA hydrogel. This result differed from the elastic modulus results obtained for films. In that work, all of the composites at a 5 wt.% filler loading had a higher modulus than the neat PVA.

Like elastic modulus, maximum compressive stress was found to vary with number of FT cycles and hydrogel composition. For a given hydrogel composition, the maximum compressive stress increased as the number of FT cycles increased. This trend was consistent with an increase in crosslinking within the samples, as shown previously in the swelling studies. The hydrogels experienced larger percentage increases between 1FT and 3FT, and smaller percentage increases between 3FT and 7FT. With regard to hydrogel composition, all hydrogels except 1CNC had a statistically different value of the maximum compressive stress as compared to the neat PVA at 1FT, though only 1CNC/4ChNF and 5ChNF had larger values than neat PVA. At 3FT, three samples had larger values of maximum compressive stress than the neat PVA. These samples were 1CNC, 1CNC/4ChNF, and 5ChNF. This result was different than that seen for elastic modulus at 3FT. At 3FT, the composite hydrogels had similar modulus values to neat PVA. This effect was not seen as widely at 7FT, where only the 1CNC/4ChNF hydrogel had a larger maximum compressive stress than the neat PVA.

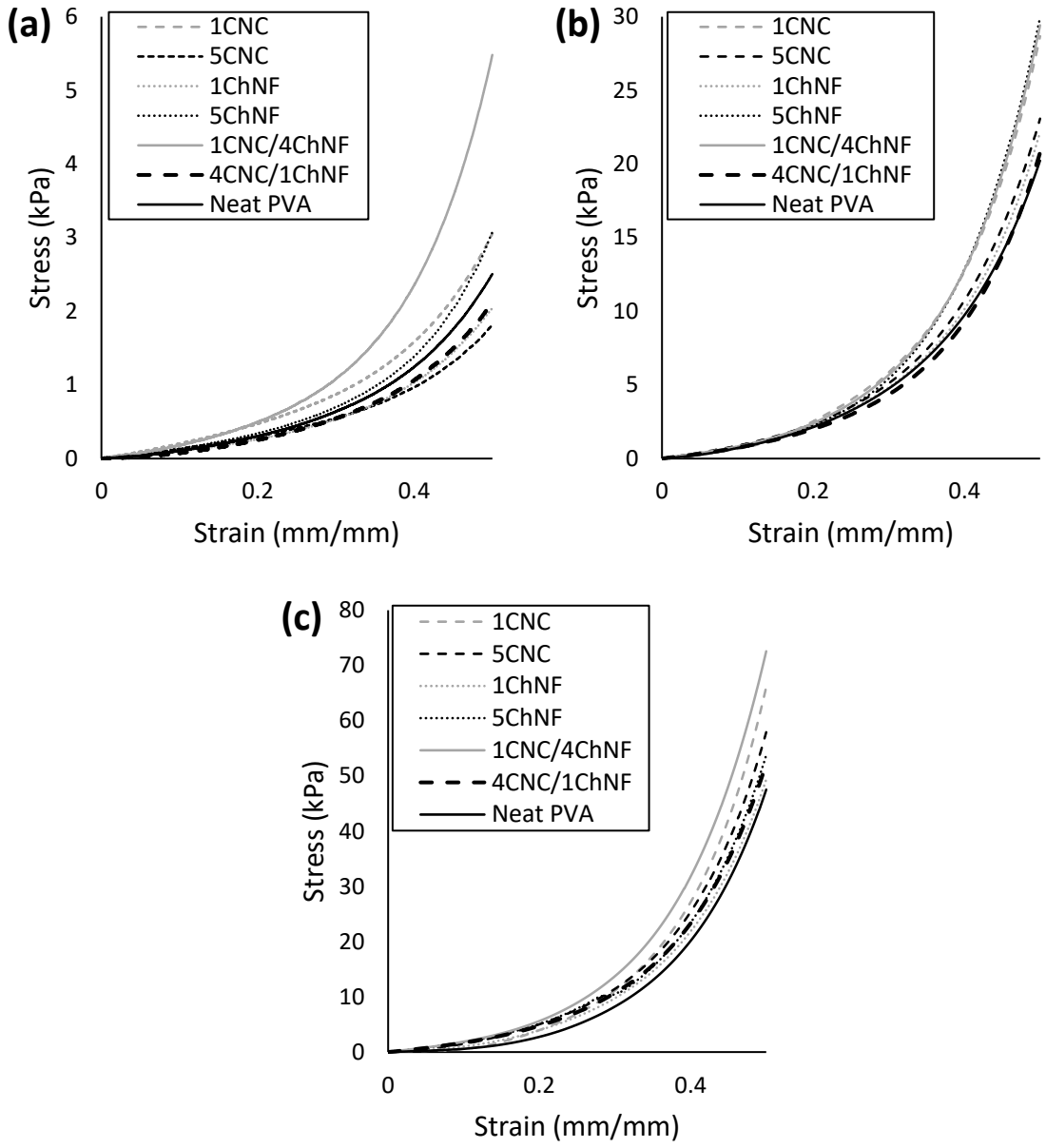

Figure 4.3 Representative curves for stress at 50% compressive strain for CNC- and ChNF-reinforced PVA hydrogel composites for (a) one, (b) three, and (c) seven FT cycle(s). Curves were chosen based on the median compressive stress value at 50% strain.

Table 4.1 Modulus and maximum compressive stress values for composite and neat PVA hydrogels at one, three, and seven freeze-thaw cycles. Statistically greater values than the neat PVA hydrogel are indicated with *.

	1FT		3FT		7FT	
	Modulus (kPa)	**Stress (kPa)**	**Modulus (kPa)**	**Stress (kPa)**	**Modulus (kPa)**	**Stress (kPa)**
Neat PVA	0.78 (± 0.12)	2.49 (± 0.13)	6.15 (± 1.8)	23.2 (± 3.7)	5.90 (± 5.0)	53.0 (± 10.9)
1CNC	0.95 (± 0.52)	2.79 (± 0.44)	5.36 (± 0.77)	28.3 (± 1.1)*	9.37 (± 6.9)	69.5 (± 13.8)
5CNC	0.89 (± 0.48)	1.69 (± 0.43)*	8.55 (± 2.0)	21.3 (± 8.3)	10.61 (± 4.0)	60.1 (± 11.2)
1ChNF	0.91 (± 0.28)	2.01 (± 0.30)*	6.57 (± 0.69)	22.7 (± 1.1)	9.91 (± 4.4)	53.6 (± 7.0)
5ChNF	0.84 (± 0.25)	3.31 (± 0.57)*	7.11 (± 1.5)	30.0 (± 1.0)*	14.54 (± 5.2)*	58.3 (± 6.6)
1CNC/4ChNF	1.81 (± 0.15)*	5.68 (± 0.54)*	6.92 (± 1.7)	29.6 (± 1.7)*	15.38 (± 2.1)*	71.5 (± 2.2)*
4CNC/1ChNF	0.82 (± 0.39)	2.07 (± 0.17)*	6.30 (± 0.78)	20.5 (± 1.0)	12.46 (± 1.2)*	52.1 (± 1.0)

Overall, the compression testing results showed that the 1CNC/4ChNF hydrogel was the highest performing of the composite hydrogels across the processing space investigated. As mentioned previously, this general result is consistent with results obtained for composite films samples with the same components.[2] As seen with the swelling test results, the mechanism for property enhancement was likely different for the different composites. The ChNFs likely had a greater ability to reinforce PVA than CNCs due to their longer length, even though there were stronger component interactions between CNCs and PVA. The mechanical testing results suggested that these factors could be working together in the 1CNC/4ChNF composite hydrogels but not as effectively in the 4CNC/1ChNF composite hydrogels.

For comparison, a study assessing 1, 2, and 3 wt.% loadings of CNCs in 85k-125k g/mol PVA hydrogels found that there was a significant decrease in mechanical properties as the weight loading was increased, which the authors attributed to poor dispersion of the

nanofillers above a critical value.[147] Similarly, in another study, 0.75, 1.5, and 3.0 wt.% CNCs in 25k g/mol pre-soaked PVA hydrogels were measured and the stress achieved at 25% strain and modulus measured were significantly higher for 1.5% compared to 3.0% and 0.75%.[91] This latter study also suggested that above 1.5 wt.% loadings, CNCs may be disturbing rather than reinforcing the hydrogel network, which agrees with the decrease in properties of 5CNC compared to 1CNC samples shown in Figure 4.3 and Table 4.1. Gonzalez et al. (2014) demonstrated a similar critical point in tensile testing of 89k-98k g/mol PVA hydrogels at 3FT cycles, as the tensile strength was highest for 3 wt.% cellulose nanowhiskers (CNWs) relative to 1 wt.% and 5 wt.%.[148] In contrast to CNCs, 5ChNF possessed a statistically significantly greater maximum stress than 1ChNF across all freeze-thaw cycles. The study of chitin nanomaterials in PVA hydrogels is very limited, but the increase in stress seen for the 5ChNF samples compared to 1ChNF seem to indicate 5ChNF did yet not exceed a specific critical point loading that limited the dispersion of the nanofibers.

For tricomponent composite hydrogels, 4CNC/1ChNF and 1CNC/4ChNF possessed among the lowest and highest achieved stresses, respectively, with 1CNC/4ChNF being statistically significantly greater than 4CNC/1ChNF for all three FT cycles. The 1CNC/4ChNF set possessed a greater compressive stress than 1CNC and 5ChNF for 1FT and 7FT, indicating that a specific combination between CNCs and ChNFs in a polymer matrix can achieve greater reinforcement than singular nanofillers at both low and high freeze-thaw cycles. The greater stress values achieved by 1CNC/4ChNF ratio are consistent with the previously mentioned study analyzing the relative modulus in CNC/ChNF/PVA nanocomposite films, with the former study's results being attributed to

a relative charge-matched ratio between CNCs and ChNFs.[2] Overall, the addition of CNCs greater than 1 wt.% resulted in a decline in maximum stress in the 5CNC and 4CNC/1ChNF sets while the addition of ChNFs greater than 1 wt.% resulted in an increase in stress in 5ChNF and 1CNC/4ChNF sets.

While the swelling and compression studies establish the macroscale properties of these polymer nanocomposites, rheological experiments were performed in order to elucidate the nanostructure formation between CNCs, ChNFs, and PVA and to more fully understand the influence of charge-driven complexes on matrix reinforcement. To this aim, CNC-only, ChNF-only and CNC/ChNF suspensions in both pure water and in PVA solutions were subjected to steady shear viscosity and frequency sweep experiments. Figure 4.4a shows the relative viscosity of the CNC, ChNF and mixed CNC/ChNF suspensions (viscosity of suspensions normalized by the viscosity of the suspending fluid, i.e. water) as a function of shear rate. The data clearly showed that the presence of CNC nanoparticles in water barely raised the viscosity and maintains Newtonian behavior, while ChNF fibers had a much greater effect on suspension viscosity and exhibit strong shear thinning; this behavior was indicative of attractive ChNF fiber-fiber interactions, most likely due to a heterogeneous distribution of surface charges with local regions with lower electrostatic repulsion. Furthermore, the data show that CNC nanoparticles interacted strongly with the ChNF nanofibers: while the addition of CNC nanoparticles barely affected the viscosity of pure water, it substantively raised viscosity when added to a ChNF suspension. The corresponding frequency sweeps for the suspensions (Figure 4.4c) supported these observations: the CNC suspension showed pure liquid-like behavior ($G'' \sim \omega$ and G' was too small to be accurately detected), the presence of ChNF fibers at 0.25

wt.% lead to slight viscoelasticity (G' was measurable, but G' < G"), and addition of CNC to the ChNF suspension pushed the mixed suspension across the gelation threshold (G' > G"). Figures 4.4a and 4.4c are indicative of the synergistic effect of these nanomaterials on mechanical properties of polymer-free suspensions. The likely explanation was that the negatively charged CNC particles bridged between the positively charged surfaces of ChNF fibers and thus enhanced network connectivity.

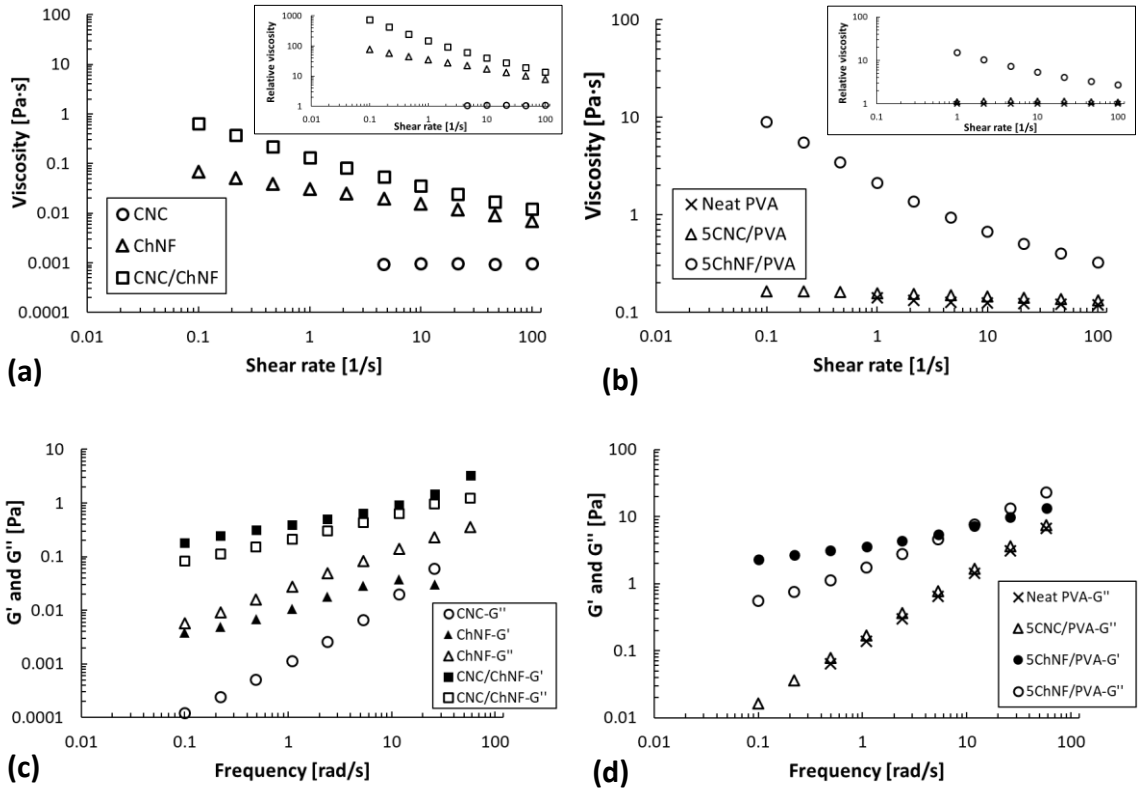

Figure 4.4 Rheological measurements of 0.125CNC, 0.25ChNF, 0.125CNC/0.25ChNF, neat PVA, 5CNC/PVA, and 5ChNF/PVA suspensions. Measurements include (a, b) viscosity with insets of relative viscosity, (c, d) storage and loss modulus.

To investigate the interactions between PVA and the nanomaterials, sample were measured in which the suspending fluid is a PVA solution. Figure 4.4b presents steady shear viscosity experiments of CNC/PVA or ChNF/PVA suspensions as well as the corresponding neat PVA solution. The figure shows that the neat PVA solution was roughly 100 times more viscous than water, and exhibited slight shear thinning; when CNC was added, the viscosity only increased slightly, similar to its effect in water (compare inset of Figure 4.4a with Figure 4.4b). In contrast, the 5ChNF/PVA sample was much more viscous and strongly shear thinning, much like the effect of adding ChNF to water. A careful comparison between the relative viscosities of 0.25 wt.% ChNF in water and PVA solutions showed that the increase of viscosity in PVA is slightly lower, suggesting that the PVA had a minor suppressive effect on attractive ChNF fiber interactions, possibly due to polymer adsorption, but the effect is quite subtle and the behavior of CNC and ChNF in PVA solutions is not very different from water. The corresponding frequency sweeps in Figure 4.4d underline this conclusion: 5CNC/PVA and neat PVA did not exhibit measurable viscoelasticity and behaved like purely viscous liquids, while 5ChNF/PVA was a weak gel (G' > G" values at low frequencies and a crossover occurred near 10 rad/s).

The difference in effect of CNC and ChNF on suspension viscosity (both with water and PVA solution as suspending liquid) can be explained by the longer length of the ChNF fibers and the lower, less homogeneous surface charges. The length led to greater fiber-fiber connectivity in ChNF suspensions, while the surface chemistry allowed for local attractive interactions between fibers, resulting in elasticity at rest and strong shear thinning under flow. As shown in Figures 4.4a and 4.4c, adding negatively charged CNC particles

to a ChNF suspension strengthened the interactions between ChNF fibers, which led to increased viscosity and elasticity.

MADLS was used to further analyse the synergistic effect between CNC and ChNF in swelling and rheology experiments and thus obtain a better understanding of how these nanofillers may be forming structures in an aqueous suspension. Size distributions for each of the angles for the tested samples are shown in Figure 4.5 below.

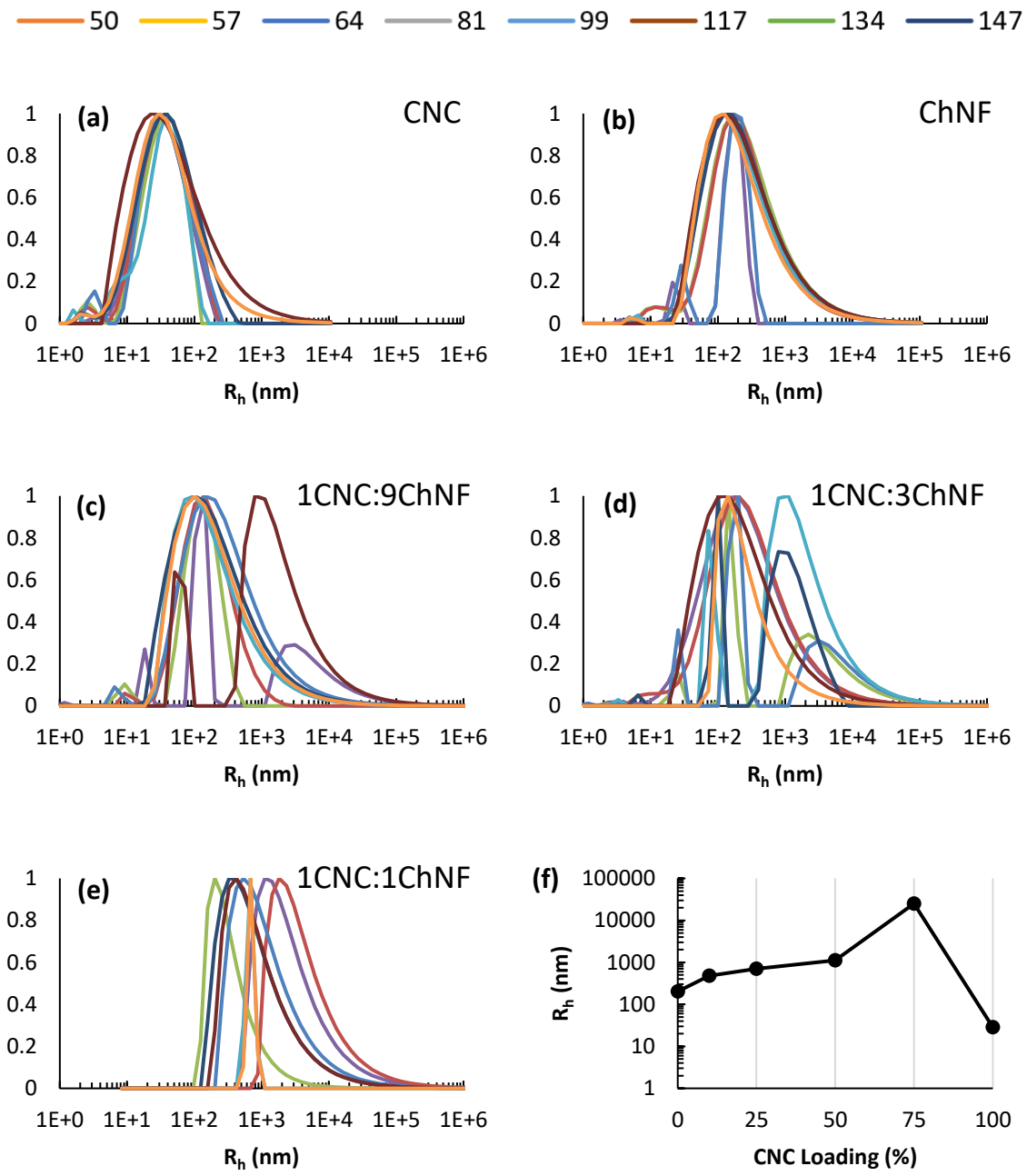

Figure 4.5 Multiangle dynamic light scattering displaying hydrodynamic apparent radius distributions for suspensions of (a) CNCs, (b) ChNFs, (c) 1CNC:9ChNF, (d) 1CNC:3ChNF, (e) 1CNC:1ChNF, and (f) a plot of the average apparent hydrodynamic radius as a function of CNC content with 0% CNCs representing 100% ChNFs. Values in the y-axis for (a) – (e) are normalized intensities. The color legend atop the figure shows the scattering angles.

The R_h values for the CNCs and ChNFs as separate components were first calculated for comparison to the literature. Extrapolations to c = 0 and q = 0 were neglected; for the purposes of this investigation, these are both minor effects for the separate components; nevertheless, these hydrodynamic radii should be considered apparent values. Graphs of q^2 vs. Γ and q^2 vs. R_h for CNCs and ChNFs are shown in the Supporting Information in Figure A.16. For the CNC-only suspension, Figure 4.5a, the estimated size distribution does not depend strongly on scattering angle, with only the two lowest angles displaying significant response at high R_h values. This observation suggests particles of reasonably good size uniformity because in a system of large scatterers with a broad size distribution, DLS under-represents large particles at high angles. Across the measured angles, the intensity-weighted average R_h was 28.5 ± 3.8 nm. A previous study by Mukherjee and Hackley (2018) using asymmetric field flow field fractionation (AF4) measured the light scattering properties of CNCs produced by sulfuric acid hydrolysis and reported a similar average R_h values that varied from 18.3 to 48.8 nm depending on the level of refinement of CNCs.[149] Using Kirkwood-Riseman's equation, the lengths of the CNCs were calculated to be between 188 – 215 nm (depending on width between 5-7 nm), which falls within a similar range as AF4 analysis of CNCs.[149-150] The apparent R_h of the ChNF-only suspension was much larger, 202 ± 30 nm, which is attributed to the larger lengths of the ChNFs. The size distributions now exhibit greater angular dependence; scattering by the larger particles in the distribution is being suppressed at the higher scattering angles. Previously, Mushi et al. (2019) showed the R_h of α-chitin nanofibers produced by high pressure homogenization to be 350-1300 nm with a curve exhibiting a shape similar to that reported by the different angles in Figure 4.5b.[151] Despite their larger size compared to Mushi's samples, the ChNFs

reported here experienced more passes through the homogenizer (30 passes compared to 10 for Mushi). These results obtained in this study for the CNC- and ChNF-only suspensions suggested that most particles were suspended individually and not assembled into large aggregates.

While CNCs and ChNFs exhibited little aggregation on their own, the mixtures between the CNCs and ChNFs showed increased apparent R_h values, suggesting aggregation. The addition of 10% CNCs in the 1CNC:9ChNF ratio showed a similar R_h value to ChNFs with 482 nm, but when the loadings were increased to 25 and 50% CNCs, the 1CNC:3ChNF and 1CNC:1ChNF ratios showed an increase in average R_h value to 708 nm and 1120 nm, respectively. These are very large particles for investigation by DLS; while the accuracy of the Rh values could be questioned, the distinct difference between these mixtures and the CNC and ChNF components taken separately cannot. Additionally, while the 1CNC:3ChNF and 1CNC:1ChNF suspensions were slightly cloudier than the pure CNC or ChNF suspensions upon visual inspection, they were still translucent. At CNC loadings greater than 50%, there was evidence of larger scale aggregation between CNCs and ChNFs. A vial containing a 2CNC:1ChNF ratio exhibited long wisps of white aggregates connected throughout the water in a web-like formation, but the mixture still acted as a fluid and moved freely inside the vial. With an increased addition of CNCs to 75% loading for the 3CNC:1ChNF charge-matched mixture, the suspension quickly began to form large aggregates only minutes after combining the CNCs and ChNFs. After 30 minutes, the mixture generated aggregates of approximately 1 mm in diameter, which appeared as white globules within the suspension. Because these particles were too large to analyze with light scattering methods, additional filtration steps were necessary in order

to analyze some of the unbound mixture at this ratio. Therefore, the visible aggregated components were separated from the suspension and the still-liquid components were placed in a separate vial. Despite separating out the largest solid aggregates that formed in the 3CNC:1ChNF mixture, the experiment resulted in an average apparent R_h value that exceeded 23,000 nm (Figure A.17). While this large R_h value for the charge-matched mixture was unreliable as a definitive measurement of particle size due to the limitations of the light scattering method, the visual observations of gel-like formation and the large shift to higher R_h measured by MADLS in Figure 4.5 indicate a type of "critical point" at which the smaller collections of CNC/ChNF particles destabilized. Additional analysis of these large particles may require ultralow angle light scattering methods to accurately capture size values for comparison to other mixtures. It can be concluded that electrostatic bonding drives the interactions between these two particles and that network formation can be controlled by using different ratios between the relative charges on the surface of two oppositely-charged nanofillers. These results suggest that aggregate formation could also be occurring in tricomponent composite hydrogels and that aggregate structures formed in composites hydrogels containing CNC/ChNF mixtures containing CNCs at loadings where the CNC loadings were less than the ChNF loading could have aggregate sizes that were disproportionately larger, consistent with observations by the authors in a previous study with tricomponent composite films. Additionally, using particle number measurements, the 1CNC/4ChNF ratio was calculated to have approximately 0.7 CNCs for every ChNF, while the 4CNC/1ChNF sample contained 10.8 CNCs for every ChNF. It is possible that the reinforcement mechanisms proposed are achieved only when there are more ChNFs in the composite than CNCs, which could influence the aggregation and structure formation

behavior of the nanomaterials. When considering the MADLS results together with the other results presented here, it may be possible for CNCs adhered to ChNFs to serve as a compatibilizing agent between the nanofiber assembly and the polymer, allowing for more efficient stress transfer.

4.3 CONCLUSIONS

This work explored the use of bio-based nanofiber mixtures as the reinforcing phase in PVA hydrogels. The two nanofiber types, CNCs and ChNFs, behaved differently in the PVA-based hydrogel, so the use of nanofiber mixtures provided an additional pathway to tune properties and, in some cases, improve properties beyond what was achievable with a single type of nanofiber. The results of the swelling studies suggested that the interface between the CNCs and the PVA was stronger than the interface between the ChNFs and the PVA. However, compression testing results suggested that in general the 5ChNF/PVA hydrogels had better mechanical performance than neat PVA and 5CNC/PVA, presumably due to the longer length of the ChNFs. Additionally, the compression testing results indicated that the composite hydrogel containing a nanofiber mixture with more ChNFs than CNCs (1CNC/4ChNF) showed mechanical property improvement more consistently across the FT conditions studied here than the other hydrogel compositions, including those hydrogels containing only one type of nanofiber. These results were somewhat contradictory, but the trends could be explained through a synergistic interaction between the CNCs and ChNFs. Since these nanofibers possessed opposite surface charges, it was possible for them to form assemblies when mixed.

The rheological and light scattering studies provided some information about the possible nanofiber structures that were present in the hydrogels. These results showed that while nanofiber aggregation was occurring when the CNCs and ChNFs were mixed, the size scale of the aggregates was the same order of magnitude as than the particle size scale observed in the ChNF suspensions. As the CNC/ChNF ratio approached the charge-matched ratio, the aggregate size became much larger, which would not likely be effective as a reinforcing phase in composites. These trends were also observed in tricomponent composite films in a separate study,[2] suggesting that the phenomena was not unique to hydrogel structures. Together the characterization results from swelling studies, mechanical testing, rheological testing and light scattering studies provided insight into the structure of the hydrogels and how mixtures of nanofibers may be useful in composite constructs. If the aggregates contained a relatively small number of nanofibers where CNCs were adhered to ChNFs, the CNCs could serve as a compatibilizer between the ChNFs and the PVA, allowing for a stronger component interface that allows for more effective stress transfer to the longer ChNFs. Overall, these results provide insight into how nanofiber mixtures and their interactions may be used in composite constructs to produce better properties than can be achieved with a single nanofiber type.

CHAPTER 5. CELLULOSE AND CHITIN-BASED NANOMATERIALS INCORPORATED INTO POLYMER AEROGELS

The combination of CNCs and ChNFs together in tricomponent polymer composites in the aerogel or foam construct has not previously been studied. The generation of these materials is beneficial to the study of CNC-ChNF interactions in that the freeze-drying process restricts the mobility of the nanofillers during the composite formation process, which therefore allows for the analysis of the three materials in a moment of stasis before any rearrangement that may occur in the formation of the film and hydrogel constructs. Additionally, these aerogel materials possess low levels of water content, which provides opportunities for study with mechanical and chemical characterization techniques that might be influenced by water.

5.1 MATERIALS AND METHODS

PVA with an average MW of 146-186 kg/mol and 99+% hydrolysis was used. Freeze-dried CNCs provided by the USDA Forest Service Forest Product Laboratory (Madison, Wisconsin) were produced through sulfuric acid digestion as previous described[143] and redispersed in water at 0.5 wt.% loadings. The sulfuric acid hydrolysis method left approximately 1% sulfur content on the surface of the nanocrystals resulting in a negative surface charge. The ChNFs were produced from a precursor material of Crabshell Fertilizer from Neptune's Harvest (Gloucester, Massachusetts). The ChNFs were produced by

grinding the crab shells and redispersing in a 1 vol.% acetic acid solution, which was then generated into nanofibers using high-pressure homogenization as previously described.[81] Glacial acetic acid was obtained from Sigma-Aldrich and used as received.

5.1.1 Neat and Nanocomposite Aerogel Processing Procedure

To generate the nanocomposite and neat polymer aerogels, PVA was first dissolved in deionized water while being mixed with a stir bar at 300-750 RPM in a water bath at 100 °C for eight hours or until no visible PVA particles were present. For nanocomposite samples, the solution was cooled to below 50 °C and acetic acid was added to achieve a 1 vol.% concentration to protonate the solution and encourage the dispersion of ChNFs.[82] A 0.5 wt.% ChNF suspension was next deposited into the solution and mixed at 750 RPM with a stir bar for at least 30 minutes. Lastly, for composites containing CNCs, a 0.5 wt.% solution of CNCs was added to the PVA solution or ChNF/PVA suspension and mixed at 750 RPM with a stir bar for at least 30 minutes. The final total solids loading of all suspensions was 5 wt.%. Nanocomposite solutions were sonicated in a Misonix Sonicator 3000 for five minutes at 80W to break up larger aggregates and encourage nanofiller dispersion. 20 mL of the prepared solutions were syringed into 20 mL cylindrical glass scintillation vials of approximately 24 mm in diameter and 45 mm in height. The glass vials were placed in a -10 °C freezer and frozen overnight for approximately 18 hours before being removed. The glass vials were then wrapped and broken, with the intact hydrogels removed in order to expose all parts of the sample and maximize the amount of surface area available for sublimation. Lastly, the frozen samples were placed in individual

glass beakers in a freeze-dryer at approximately -50 °C and 0.1 mBar pressure for three days to sublimate water out of the neat and composite samples. Resulting aerogels were cut with a razor blade to generate cylindrical samples of approximately 10 mm in height for compression testing, with 5 mm portions from the center cut out and set aside for scanning electron microscopy (SEM) analysis. The naming convention for samples in this study use the following structure: [wt.%]CNC/[wt.%]ChNF. Nanocomposite samples were kept at a consistent 1 wt.% loading with five total sample groups: 1CNC, 1ChNF, 0.2CNC/0.8ChNF, 0.8CNC/0.2ChNF, and Neat PVA. Tricomponent ratios were chosen to be consistent with 1:4 and 4:1 ratios analyzed in previous studies on polymer films[2] and hydrogels.

5.1.2 SEM Imaging

The neat polymer and composite aerogels were analyzed with SEM in order to assess the influence of the nanofillers on the pore structure. To prepare the samples for SEM, the 5 mm tall sample section cut from the center of the aerogel cylinder was submerged in liquid nitrogen until the sample was completely frozen, then it was removed, cryo-fractured, and positioned on an SEM sample holder with the broken end facing upward. This preparation was used to minimize damage to the internal structure. Aerogel samples were then mounted on carbon tape covered SEM stubs and were sputter coated with gold-palladium alloy using a Quorum® Q150T ES sputter-coater coating approximately a 10 nm layer on the surface. SEM was performed on a Hitachi SU8010. After acquiring the SEM images, the pore size and structure were analyzed using ImageJ

software. No additional modifications were applied to the images and size scales were based on the number of pixels along the length of the image scale bars. Pores were analyzed using an image of each sample at 100x magnification. Average pore area was calculated based on the length and width of 20 selected pores and they were compared to each other statistically using a two-tailed Student's T-Test assuming unequal variances and an alpha value of 0.05.

5.1.3 FTIR Characterization

Chemical structure changes were measured with FTIR with an ATR fixture. A Shimadzu Prestige 21 Infrared Spectrometer was utilized for this testing. Each spectra curve generated was based on the average of 64 scans with a resolution of 4 cm^{-1}, then each curve was normalized to the 2910 cm^{-1} C-H stretching peak that did not shift between samples. The curves were staggered for clarity.

5.1.4 Compression Testing

Neat and nanocomposite aerogel samples approximately 10 mm in height and 18 mm in diameter were used for compression testing to assess the impact of the CNCs and ChNFs on the mechanical behavior. The samples were cut from the as prepared aerogels from the top to the bottom with a single cylinder yielding up to three samples. The individual samples were then weighed, and the diameter was taken from the average of four measurements. The height was determined from the Instron prior to running the

compression testing by lowering the compression head until a 0.1 N force was registered. These measurements were used to calculate the density of the samples with the following equation:

$$\rho = \frac{m}{(d\pi h)}$$

In this equation, ρ is the density, m is the mass, d is the diameter, and h is the height of the sample. The samples were assumed to be cylindrical for volume measurements, and the density of each sample set was compared to one another.

Compression testing was performed by applying a 10 N preload to the samples and then compressing at 10% strain per minute up to 80% strain. The modulus was measured as the slope of the stress-strain curve over the initial 1% strain, and the energy associated with deformation was measured as the area under the stress-strain curve. The solids modulus and solids stress were also calculated in order to adjust the measured values to the differences in densities of the neat and composite materials. The values were calculated from a method described by Gibson and Ashby (1982) and were based on the relative density of the materials, or the ratio of aerogel density to solid density.[152] Below is the formula for calculating these two values:

$$\frac{E^*}{E_s} = \left(\frac{\rho^*}{\rho_s}\right)^2$$

$$\frac{\sigma_{pl}^*}{\sigma_{ys}} = 0.3\left(\frac{\rho^*}{\rho_s}\right)^{\frac{3}{2}}$$

In these equations, E^* is the aerogel modulus, E_s is the moduli for cell wall material, ρ^* is the aerogel density, ρ_s is the solids density, σ^*_{pl} is the aerogel stress at yield, and σ_{ys} is the solids yield stress. The density of the solids was calculated as a ratio of the individual weight loadings and densities of the components in each sample set. To compare values of each set, the median was chosen from the data sets. The yield stress was determined by calculating the stress value at the intersecting strain value between the elastic modulus and the linear trend line calculated from the 20-23% plateau range of the curves. Yield stress values calculated with this methodology that either occurred at strain values larger than 20% or less than 0% strain were not considered and those curves' values were manually chosen based on the point of greatest slope change between 0-20%.

5.2 RESULTS AND DISCUSSION

5.2.1 Aerogel Appearance and Densities

Neat and composite PVA aerogels were generated and characterized in order to more fully understand the influence of the nanofillers on the structure both individually and in conjunction. After the sublimation process, the aerogels possessed a white, opaque appearance with no discernible visual differences between samples of different nanofiller loadings. An image of aerogel samples after freeze-drying are shown in Figure 5.1.

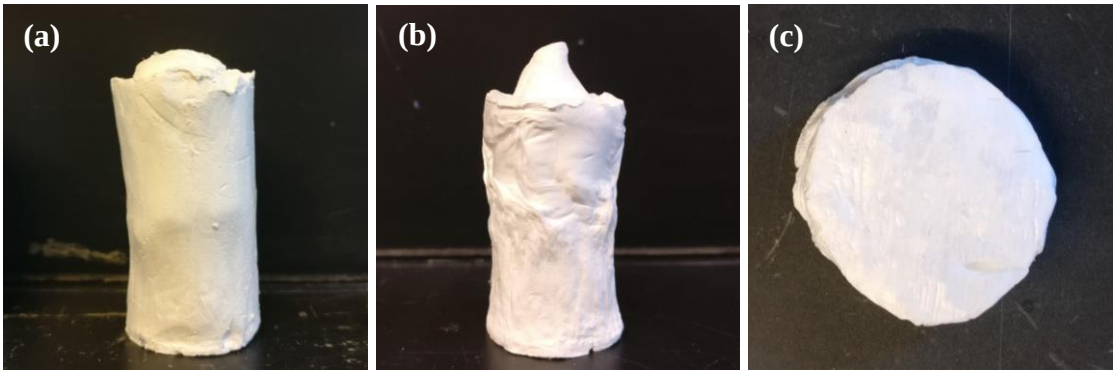

Figure 5.1 Images of (a) whole neat PVA aerogel, (b) whole 1CNC aerogel, and (c) cut 1ChNF aerogel sample. All samples are approximately 17-19 mm in diameter.

Density was first measured in order to assess the level of macro-scale structural shrinkage that the nanofillers may have caused during the freeze-drying process. Neat PVA had the highest average density of the sample sets at 138 kg/m^3, which was evident by the smaller diameters of the neat PVA aerogels relative to the nanocomposite samples. Conversely, 1CNC had the lowest density of the tested samples at 99 kg/m^3, while samples containing any amount of ChNFs had density values that were between neat PVA and 1CNC aerogels at about 110 kg/m^3.

The shrinkage of aerogel structures with the freeze-drying methodology is generally attributed to surface tension arising from the liquid to gas transition of residual water,[153-154] which can be reduced through with the introduction of a highly crystalline and high modulus nanofiller to reinforce the cell walls of the matrix.[155] For instance, Liu et al. (2014) reported that the density of freeze-dried PVA aerogels drastically decreased with loadings of CNFs at 20 wt.%, and continued to decrease up to 30 wt.%.[156] Liu noted that the pore sizes of the PVA aerogels changed when the solutions were stored in colder temperatures, which was attributed to the impedance of ice crystal growth with increased

cooling rates. Mueller et al. (2015) similarly reported that CNCs suppressed the shrinkage of PVA aerogels, and that the level of suppression was dependent on the source of the CNCs and loadings relative to the polymer matrix.[155] Mueller also reported that PVA aerogels reinforced with the longer microfibrillated celluloses (MFCs) possessed larger densities than the shorter CNCs. The authors attributed this effect to the lower crystallinity of the MFCs, which would result in a lower stiffness and a lower ability to restrict pore shrinkage during sublimation. While the study of ChNF-reinforced PVA aerogels is limited, this reasoning for higher density MFC-reinforced PVA could explain why the composites containing ChNFs had larger shrinkage/densities than that of 1CNC. For composites utilizing a different nanofiller, Víctor-Román et al. (2015) prepared PVA aerogels with carbon nanofibers as the nanofiller and similarly showed a progressive decrease in density of the aerogels with increased loadings from 0.5 to 3 wt.%.[157]

5.2.2 SEM Imaging

SEM images were taken of the neat PVA and composite samples, and pore sizes were measured with ImageJ image analysis software. Images at 100x and 1000x magnification are shown in Figure 5.2 and these images were utilized to compare the size and structure of the pores within the neat and composite aerogels.

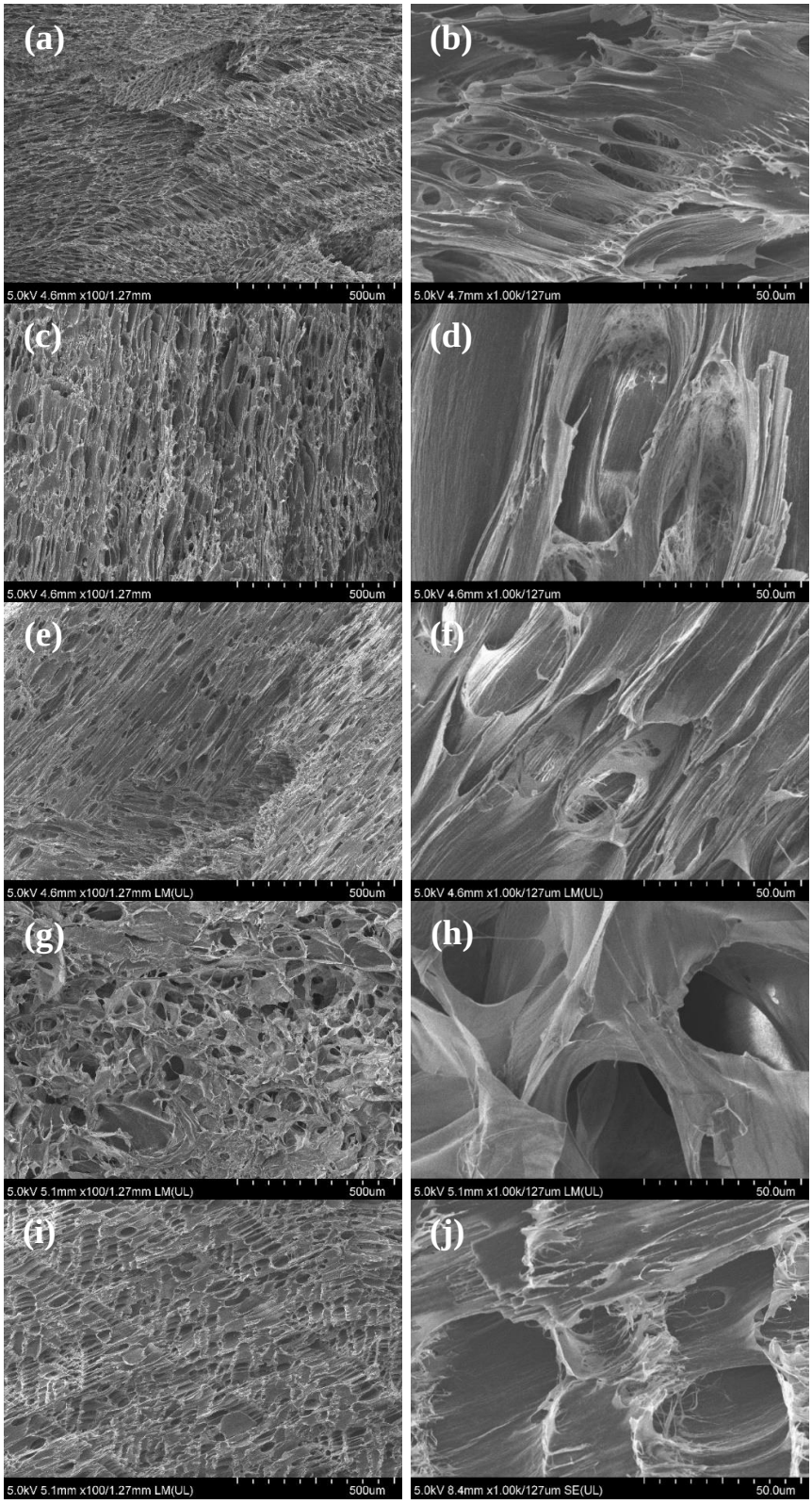

Figure 5.2 SEM images at 100x (left) and 1000x (right) magnification of cryo-fractured aerogel surfaces. (a, b) Neat PVA, (c, d) 1CNC, (e, f) 1ChNF, (g, h) 0.2CNC/0.8ChNF, and (i, j) 0.8CNC/0.2ChNF.

SEM images of neat PVA showed a relatively uniform lamellar sheet-like porous structure, which is typical of the PVA aerogel construct.[158] All sample set average pore areas were statistically different from one another unless otherwise mentioned. Pore areas for neat PVA were approximately 255 ± 66 μm^2 and have a "plate-shaped" pore structure previously described,[116] with long PVA wisps stemming from the sharp edges of the cryo-fractured surface. 1CNC samples had a similar plate-shaped pore structure, though the pore areas were larger at 972 ± 320 μm^2. The 1ChNF samples possessed a pore area between 1CNC and neat PVA at 575 ± 200 μm^2. The 0.2CNC/0.8ChNF and 0.8CNC/0.2ChNF aerogels possessed the largest pore areas at 1240 ± 420 μm^2 and 1190 ± 320 μm^2, respectively, but were not statistically different from each other. Additionally, the 0.2CNC/0.8ChNF aerogels exhibited a more equiaxed structure with pore widths more similar to their lengths, where large pores clearly appeared interconnected and large PVA bridges extended from one pore edge to another. This effect was supported by previous studies that suggested that strong gel-like structure formation between nanofillers can promote a more 3D structure.[116, 159] Another observation from these SEM images was the appearance of nanosized bridges extending from one end of the pore to the other in each of the samples, which was an observation seen previously in CNF/PVA aerogels.[117] The changes in pore size can be connected to the differences in growth of ice crystals within the polymer matrix. In general, a higher freezing rate typically leads to the formation of smaller ice crystals.[160] Mueller et al. (2014) compared CNC/PVA aerogels produced through fast freezing (-196 °C) to slow freezing (-20 °C) cross-link procedures and showed that the slow freezing aerogels had much larger, cube-like pores as ice crystals were allowed to expand further over time.[113] Therefore, the statistically larger pores of

nanocomposite samples compared to neat PVA inferred that nanofillers encouraged the nucleation and growth of ice crystals within the PVA matrix.

5.2.3 FTIR-ATR Characterization

FTIR-ATR analysis was utilized in order to measure any chemical bonding differences between the neat and composite samples. This analysis was similar to what was studied previously with the CNC/ChNF/PVA films,[2] though the presence of water in those samples complicated data analysis. The results of this analysis are shown below in Figure 5.3.

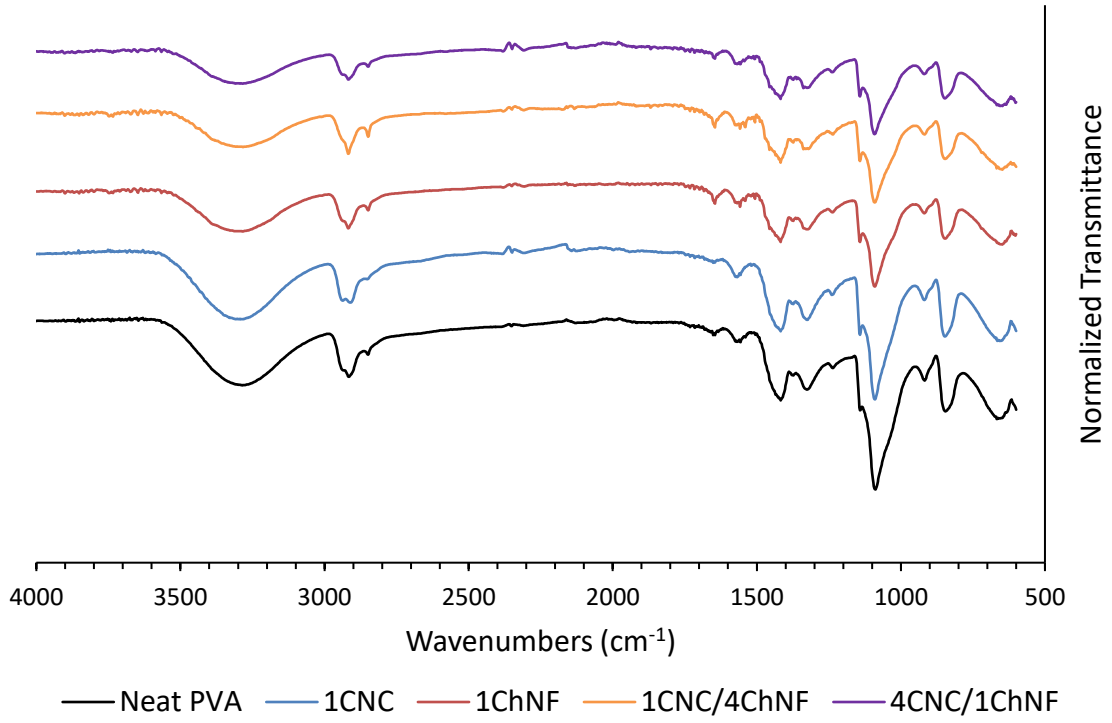

Figure 5.3 FTIR analysis of neat and composite PVA aerogels and spectra are staggered for clarity.

The spectra shown in Figure 5.3 show a large peak in the 3500-3000 cm^{-1} range which was attributed to the stretching of hydroxyl groups. The intensities of these peaks were slightly lower for samples containing ChNFs, which indicated ChNFs may have increased dehydration leading to lower amounts of water relative to neat PVA or 1CNC aerogels. An additional peak intensity difference can be seen at 1640 cm^{-1}, which is greatest in samples containing higher amounts of ChNFs. This peak is attributed to C=O stretching in the ChNFs and is an indicator of their presence within the tested aerogels. However, no significant peak shifts could be observed, which implied there was no observable increase or decrease in hydrogen or electrostatic bonding with the differences introduction of CNCs or ChNFs.

5.2.4 Mechanical Analysis

To analyze the effects of the nanofillers on the mechanical properties of the aerogels, samples were compressed between two plates to a total strain of 80% and various values were extracted from the resulting stress-strain curves. Representative curves were chosen based on the median stress at 80% strain value measured and are shown in Figure 5.4, which also exhibits the three distinct phases of the aerogel compression described previously.[113, 117, 146]

The first stage consisted of linear elastic deformation before plateauing around 10% strain. In this stage, neat PVA possessed the highest slope between 0% and 10%, followed

by 1CNC, 1ChNF, 0.2CNC/0.8ChNF, and 0.8CNC/0.2ChNF. The second stage involved plastic yielding as a result of pore cracking in which the pores of the sample would continually collapse under the force of the compression and limit any increase in recorded stress. This stress plateau would continue until about 40% strain at which point the pore structure would be completely collapsed. The neat PVA, 1CNC, and 1ChNF curves exhibit a clear yield point and transition between phases 1 and 2, whereas the tricomponent curves appear to experience a lesser difference in slope change as they hit their plateau. This qualitative difference can be inferred as the tricomponent samples quickly experiencing pore cracking in response to compression with little elastic response. The third stage consisted of an exponentially increasing stress-strain curve as the collapsed pores would densify the polymer structure. All samples exhibited similar shapes here, though the pore cracking plateau differed as they appeared to end around 50% for 1CNC, 60% for neat PVA and 1ChNF, and 65% for the tricomponent composites. This implied that despite entering the pore cracking stage at an earlier point than 1CNC, 1ChNF, and neat PVA aerogels, the tricomponent samples possessed a greater volume of pores as their densification was slowed.

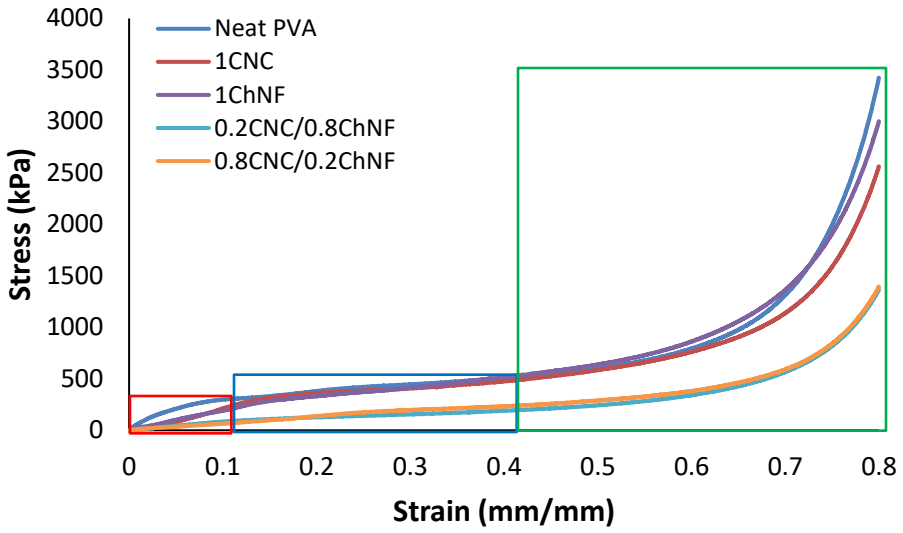

Figure 5.4 Representative curves of aerogel samples that experienced three distinct compression phases identified by a red (phase 1), blue (phase 2), and green (phase 3) box.

While the bulk property values provided information about the overall structure of the PVA aerogels, the density could be used to adjust mechanical properties for a more complete understanding of how the nanofillers may be reinforcing or weakening the PVA matrix structure on the nanoscale. In order to adjust the density, the solids density of the constituent materials first needed to be calculated. The solids densities of each material were calculated based on the volume and densities of the constituent materials where the density of PVA was 1260 kg/m^3, the density of CNCs was 1600 kg/m^3, and the density of ChNFs was 1425 kg/m^3. The resulting solids densities were 1260 kg/m^3 for neat PVA, 1263 kg/m^3 for 1CNC, 1261 kg/m^3 for 1ChNF, and 1262 kg/m^3 for both 0.2CNC/0.8ChNF and 0.8CNC/0.2ChNF. The average density, pore size, and mechanical properties for each sample set are reported in Table 5.1, while median mechanical values and their corresponding solids properties are reported in Table 5.2.

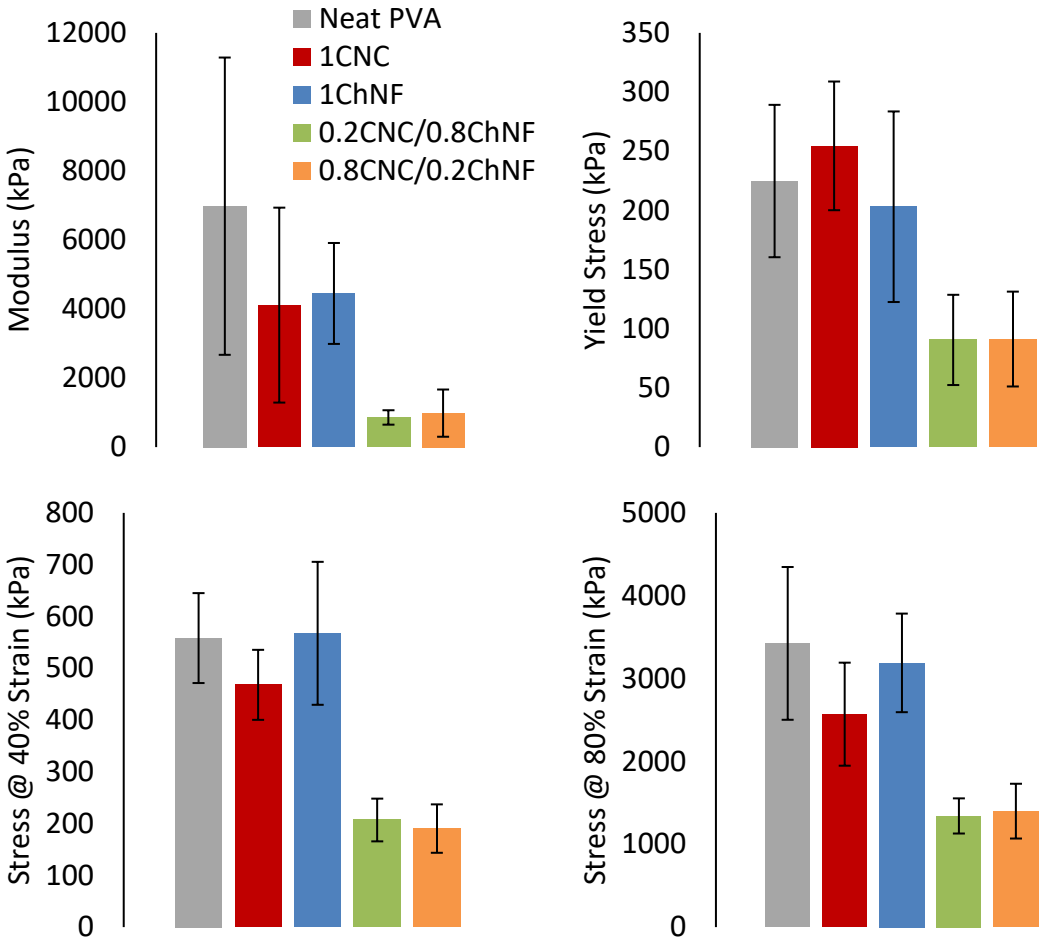

Figure 5.5 Mechanical properties of neat and composite aerogels including (a) modulus, (b) yield stress, (c) stress at 40% strain, and (d) stress at 80% strain.

Table 5.1 Density, pore size, and mechanical properties of neat PVA and composite samples. Values are reported as averages ± standard deviations. Statistically different properties from neat PVA are denoted with a *.

	Density (kg/m³)	Pore Area (nm²)	E (MPa)	σ_y (kPa)	Energy of Deformation (kPa)
Neat PVA	138 ± 15	255 ± 66	6.98 ± 4.3	225 ± 64	620 ± 120
1CNC	99 ± 9.9*	972 ± 320*	4.11 ± 2.8	255 ± 54	509 ± 91
1ChNF	113 ± 8.0*	575 ± 200*	4.45 ± 1.5	203 ± 81	614 ± 130
0.2CNC/0.8ChNF	109 ± 6.3*	1240 ± 420*	0.860 ± 0.21*	90.6 ± 38*	234 ± 44*
0.8CNC/0.2ChNF	113 ± 13*	1190 ± 320*	0.985 ± 0.68*	91.3 ± 40*	224 ± 51*

From Figure 5.4, it can be observed that each of the representative curves possessed the same general three stage stress-strain shape previously described, though differences in each region can describe changes in structural properties of the materials. For instance, the reported moduli for each of the aerogel samples (Table 5.1) reflect the pore structure of the materials, as the larger pores can be expected to crack at lower strains than that of smaller pores. As shown previously in the SEM images, neat PVA had a much lower average pore size, which could be a primary factor in the largest measured modulus values. Conversely, it was seen that the initial slope of the tricomponent composite curves was low, which was the result of the larger pores beginning to crack quickly under the initial pressure of the compression plate. While 1CNC and 1ChNF also possessed larger average pore sizes than neat PVA and correspondingly lower moduli values, their stress-strain curves more closely resembled that of neat PVA rather than the two tricomponent samples. This similarity in stress response indicated that the pore walls had been reinforced with the introduction of singular nanofillers, while the aggregated nanofillers in the tricomponent composites may be weakening them. Statistically, 0.2CNC/0.8ChNF and 0.8CNC/0.2ChNF had lower yield stress, solids yield stress, modulus, solids modulus, and toughness values than 1CNC, 1ChNF, or neat PVA sample sets, while not being statistically different from each other. Furthermore, while 1CNC possessed a larger solids yield stress than that of neat PVA and 1ChNF, no other statistical differences were found between all other data sets.

Table 5.2 Median aerogel and solids mechanical properties of neat and composite data sets. Solids properties are denoted with a subscript *s*.

	E (MPa)	σ_Y (kPa)	E_s (MPa)	σ_{ys} (MPa)
Neat PVA	5.91	214	460	19.1
1CNC	3.27	255	629	39.1
1ChNF	4.27	204	540	26.1
0.2CNC/0.8ChNF	0.818	82.5	114	10.5
0.8CNC/0.2ChNF	0.881	85.5	106	11.1

In order to account for the effects of density, median values for modulus and yield stress were chosen and used to convert to solids property values previously described by Gibson and Ashby (1994).[152] While the median 1CNC aerogel possessed a 45% lower modulus and 19% greater yield stress than neat PVA, the density-adjusted 1CNC solids modulus and yield stress were 37% and 105% greater than neat PVA, respectively. Similarly, the 1ChNF aerogel possessed a 28% lower modulus and 5% lower yield stress than neat PVA, but the solids modulus and yield stress were 17% and 37% greater than that of neat PVA, respectively. This increase in solids mechanical properties with singular nanofiller addition is attributed to the reinforcement of the cell wall between pores that generates a greater resistance to collapse.[116-117, 146] For tricomponent composites, the solids properties were still lower than that of neat PVA. This reduction in mechanical properties for charge-matched ratios (i.e. 0.8CNC/0.2ChNF) relative to other composites was consistent with what has been previously observed in PVA films[2, 73] and hydrogels, though these previously discussed constructs also showed an improvement in mechanical properties for a 1CNC:4ChNF ratio that is inconsistent here. To better understand the relationship between constructs, a 0.2CNC/0.8ChNF hydrogel was produced and compared

to the hydrogels from chapter 4 (Table A.2). After 1FT cycle (most similar processing to the aerogels), the 0.2CNC/0.8ChNF hydrogel possessed the lowest modulus and second lowest compressive strength relative to all other hydrogels and this reduction in properties is consistent with what is observed with the aerogel data. However, for 3FT, 5FT, and 7FT cycles, the 0.2CNC/0.8ChNF hydrogel was among the three highest modulus and compressive strength values relative to other hydrogels, indicating a potential influence of increased physical crosslinking on nanofiller ratio performance.

Simón-Herrero et al. (2016) analyzed the effects of carbon nanofibers and different processing conditions on the structure of PVA aerogels and demonstrated that long freezing times above 8 hours would lead to nanofiber agglomerates, which the authors attributed to a reduction in reinforcement capacity and resulting lower mechanical properties.[161] The 16 hour freezing times of the aerogels in the present study would understandably allow for a great amount of phase separation between the water and oppositely-charged nanofillers, thus encouraging larger amounts of agglomerates. While aggregates may still be forming within the 1CNC and 1ChNF compositions, the repulsion forces from the like-charged nanofillers may be mitigating this effect. As discussed previously in the pore size measurements, Mueller et al. (2014) showed that slow freezing aerogels had much larger pore sizes than that of fast freezing aerogels, which demonstrated the inverse relationship between ice crystal growth rate and ice crystal size.[155] Furthermore, it is well documented within food science that increases in suspension viscosity retard ice crystal growth rates due to lower molecule mobility,[162-164] which would suggest that the ice crystal growth would be slowest in tricomponent composite samples. This may explain the increased pore size of tricomponent composites relative to 1CNC, 1ChNF, and neat PVA, as well as the

resulting difference in pore structure. Liu et al. (2017) studied 50:50 montmorillonite clay and PVA aerogels reinforced with cellulose nanofibers loadings between 2-19%, where lower loadings of CNFs (2% and 4%) were shown to slightly decrease total compressive strength relative to neat MTM/PVA composites. This was attributed to cell wall defects represented by noncontinuous cell wall edges, which limits the load transfer within the aerogel.[116] Therefore, the larger noncontinuous 3D cell wall structure of the tricomponent composites as a result of the slower freezing rates and larger ice crystals could explain the reduction in mechanical reinforcement.

5.3 CONCLUSIONS

Neat and composites PVA aerogels were generated from the mixture of CNCs, ChNFs, PVA, and water, which resulted in stiff materials with properties that could be modulated with nanofiller type and ratio. SEM analysis showed that the pores of the aerogel expanded with the introduction of CNCs and ChNFs, which was largest for the tricomponent composites and formed a 3D structure with the 0.2CNC/0.8ChNF loading. This shift in pore structure may be attributed to changes in suspension viscosity, which would allow for larger ice crystals after the 16-hour freezing period. Mechanical properties measured through compression demonstrated that CNCs and ChNFs were able to increase the strength of the PVA aerogel, but the tricomponent composites resulted in a reduction in aerogel strength. This differs from results previously discussed in PVA tricomponent films and hydrogels, which showed an increase in mechanical properties with the 1CNC:4ChNF ratio beyond that of individual nanofillers. However, while the larger pores of the

tricomponent aerogels may produce a weaker bulk structure, it has been previously shown that these sizes of pores are better for oil absorption[160] and could be further investigated for those applications. The work in this study generates greater fundamental understanding of the interactions between CNCs and ChNFs both on their own in an aqueous suspension and in a polymer matrix.

CHAPTER 6. VALORIZATION OF CELLULOSE AND CHITIN-BASED NANOMATERIALS

The last component of this study aimed to combine the knowledge gathered of the previous three chapters on tricomponent composite films, hydrogels, and aerogels, respectively, and explore new applications of CNCs and ChNFs as reinforcement materials. In addition to individual efforts, this chapter utilized the resources and advice of groups in other disciplines through a designed collaboration initiative to develop a more complete understanding of the process-structure-property relationship of the developed materials and their applications. While these materials have a high level of versatility and potential for many different fields, biomedical and packaging industries were the primary focus. The goal was to expand on the usage of renewable biomaterials in commercial applications and drive towards developing customizable environmentally friendly and bioinert materials that possess similar levels of long-term mechanical performance as the industry standard.

6.1 Intervertebral Disc Replacement

6.1.1 Background of IVDs

Back pain is a very common modern day ailment that has been reported in 80% of the world's population with 75% of these cases being attributed to degenerated intervertebral discs (IVD).[23] Artificial IVDs are becoming a more often utilized solution that seeks to replace the damaged fibrocartilage discs to supplant the more common spinal fusion procedure. The IVD is a relatively simple structure composed of two major

components: (1) an outer fibrous set of lamellar rings called the annulus fibrosus (AF) and (2) a gel-like material at the center called the nucleus pulposus (NP). The stiffer AF takes the bulk of the load in most situations, while the NP acts a kind of shock absorber for instant-impact forces. A diagram for the location and structure of this organ is shown below in Figure 6.1.

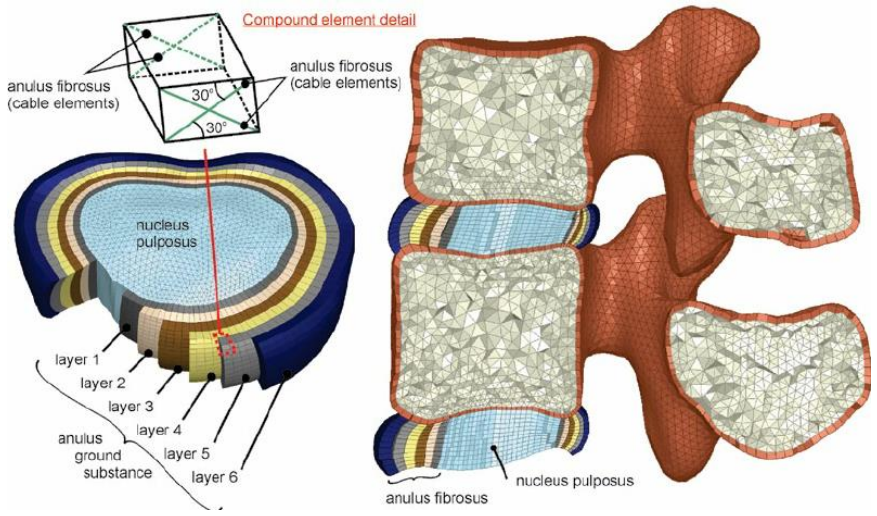

Figure 6.1 IVD diagram showing a (A) a side view between two vertebrae in the spine and (B) an alternate three dimensional view showing the nucleus pulposus (NP) and annulus fibrosus (AF).[165] (f5)

The NP sits at the center of the disc and is a material of high water content, often characterized as a hydrogel. The main components of this structure are proteoglycan, collagen type II fibrils, and water, with the water taking up approximately 90% of the weight that decreases to 70% with age. Collagen makes up approximately 5-20% of the

(f5) Image taken from Figure 2 of Tsouknidas et al. (2012) in *Journal of Applied Biomechanics.* DOI: https://doi.org/10.1123/jab.28.4.448

dry weight of the NP, while proteoglycans, which enable water binding to the collagen, make up approximately 35-65%. The remaining components are elastin and proteins. The outer AF is constructed of approximately 15-25 concentric layers, with increasing layer thickness between 0.05 – 0.5 mm as you progress towards the center. About half of these layers do not form a complete circle, however, and the number of complete layers decreases with age. Similarly to the NP, the AF is made up of collagen fibers, both type I (found in bones and skin) and type II (found in cartilage). The increased amount of collagen type II as you move radially towards the center of the IVD allows for the structure to take larger amounts of compressive forces. Also similar to the NP, the AF is made up mostly of water, which accounts for approximately 65-70% of its mass. The dry components then consist of about 20% proteoglycan for water binding, 50-70% collagen, and a small amount of elastin. The NP and AF are connected through collagen fibers rooted in between the two components.[166]

Mechanically, the loads needed for proper support for the IVD and its two sections depend on the location, size, gender, and age of the patient, in addition to the levels of activity. For instance, Wilke et al. (1999) implanted a pressure transducer into the L4-L5 lumbar region of the spine of a 45-year-old male weighing 70 kg and measured the forces present on the NP during different activities. These researchers found that activities such as laying prone applied 0.1 MPa to the NP, standing provided 0.5 MPa of pressure, and lifting a 20 kg weight produced the maximum recorded 2.3 MPa of pressure.[167] In measurements of a total IVD, Stemper et al. (2010) measured thoracic IVDs that possessed compressive moduli of 17.7 MPa for 20 – 36 year old men and 21.3 MPa for 20 – 36 year old women, with a much lower 9.7 MPa and 11.5 MPa for 63 – 77 year old men and

women, respectively.[168] In finite element analysis of cervical IVDs (C3 – C6), Ha et al. (2006) reported a Young's modulus of 1.0 MPa for NP and 4.2 MPa for AF, which was then used to validate the usage of a 5.9 MPa polyurethane elastomeric material as an IVD replacement.[169] However, Umehara et al. (1996) demonstrated that the larger lumbar discs (L3 – L5) tested through indentation tests possessed a compressive elastic modulus of 5.8 kPa for NP and 110.7 and 75.8 kPa for anterior and posterior AF, respectively.[170] Interestingly, the modulus of the IVD increases if it is degenerated. Literature shows that healthy and degenerated AF possess moduli of 2.56 and 12.29 MPa, respectively, while healthy and degenerated NP possess moduli of 1.0 and 1.66 MPa, respectively. These results highlight the importance of using reinforcement materials to tune the mechanical properties to whatever is necessary for the patient. If the strength of the implant is too low there is risk of failure under pressure, but if it is too high it may bear too much of the load on the spine and deteriorate much more quickly.

PVA composites for biomedical applications has been previously studied with a heavy focus placed on their application to biomedical cartilage, wound dressing, and tissue engineering applications.[171-174] Regarding their applications to tissue engineering, PVA hydrogels have a documented history of being generated as an artificial replacement for the NP in intervertebral discs.[27, 93, 171, 175] Additionally, as previously mentioned, cellulose and chitin have excellent mechanical properties, high levels of biocompatibility, little to no toxicity, and they encourage cellular growth given their natural role in cellular systems.[121] Therefore, their incorporation into PVA hydrogels and aerogels tunes mechanical performance and provides potential point of growth for cells without concern for a negative response from the surrounding tissue. Utilizing nanofillers within these different constructs

makes it possible to mimic the natural structure of the IVD, as it serves the role of the natural reinforcement fibers of collagen dispersed throughout the cartilaginous tissue. More specifically, the outer fibrous ring can take advantage of the PVA aerogels in a similar way that other studies have generated PVA/CNC aerogels for meniscus implants,[113] while PVA hydrogels can mimic the inner gel-like shock absorber.

This study aimed to generate these structures with a combination hydrogel/aerogel hybrid system made up of CNCs, ChNFs, and PVA. The most important aspects of generating an artificial IVD are to use biocompatible materials that will not cause medical complications and to match the mechanical capabilities of a natural IVD. Also, another important component is generating a material that can retain its water content and absorb the surrounding fluid so that it will increase material longevity within the application space. Regarding biocompatibility, it was previously mentioned that cellulose, chitin, and PVA have all been shown to be biocompatible and used in tissue engineering applications, so these materials are expected to operate without biological complications. However, this aspect of performance could be of interest in a future study.

6.1.2 IVD Construction and Characterization

In this study, a prototype of an artificial IVD was constructed with a composite aerogel serving as the AF and a composite hydrogel served as the NP, which was then mechanically characterized. To construct this aerogel/hydrogel hybrid and shape it to the dimensions and properties necessary of a natural IVD, the knowledge garnered from the film, hydrogel, and aerogel studies was utilized. Firstly, a 1CNC/PVA solution with 95% water was

prepared as outlined in chapter 2, with the suspension being poured into a 75 mm diameter and 26 mm high Teflon mold and frozen for 16 hours as described previously in chapter 5. 1CNC/PVA was chosen due to its high-performing mechanical properties in compression relative to the other tested composite and neat samples outlined in in this chapter. The frozen 1CNC/PVA hydrogel was then placed into a freeze-dryer and allowed to sublimate for three days to remove water. After the freeze-drying process was completed, a one-inch diameter die was used to cut out a hole from the center of the aerogel. This hole was filled with a prepared solution of 1CNC/4ChNF/PVA at 95% water, which was chosen due to its performance in both compression tests and water absorption hydrogel studies from chapter 4. This sample was then placed in the freezer and subjected to up to five freeze-thaw cycles as described in chapter 4. This number of FT cycles was chosen given its similarity to the measured mechanical properties of natural NPs. The resulting structure is shown in Figure 6.2 below, which mimics the structure of a natural human IVD.

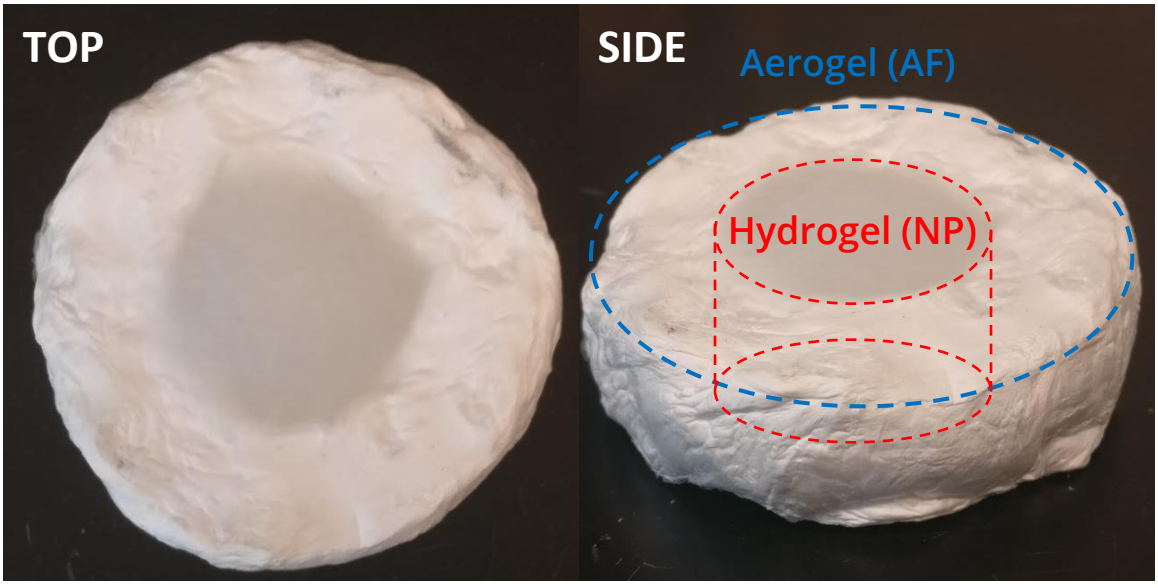

Figure 6.2 CNC/ChNF/PVA hydrogel/aerogel hybrid.

The resulting 10 mm tall and 56 mm wide hydrogel/aerogel hybrid sample was compressed between plates in order to mechanically characterize it and compare to the average human IVD. After compression, the plates were then reversed at the same strain rate in order to generate hysteresis curves and demonstrate the recovery behavior of the material. Compression was performed at a strain rate of 2 mm per minute to 50% compression. The stress-strain data obtained from the compression test is shown in Figure 6.3.

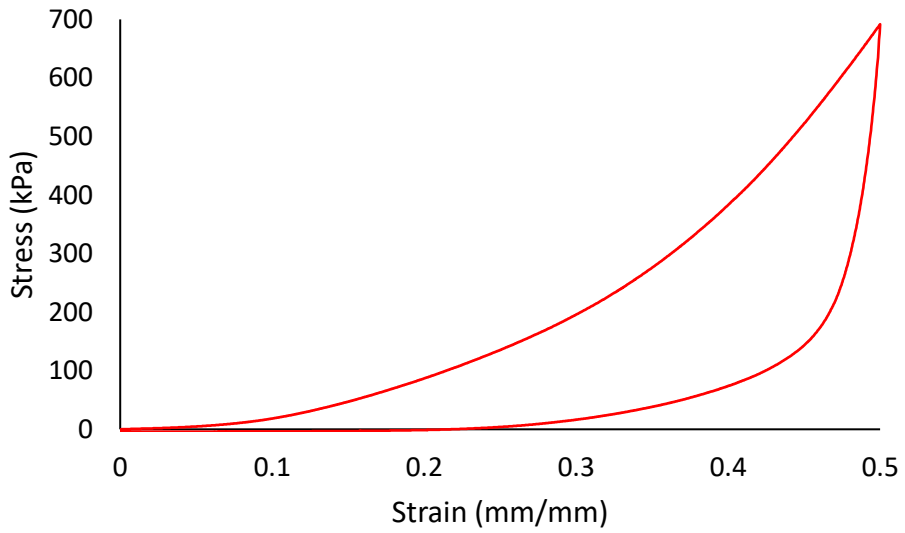

Figure 6.3 Stress-strain curve of an artificial intervertebral disc.

The tested sample shown in Figure 6.3 displays an exponential increase in stress with increased strain, which then quickly relaxed on the return curve. This behavior was similar to that of natural IVDs[166] with mechanical properties summarized in Table 6.1. The peak stress achieved at 50% compression was 691 kPa, which was within the reasonable range of pressure expected for an IVD. The stress value for this hybrid material was nearly 10x

larger than the highest stress achieved by the 1CNC/4ChNF hydrogel of chapter 4 (71.5 kPa), indicating a high level of support provided by the aerogel construct. Interestingly, the shape of the stress-strain curve was more similar to those of the hydrogel samples of chapter 4 and did not possess the three-stage compression shape of the stress-strain curves for aerogels outlined in chapter 5. It was possible that the introduction of the hydrogel may have led to increased flexibility of the aerogel struts, resulting in a more hydrogel-like mechanical response. Though the volume of the hydrogel and the aerogel components were approximately 5,070 and 19,600 mm^3, respectively, and the density measurements from previous chapters for 5FT 1CNC/4ChNF hydrogels (0.97 mg/mm^3) and 1CNC aerogels (0.099 mg/mm^3) lead to a hydrogel:aerogel mass ratio of 2.5:1. Therefore, the mass majority hydrogel component may be dominating the mechanical behavior in response to the compressive stress. The elastic modulus of this hybrid material after the first 5% of compression was 94 kPa, which was within the range reported for the larger lumbar discs' annulus fibrosus (75.8 – 110.7 kPa).[170] However, it was worth noting that these values were much lower than that of the thoracic[168] and cervical[169] moduli of 9.7 – 21.3 MPa and 1.0 – 4.2 MPa, respectively, reported earlier. Additionally, the energy associated with deformation of the material upon loading and unloading was 100 kPa and 24.1 kPa, respectively, indicating a total loss of approximately 76 kPa of energy. This energy loss was attributed to some plastic deformation of the hybrid material, which could be investigated further in fatigue testing for long-term performance.

Table 6.1 Mechanical property summary of IVDs. Hydrogel/Aerogel hybrid material highlighted in grey for comparison.

NP or AF	Men or Women	Spinal Region	Modulus (MPa)	Reference
Both		Lumbar	0.094	Hybrid Hydrogel/Aerogel
AF	NA	C3 – C6	1.0 – 4.2	Ha (2006)[169]
Both	M	Thoracic	9.7 – 17.7	Stemper (2010)[168]
Both	W	Thoracic	11.5 – 21.3	
NP	NA	L3 – L5	0.0058	Umehara (1996)[170]
AF	NA	L3 – L5	0.0758 – 0.1107	

The development of a hybrid aerogel/hydrogel biomimetic IVD replacement prototype reinforced with CNCs and ChNFs helped display how these nanomaterials can be used to mimic the properties of body tissue with highly tunable mechanical properties. Previous studies on PVA aerogel and hydrogels reinforced with these nanofillers allowed for the selection of different nanofiller types and loadings, ultimately resulting in a hybrid material that was able to achieve the mechanical properties necessary to perform in its application space. However, while the measured modulus of the device was within range of that of lumbar discs, smaller thoracic and cervical IVDs require a much larger modulus to operate. Therefore, additional testing on smaller aerogel/hydrogel hybrid artificial IVDs, as well as hybrids incorporating different compositions of CNCs and ChNFs, is necessary to evaluate the mechanical viability of these devices in different regions of the spine.

6.2 IGER Collaboration Packaging Materials

Flexible packaging is an additional application area for these materials. Petroleum-based multilayer polymer films currently dominate the packaging material market as a

result of their barrier properties and cost-effective production, but environmental concerns have encouraged the industry to investigate alternative options with lesser environmental impact. Cellulose and chitin-based materials offer a potential option in this area as a coating due to their transparency and mechanical and barrier properties. In order to evaluate these types of high-performance packaging materials, a greater collaboration effort called the Integrated Graduate Education and Research (IGER) program was formed involving a multidisciplinary team of researchers from Georgia Tech. The following section identifies key points within the two studies that tie to the research discussed in chapters 3-5. The studies discussed here were led by Chinmay C. Satam of Professor J. Carson Meredith's group, where Satam is credited as the first author on the two resulting publications. C. W. Irvin, among others, contributed to these studies in the form of sample preparation and characterization of the materials, as well as discussion of the results.

6.2.1 CNC and ChNF Spray-Coated PLA Films

The first study titled "*Spray-Coated Multilayer Cellulose Nanocrystal-Chitin Nanofiber Films for Barrier Applications"* was published in 2018 in *ACS Sustainable Chemistry & Engineering*.[82] In this study, the thermomechanical and transmission properties of CNC-ChNF spray-coated PLA were assessed and compared to neat PLA films. CNCs and ChNFs were produced as described in previous chapters and utilized in 0.5 wt.% aqueous suspensions. Using a 1.52 mm spray nozzle, 30 mL of CNC or ChNF suspensions were sprayed onto a PLA film affixed to a heated plate held at 60 °C with 2 minutes drying between added layers. The degree of acetylation of the ChNFs was

measured to be 92.6%, which possessed a similar magnitude, but opposite surface charge to that of the CNCs. Single nanofiller sample sets included PLA films spray-coated with one layer of CNCs, one layer of ChNFs, five layers of CNCs, or five layers of ChNFs. Films with alternating layers of CNCs and ChNFs were generated for two, three, four, and five layers, with the ChNFs always applied first. Therefore, for the odd numbered layers, there was one more layer of ChNFs compared to CNCs. Uncoated control films were prepared by spray-coating PLA with water. The films were then characterized with TGA, DSC, light transmission, atomic force microscopy (AFM), high-throughput mechanical characterization (HTMECH), oxygen permeability (OP), and water vapor transmission (WVTR) testing.

The main results from this study demonstrated advantages to using both cellulose and chitin as spray-coated layers. Firstly, all films, regardless if they were coated or uncoated, were transparent and exhibited little haze. This result was attributed to close packing between the CNC and ChNF layers through electrostatic interactions that provide fewer voids for light scattering. It was also theorized that the repulsion forces between like-charged layers promotes rearrangement of the layer in between, thus leading to a more efficiently packed structure. Thickness measurements further supported this where five alternating layers between CNCs and ChNFs (3.7 μm) were thinner than that of five layers of just CNCs (6.4 μm) or just ChNFs (7.7 μm), providing additional evidence of the electrostatically-driven effective packing of the alternating layers.

In measurements of oxygen permeability at 50% relative humidity (RH), single layers and five layers of CNCs or ChNFs were found to not be statistically different from that of the PLA film. However, two alternating layers of CNCs and ChNFs showed a significant

70% decrease in OP compared to neat PLA, dropping from 70 cm^3-μm/m^2/day/kPa to 20 cm^3-μm/m^2/day/kPa. This improvement in OP did not increase further with additional layers of CNCs or ChNFs and was a relatively consistent value between the two, three, four, and five-layer coated films. This improvement in OP over the neat PLA films was also consistent when alternating layer films were measured between 10-80% relative humidity, but not above 80%. These oxygen permeability results provided further evidence of close packing of the CNCs and ChNFs alternating layer films as a result of their electrostatic interactions. These results demonstrated that alternating CNC/ChNF layers can be used to drastically improve the OP of the films beyond that of what is capable by PLA on its own or with the aid of CNCs or ChNFs alone, which largely agree with the results outlined in chapters 3 and 4, which demonstrated that ratios between CNCs and ChNFs can provide improvements in certain properties not possible with singular nanofillers.

Lastly, the mechanical properties were measured with an HTMECH device and the ultimate tensile strength (UTS) and strain at break were reported. Layers of CNCs or ChNFs in any combination were found to decrease both the UTS and strain at break values, but the five-layer samples experienced the largest decrease. This reduction in strength was suggested to be the result of stress points that developed where there is thermal contraction as the layered sheets cooled in addition to volumetric contraction during the film drying phase, which caused fracture in the coated layers first and then propagated down to the PLA layer. These brittle materials were consistent with the decrease in strain at break properties found in CNC/ChNF/PVA films outlined in chapter 3, which were considerably more brittle than the neat PVA films.

6.2.2 CNC and ChNF Blended Films

The second study titled "*Barrier Materials Based on Direct Blending of Cellulose Nanocrystals and Chitin Nanofibers*" was published in *Biomacromolecules* in 2019 and assessed the properties of CNC/ChNF blended films generated with varying ratios of CNCs to ChNFs.[55] This study also analyzed ChNFs with different levels of deacetylation, denoted as LChNFs for low and HChNFs for high deacetylation. It is worth noting that the ChNFs utilized in the tricomponent composites from chapters 3-5 were the LChNFs for comparison purposes. The titration results showed that CNCs had a charge of -0.49 ± 0.09 meq/g, as previously reported, while HChNFs possessed a 0.35 ± 0.12 meq/g charge and 93% deacetylation and LChNFs possessed a 1.37 ± 0.08 meq/g charge and 74% deacetylation. These charges governed the mixing ratios, resulting in 1:3, 1:1, and 3:1 ratio for CNCs:LChNFs and a 1:1 ratio for CNCs:HChNFs. These films were tested and compared to neat films of only CNCs, LChNFs, or HChNFs. After mixing, the suspensions were then cast into molds where they were dried for 10-14 days. The characterization of these films included analysis of the thickness, light transmission, oxygen permeability (OP), mechanical, and structural and ordering properties of the materials.

Like the previous study, these experiments further supported the generation of cellulose- and chitin-based materials. In appearance, the CNC films were iridescent due to the chiral nematic nature of the CNCs after drying, which did not occur in films containing ChNFs. Polarized optical microscopy (POM) was able to confirm the presence of birefringent domains that resulted in the CNC film iridescence. These domains were represented by large, bright white regions on the order of 200 μm, which were broken up into smaller and smaller sizes while ChNF loadings were increased down to approximately

50 μm in the 1CNC:3LChNF film. This decrease in nematic ordering and improved dispersion were attributed the higher amounts of interfibrillar hydrogen bonding of ChNFs, which lowers the long-range orientation of the nanomaterials and disrupts CNC ordering through electrostatic binding. Furthermore, 1CNC:1HChNF films possessed nearly no evidence of CNC agglomerates, which were suggested to be due to the lower surface charge of the HChNFs leading to less CNC aggregation and subsequent ordering along the chitin surfaces. These results were similar to that found in the CNC/ChNF/PVA film study of chapter 3, with birefringent CNC domains appearing as bright spots that became smaller and more homogeneous with increased ChNF loadings (Figure 3.1). Furthermore, CNCs were shown to increase the haziness of both the LChNF and HChNF films, which was attributed to aggregation between the two oppositely-charged particles and agrees with light scattering results discussed previously in chapter 4. In thickness measurements, the addition of ChNFs was shown to decrease the thickness compared to the neat CNC films, which was the result of more efficient packing with the introduction of higher aspect ratio nanofibers and the repulsion forces between them.

In oxygen permeability studies, CNC films possessed a high OP of 14.1 cm3-μm/m2/day/kPa, LChNFs possessed an OP of 1.0 cm^3-μm/m^2/day/kPa, and HChNFs possessed an OP of 4.4 cm^3-μm/m^2/day/kPa. The addition of ChNFs to CNCs in blended films was found to significantly improve the barrier properties compared to CNCs alone, though there was little difference between the CNC/ChNF films regardless of ratio that is indicative of an “all-or-nothing” type effect. It is believed that the larger aspect ratio and structure formation exhibited by ChNFs produced a longer diffusion path for oxygen and, thus, reduced the permeability to that gas. These results were supported by SEM analysis

that showed lamellar and honeycomb structure formation between ChNFs, which were encouraged by the addition of CNCs that act as binding particles between parallel ChNF layers, thus creating a more tortuous path for oxygen transportation.

Mechanically, the 1CNC:3LChNF ratio had the highest median ultimate tensile strength (UTS) and second highest median breaking strength, though it was not statistically different from the other blended films similar to the OP results. These experiments demonstrated the dominance of the ChNFs over the CNCs in improving UTS and strain at break properties as a result of greater capacity for physical entanglement, though the CNCs provided reinforcement to these ChNF films to achieve mechanical properties not possible with ChNFs alone. Additionally, though it is not statistically different than the other blended films, the 1CNC:3LChNF ratio exhibited the highest UTS of the measured neat and blended films, which agrees with the ratio found to outperform the others in modulus and UTS for HPVA composites discussed in chapter 3.[2]

Lastly, analysis of AFM images was used to measure the surface properties of the CNC/ChNF films. Both the LChNF and HChNF films were shown to possess little apparent ordering in the images, though the CNCs were visually shown to be highly ordered. In the blended films, the charge-matched 3CNC:1LChNF and 1CNC:1HChNF ratios exhibited ChNF fibers with CNCs aligned along their surfaces, where CNC ordering appeared to decrease with increased ChNF loadings. This evidence of CNCs along the surface of the ChNF supported a theory proposed in chapter 4, where it was suggested that CNCs could act as a compatibilizer between the PVA and ChNFs while adhered to both.

6.2.3 IGER Collaboration Conclusions

This multi-disciplinary IGER project worked to characterize the individual nanofillers and how we could use their synergistic differences to develop better packaging materials. The study of the CNC/ChNF-coated PLA films demonstrated the aggregation behavior of CNCs and ChNFs and how they could effectively pack together and create effective oxygen barriers. The results showed that the combination of these two nanomaterials can surpass the capabilities of single nanofillers, which agrees with results discussed in previous chapters regarding tricomponent composite materials. The study on CNC/ChNF blended films provided insight into the structure formation of the CNCs and ChNFs, which developed a greater understanding of how they may be interacting within the PVA tricomponent composites. Particularly, the observation that CNCs are aggregating along the surfaces of the ChNFs provided credence the theory that CNCs act as a compatibilizer that increases the affinity of ChNFs for the PVA matrix in tricomponent composite materials, thus leading to an overall enhanced reinforcement of the network structure. Altogether, these two studies developed potential in packaging applications by producing high-performance barrier materials that can improve renewability and sustainability in an industry looking to move away from petroleum-based plastic products. Both studies demonstrated valorization of CNCs and ChNFs and provided value-added products that take advantage of their synergistic interactions for enhanced levels of performance beyond singular nanofillers.

CHAPTER 7. CONCLUSIONS AND FUTURE WORK

In this chapter, the major conclusions from each of the preceding chapters will be summarized in a series of bullet points with discussion at the end on how they contribute to the overall project goals of understanding how the nanofillers influence the polymer matrix and how their synergistic interactions can be manipulated to create high-performance materials beyond that of singular nanofillers. Based on the findings of this thesis, recommended future work is included at the end of this chapter.

7.1 Chapter Conclusions

7.1.1 Chapter 3 Conclusions

- Mechanical analysis of CNC/ChNF/PVA films demonstrated that 5 wt.% CNCs and 5 wt.% ChNFs possessed similar modulus and tensile strength values for both high and low MW PVA, though the 1CNC/4ChNF/HPVA and 2.5CNC/2.5ChNF/LPVA films were capable of surpassing singular nanofillers and achieving mechanical improvement over neat HPVA and LPVA, respectively. In contrast, the charge-matched nanofiller ratio of 4CNC/1ChNF decreased the modulus and tensile strength relative to singular nanofillers.
- Polarized optical microscopy (POM) indicated that aggregation and ordering between CNCs was decreased with the introduction of ChNFs, with ordered CNCs represented as bright white regions in the microscopy images.

7.1.2 Chapter 4 Conclusions

- Water absorption/retention of PVA hydrogels containing ChNFs was higher than that of neat PVA and CNC-only hydrogels across various freeze-thaw cycles.
- The compressive stress of 1CNC/4ChNF hydrogels was higher than that of neat PVA, singular nanofillers, and 4CNC/1ChNF hydrogels, which shows that particular ratios of CNCs and ChNFs can lead to a greater overall mechanical reinforcement of a polymer hydrogel.
- Rheological analysis showed that the addition ChNFs to water resulted in a great increase in viscosity and elasticity, while there were little changes to these values with only CNCs. Furthermore, the combination of CNCs/ChNFs resulted in even greater values of viscosity and elasticity relative to ChNFs alone. Additionally, there is little change in properties of the PVA solution with the addition of CNCs, though there is a small increase in the elasticity of the system indicated by a slightly higher storage modulus. However, the addition of ChNFs into the PVA solution caused a drastic increase in viscosity and storage modulus.
- Light scattering analysis indicated that there is aggregation between the CNCs and ChNFs that reaches a relative plateau in hydrodynamic radius between 10 to 50% loadings of CNCs. However, when loadings surpassed 50% CNCs, there is visual evidence of network formation in the CNC/ChNF mixtures, which reached a critical point of mass aggregation and hydrogel formation at the charge-matched 3CNC:1ChNF ratio that is indicative of a destabilization of the particles.

7.1.3 Chapter 5 Conclusions

- PVA aerogels incorporating 1 wt.% CNCs and 1 wt.% ChNFs do not increase the modulus and compression strength relative to neat PVA. However, tricomponent PVA aerogels have decreased the mechanical properties relative to neat PVA, which is indicative of the weakening of the internal pore structure.
- SEM images indicated that the average size of the pores increased with the introduction of nanofillers compared to that of neat PVA aerogels, while tricomponent composites appeared to change the structure of the aerogel from a 2D lamellar assembly of sheets to a 3D interconnected network.

7.1.4 Chapter 6 Conclusions

- An artificial intervertebral disc replacement was generated that possessed similar mechanical properties to that of natural human fibrocartilage. The utilization of different CNC/ChNF ratios in the aerogel and hydrogel components of this biomimetic hybrid device allow for a level of customization in the mechanical properties to a potential patient's needs, while also potentially providing cell growth points along the highly biocompatible CNCs and ChNFs.
- Materials generated for packaging applications including multilayer CNC/ChNF-coated PLA films and CNC/ChNF films without a polymer substrate exhibited increases in barrier and mechanical properties beyond that of what is capable by the utilization of single nanofillers. POM and atomic force microscopy results from these two studies provided evidence that electrostatic interactions between CNCs and ChNFs drive the formation of ordered CNCs along the surface of the ChNFs.

The goal of analyzing the three polymer constructs was to characterize each fully and piece together their collective information to generate an overall picture of how the nanofillers are interacting with one another within a selected polymer matrix, how this mechanism may be controlled, and how the impact on the polymer matrix changes across each construct. A series of characterization techniques including titration, zeta-potential, and multi angle light scattering experiments all indicated that the CNC/ChNF complexes were driven by electrostatic interactions and that CNC aggregation and ordering could be influenced by controlling the ratios of the two nanofillers. In the film and hydrogel studies, both systems showed an increase in mechanical properties with the 1CNC/4ChNF ratio that was not able to be achieved using singular nanofillers alone (i.e. 5CNC or 5ChNF). Specifically, the 1CNC/4ChNF films possessed a 43% increase in modulus compared to neat PVA, while 1CNC/4ChNF hydrogels possessed a 131% and 161% increase in modulus for 1FT and 7FT, respectively.

The reason for this increase in mechanical properties can be linked to the formation of CNC/ChNF/PVA complexes generated by physical and electrostatic interactions. In the preparation of the tricomponent composites, the PVA solution was always first protonated with acetic acid in order to encourage the dispersion of the ChNFs that were always added prior to the CNCs. Rheological studies provided evidence that the longer ChNFs possessed a greater amount of entanglement with the PVA molecular chains than the shorter CNCs. Additionally, the ChNF/CNC film paper showed through AFM imaging that the CNCs align themselves along the surface of the ChNFs, and that this alignment and ordering decreases at lower ratios of CNCs, particularly lowest at the 1CNC:3ChNF ratio. This reduction in CNC aggregation and ordering with the use of ChNFs was also previously

shown with polarized optical microscopy (POM) in both the tricomponent PVA films[2] and CNC/ChNF mixed films.[55] Nakagaito et al. (2018) previously showed that the tricomponent composites of CNFs, CHNFs, and PLA mechanically outperformed CNFs or ChNFs alone, where they suggested that ChNFs act compatibilizer between hydrophobic PLA and the hydrophilic CNFs.[126] A similar mechanism could be occurring in this work, where CNCs bound along the surface of the ChNFs, which then allow for a connection between the hydrophobic ChNFs and the hydrophilic PVA. Another study by Bian et al. (2018) showed that physically entangled CNFs within a PVA matrix could be partially linked by lignin molecules, thus increasing the interconnectivity between the CNF chains and increasing the mechanical properties beyond that of CNFs alone.[118] Again, this mechanism could also be taking place between the oppositely charged CNCs and ChNFs, where bound CNCs may be able to allow additional structure formation between the ChNFs while in the PVA solution, allowing for additional degrees of entanglement. Altogether, these mechanisms may explain the high-performance ratio of 1CNC/4ChNF for both the films and hydrogels, where nanostructure formation between the CNCs, ChNFs, and PVA matrix allow for increased compatibility and reinforcement. Furthermore, the large scale aggregation behavior at the charge-matched 3CNC:1ChNF ratio suggested that this aggregation creates a poor dispersion in PVA composites, which may generate points of failure within the composite that negatively impacts the properties relative to other composites as shown in both PVA films[2] and in the hydrogels. However, while the films and hydrogels exhibited an increase in mechanical properties with the 1CNC:4ChNF ratio, the aerogels saw a reduction in properties relative to neat PVA and single nanofiller composites. These results were explained by the larger pores of the tricomponent

composites that generated a 3D network structure that potentially allowed for easier collapse under force, which may have been the result of higher viscosities slowing the ice crystal growth rates thus increasing overall ice crystal size during freezing. The difference in results may be also linked to the inability for nanoparticle rearrangement due to the freeze-thawing process. It is possible that the air-drying and thawing aspects of the film and hydrogel constructs, respectively, is essential for allowing for the formation of nanofiller network structures described with the light scattering, POM, and AFM analyses.

In conclusion, these highly customizable and biodegradable film, hydrogel, and aerogel structures were constructed, which opens avenues in the applications towards packaging materials, biomedical devices, or any industry aiming to decrease their environmental impact. Additionally, this work contributed to the understanding of the processing-structure-property relationship between multiple materials and how the electrostatic forces within a composite system can be manipulated to achieve more desirable properties. Lastly, this work contributes to developing applications for nanocellulose and nanochitin composites, further advancing the potential for these renewable, abundant, and high-performance nanomaterials.

7.2 Recommendations for Future Work

7.2.1 Additional Characterization of CNC/ChNF/PVA Tricomponent Composites

Additional characterization techniques could be utilized in order to more fully understand the interactions between the CNCs, ChNFs, and PVA matrix. Cryogenic Electron Microscopy (cryo-EM) is currently being conducted in order to freeze the hydrogels and PVA solutions and study the internal structure of the materials more directly. Provided that the constituent materials do not degrade under the electron beam, it could be possible to see the formation of the CNC/ChNF aggregate structures and how the particles disperse throughout the PVA matrix. Another characterization technique could include asymmetric flow field flow fractionation measurements, which would allow for the measurement of aggregate mass coupled with light scattering measurements. This type of analysis was previously performed on CNCs alone,[149-150] though the characterization of ChNFs or CNC/ChNF aggregates utilizing this technique has yet to be performed.

In addition to physical characterization techniques, computational modelling could be used to assess the movement of the molecular components of the composites while in solution. It would be possible to model the PVA molecular chains within a confined water chamber, followed by the addition of charged acetic acid particles, then ChNFs with an assigned cationic charge, and then CNCs with an assigned anionic charge. This type of analysis could lead to a sophisticated simulation tool for analyzing different processing conditions and their effects on the overall system. For instance, through this modelling it would be possible to computationally simulate how different surface charges influence the

aggregation behavior of the individual particles or how the particles may react to different ratios or acid treatments.

7.2.2 Modifying Processing Steps

The development of each of the constructs started with the same processing steps to maintain uniformity across all the tested samples. To briefly reiterate the tricomponent composite solution steps outlined in previous chapters, the PVA solution was prepared by dissolving PVA into water, cooling to below 50 °C, then adding 1 vol.% acetic acid to protonate the solution, followed by ChNFs addition, and finishing with CNCs addition. There was no variation in this process throughout the generation of the different construct composites, therefore it is recommended that future work include changing the order of the steps or slightly changing the methodology of each step. For instance, adding the CNCs prior to the ChNFs may result in a worse dispersion of the CNC particles where there are no ChNF particles to electrostatically bind to. Additionally, as discussed in chapter 6, it is possible to generate ChNFs of different degrees of acetylation (DA) which impact the charge on the surface of the particles, so varying the source and DA of ChNFs could be a potential avenue for further tuning the aggregation behavior of CNCs and ChNFs. Another potential change could include maintaining the elevated temperature of the PVA solution during the addition of nanofillers or adding a stronger acid than acetic acid to the solution to lower the pH even further.

7.2.3 Additional IVD Generation and Characterization

The artificial IVD developed in chapter 6 acts as a proof-of-concept that artificial fibrocartilage can be generated from a PVA hydrogel and aerogel interconnected material that is highly tunable with the addition of renewable nanofillers. However, due to processing limitations regarding freeze-dryer complications, additional artificial IVDs of different shapes and sizes could not be generated and tested. Therefore, it is recommended that changes in the processing of the IVDs be made that are suggested to improve the mechanical capabilities. And while decreasing the size of the aerogel/hydrogel composite material may increase the mechanical properties to that necessary for thoracic and cervical IVD devices, additional processing changes may be necessary. Therefore, it is recommended that the PVA content of the aerogels be increased above 5 wt.%, which would create a stiffer outer structure.

Additionally, the viability of any medical device would require time-intensive testing including rotational studies, fatigue testing, and cell studies, among other tests. Additionally, any further mechanical testing would have to be performed under proper body conditions, particularly with the compression plates submerged in a water or other aqueous solution held at 37 °C. This would mimic the conditions that the IVD would be expected to perform, which may be influenced by the surrounding liquid. Additionally, cell studies on the hydrogel/aerogel complex with and without the nanofillers should be performed in order to assess the level of cell growth possible and whether or not the addition of the nanofillers aids in the development of cell growth. The importance of the material properly adhering to the surrounding tissue after implementation is paramount and would ultimately drive whether the device could be applied in its current state.

7.2.4 Further Studying Multi-Construct Materials

The multi-construct hybrid aerogel/hydrogel material described in chapter 6 for the development of an artificial IVD appears to be the first of its kind for its application. Therefore, the further study of multi-construct materials and how one construct positively influences the other could potentially lead to a variety of unique devices. For instance, it is possible that applying the proper film-like coating along the surface of the aerogel/hydrogel could provide additional biocompatibility or slow bacterial growth, in addition to potentially slowing dehydration of the hydrogel component of the IVD. Another possibility is combining separate polymers (one for the aerogel, another for the hydrogel) to generate a stiffer outer aerogel region for larger loads. Additionally, materials consisting of alternating layers of films, hydrogels, and/or aerogels may be of interest to generate shock absorption materials, where each layer can incorporate different types or amounts of nanofillers to modulate the overall properties.

APPENDIX A. PVA FILM, HYDROGEL, AND AEROGEL

SUPPLEMENTARY DATA

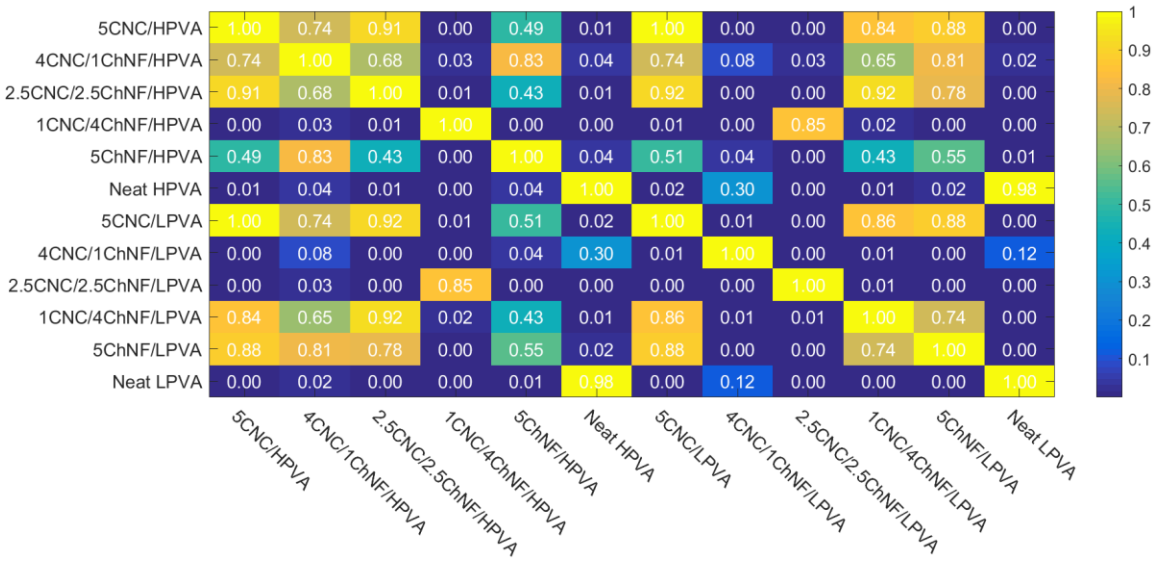

Figure A.1 Modulus statistical map showing comparisons between all data sets using a two-tailed Student's T-Test (alpha = 0.05).

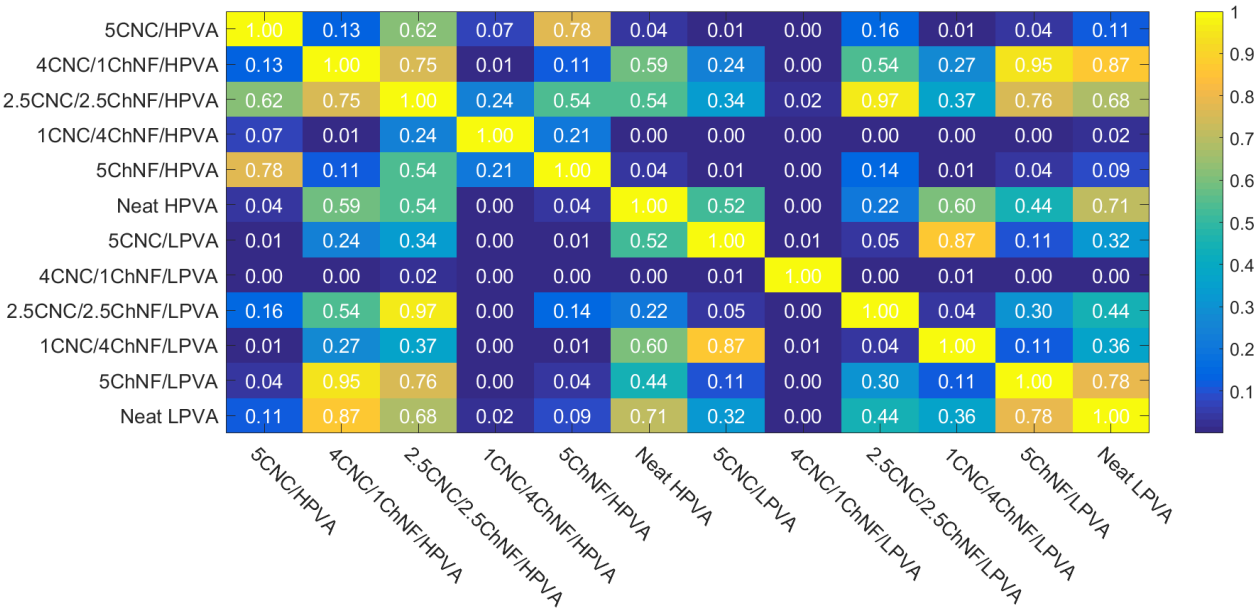

Figure A.2 Tensile strength statistical map showing comparisons between all data sets using a two-tailed Student's T-Test (alpha = 0.05).

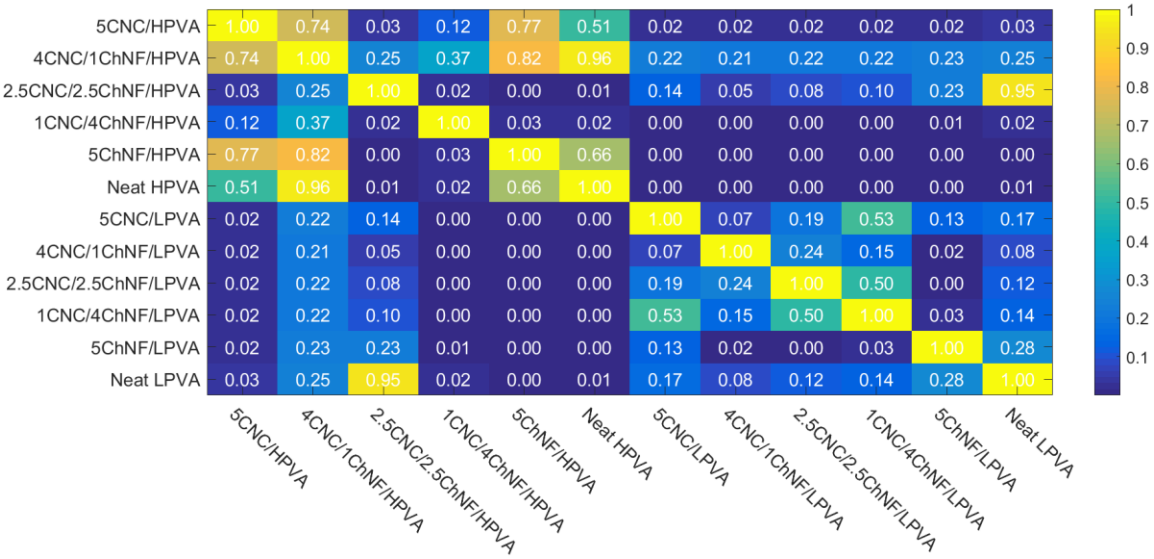

Figure A.3 Strain at break statistical map showing comparisons between all data sets using a two-tailed Student's T-Test (alpha = 0.05).

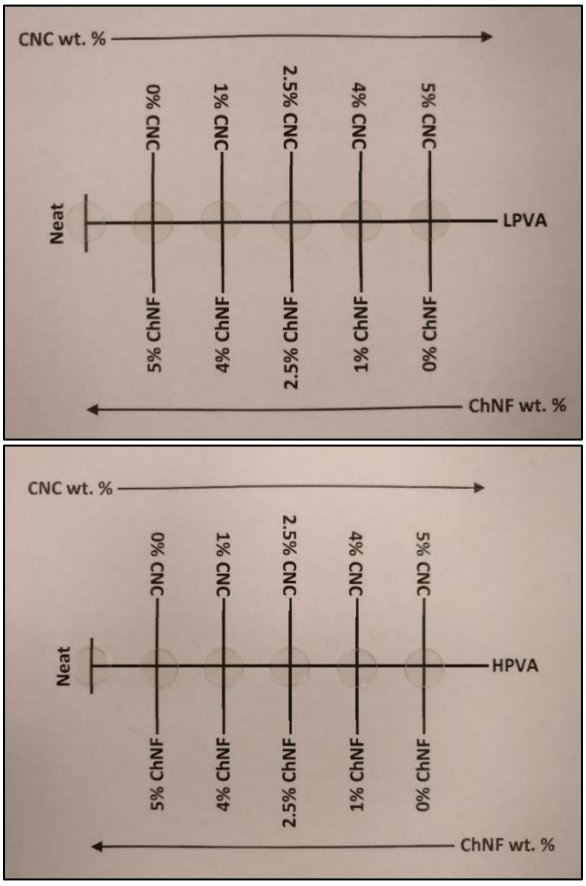

Figure A.4 Disks of approximately 7 mm in diameter of neat PVA and nanocomposite samples.

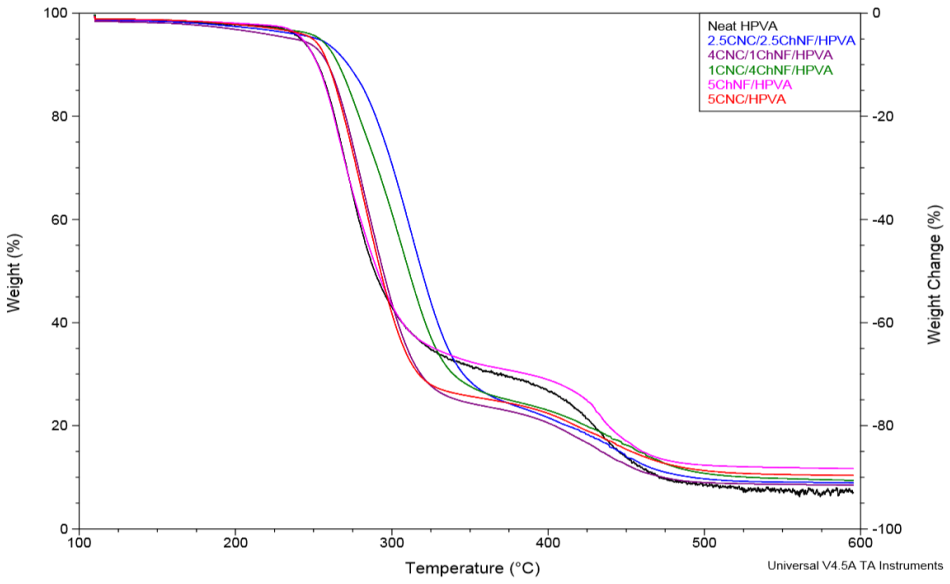

Figure A.5 Thermogravimetric Analysis of HPVA at various 5 wt.% loadings of CNC/ChNF.

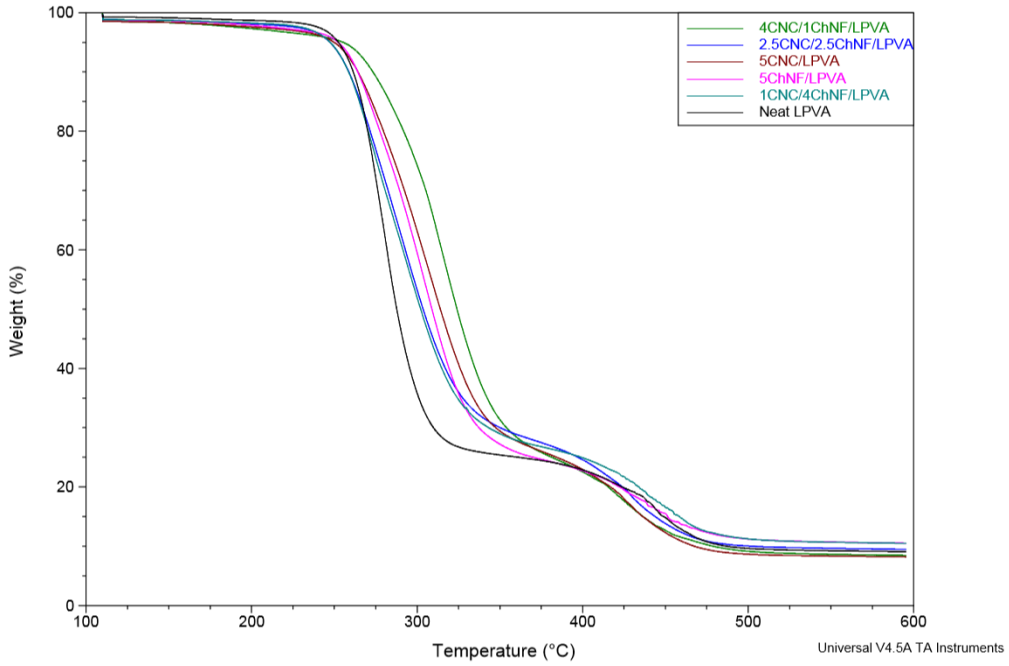

Figure A.6 Thermogravimetric Analysis of LPVA at various 5 wt.% loadings of CNC/ChNF.

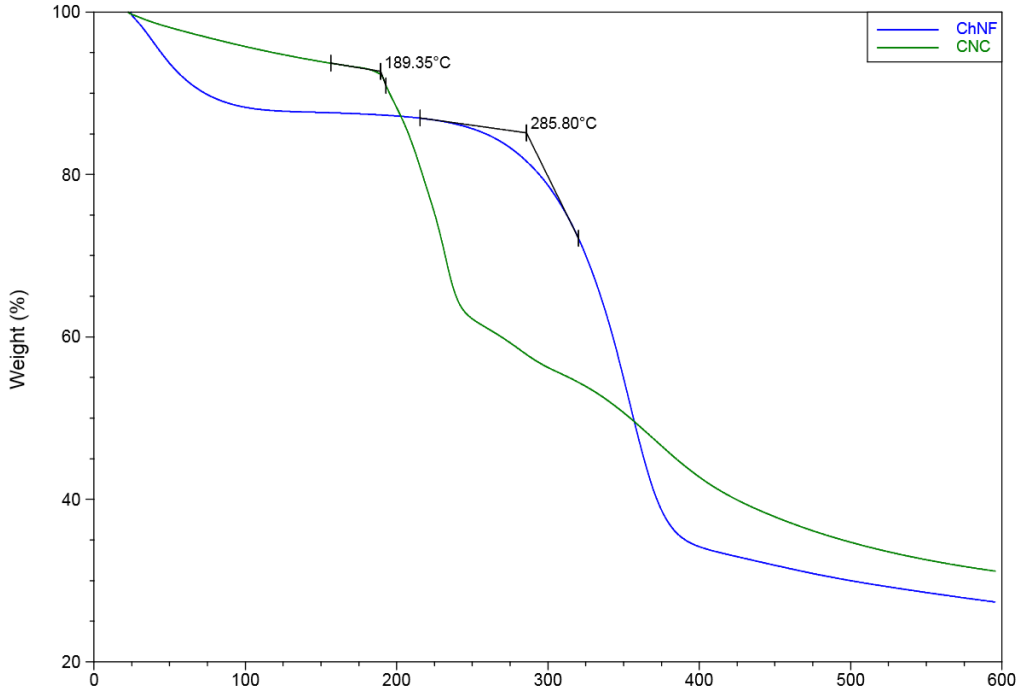

Figure A.7 Thermogravimetric Analysis of CNC and ChNF.

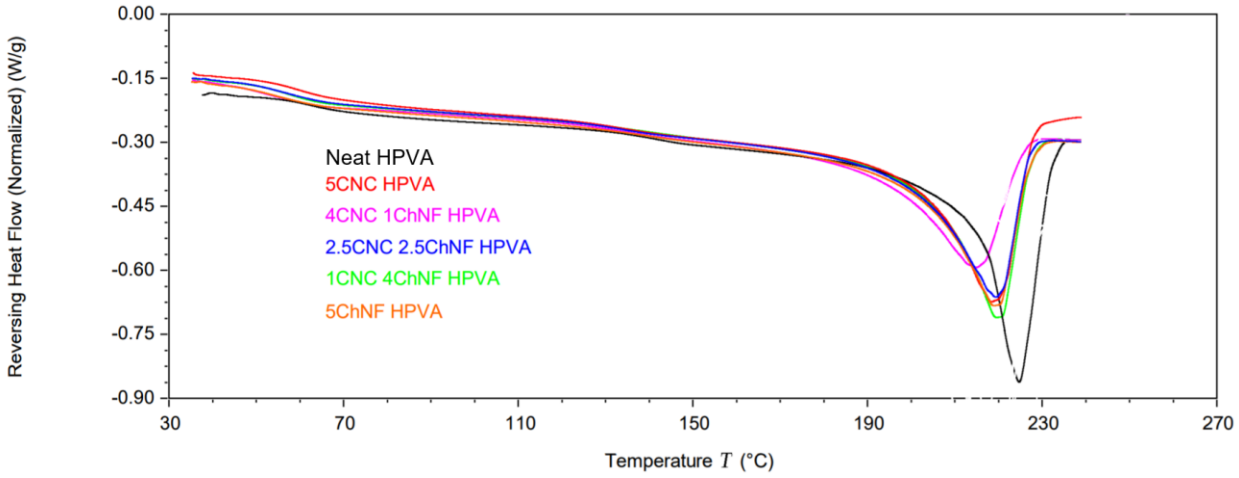

Figure A.8 Differential Scanning Calorimetry analysis of the largest melting peak for each of the six HPVA samples.

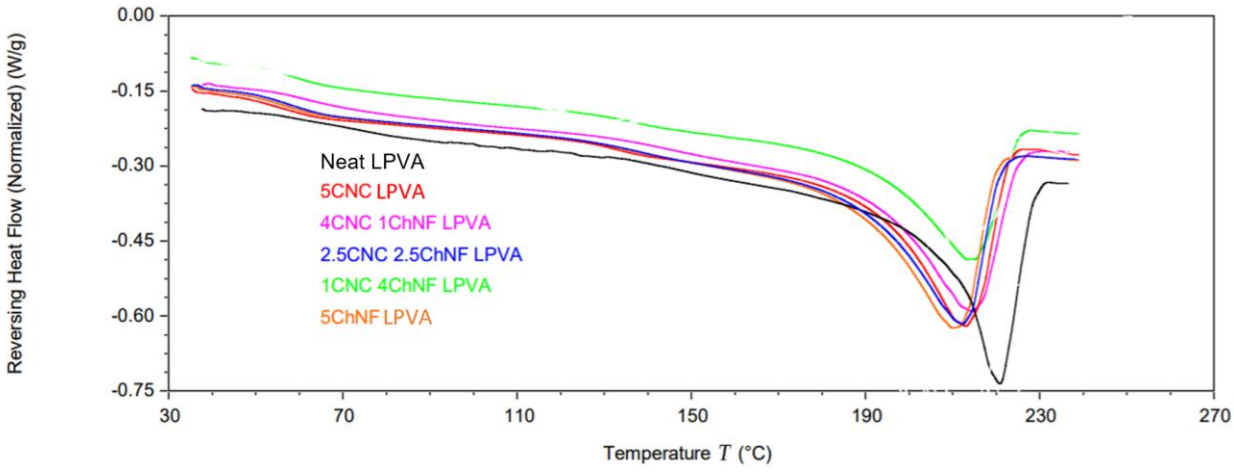

Figure A.9 Differential Scanning Calorimetry analysis of the largest melting peak for each of the six LPVA samples.

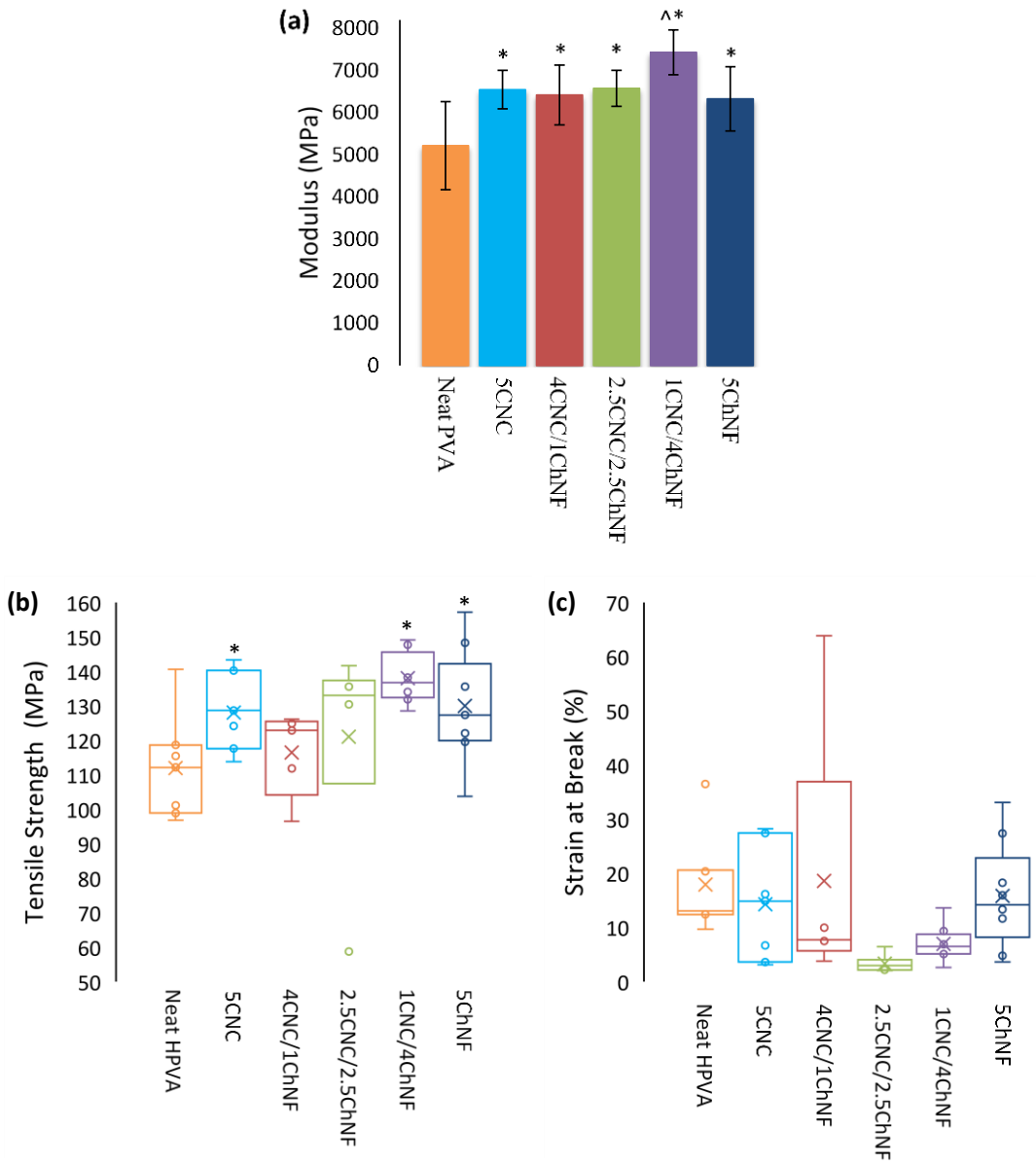

Figure A.10. (a) Modulus, (b) tensile strength, and (c) strain at break of HPVA-based samples. In box plots of (b) and (c), individual values marked by a circle, while an X indicates the average value, and the upper, middle, and lower lines of the box indicate third, second (median), and first quartile, respectively. Sample set averages that are statistically significantly greater than the neat PVA film are indicated with an *, while a ^ indicates a sample set average that is statistically significantly greater than all other values.

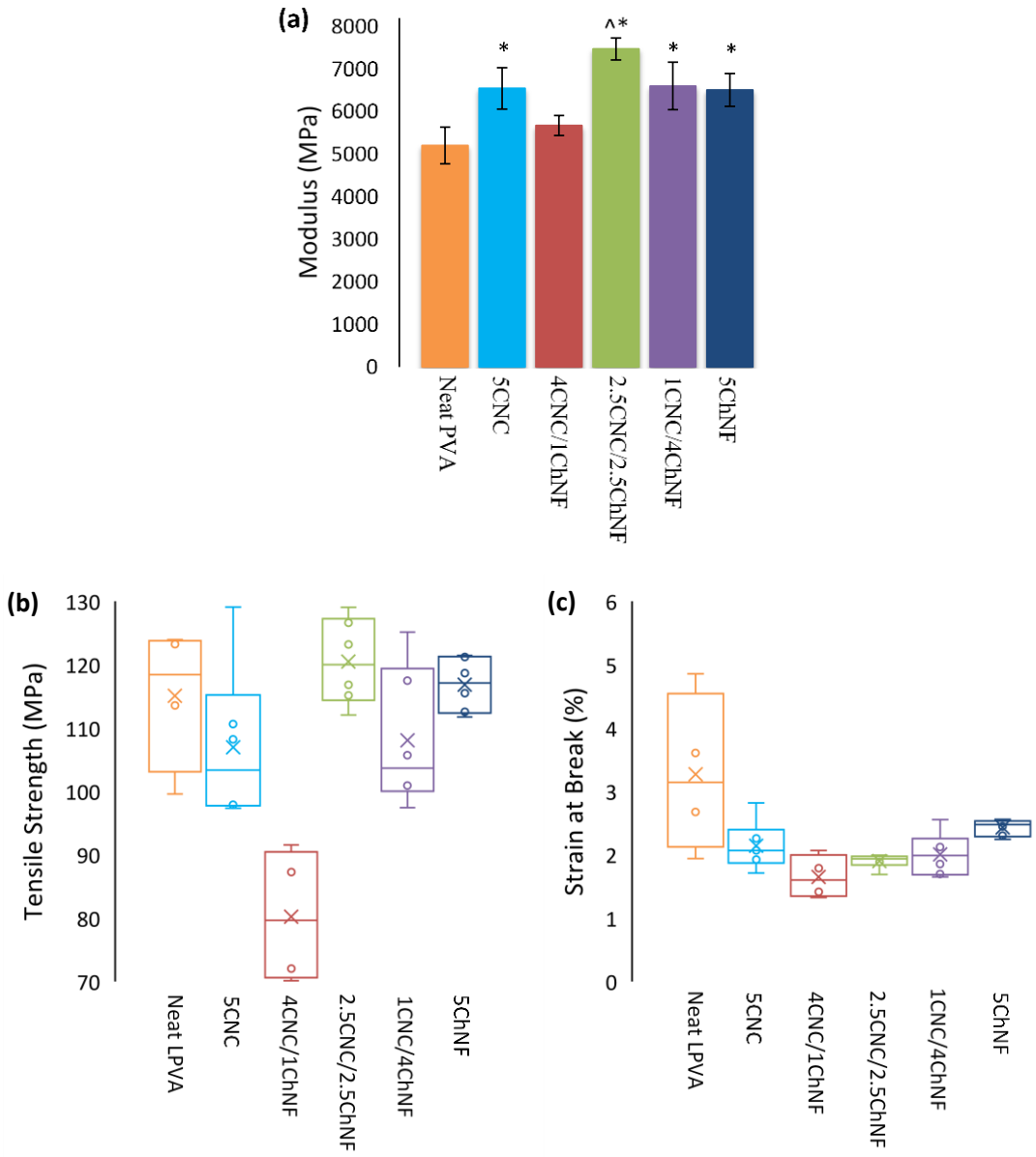

Figure A.11 (a) Modulus, (b) tensile strength, and (c) strain at break of LPVA-based samples. In box plots of (b) and (c), individual values marked by a circle, while an X indicates the average value, and the upper, middle, and lower lines of the box indicate third, second (median), and first quartile, respectively. Sample set averages that are statistically significantly greater than the neat PVA film are indicated with an *, while a ^ indicates a sample set average that is statistically significantly greater than all other values.

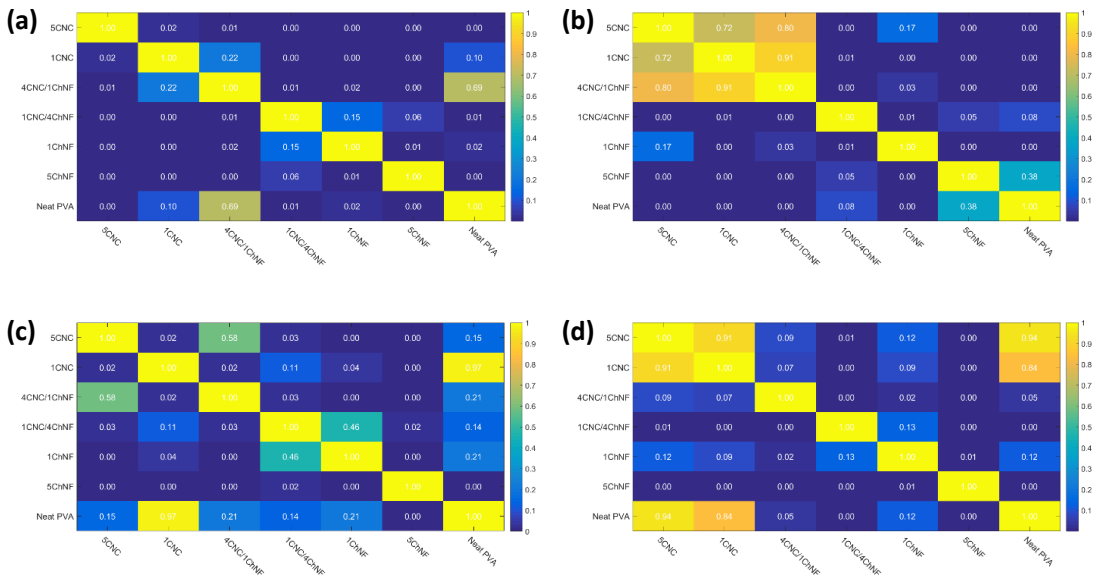

Figure A.12 Water absorption after 6 hours statistical map for (a) 1FT, (b) 3FT, and (c) 5FT, and (d) 7FT PVA hydrogels showing comparisons of all data sets using a two-tailed Student's T-Test (alpha = 0.05).

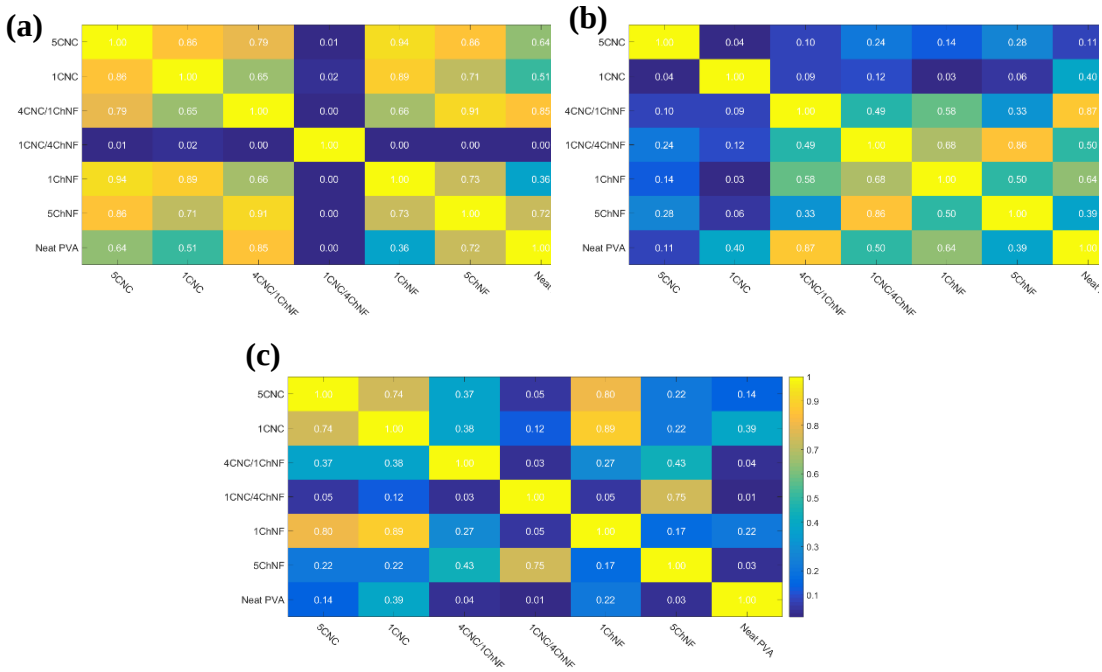

Figure A.13 Modulus statistical map of (a) 1FT, (b) 3FT, and (c) 7FT PVA hydrogels showing comparisons of all data sets using a two-tailed Student's T-Test (alpha = 0.05).

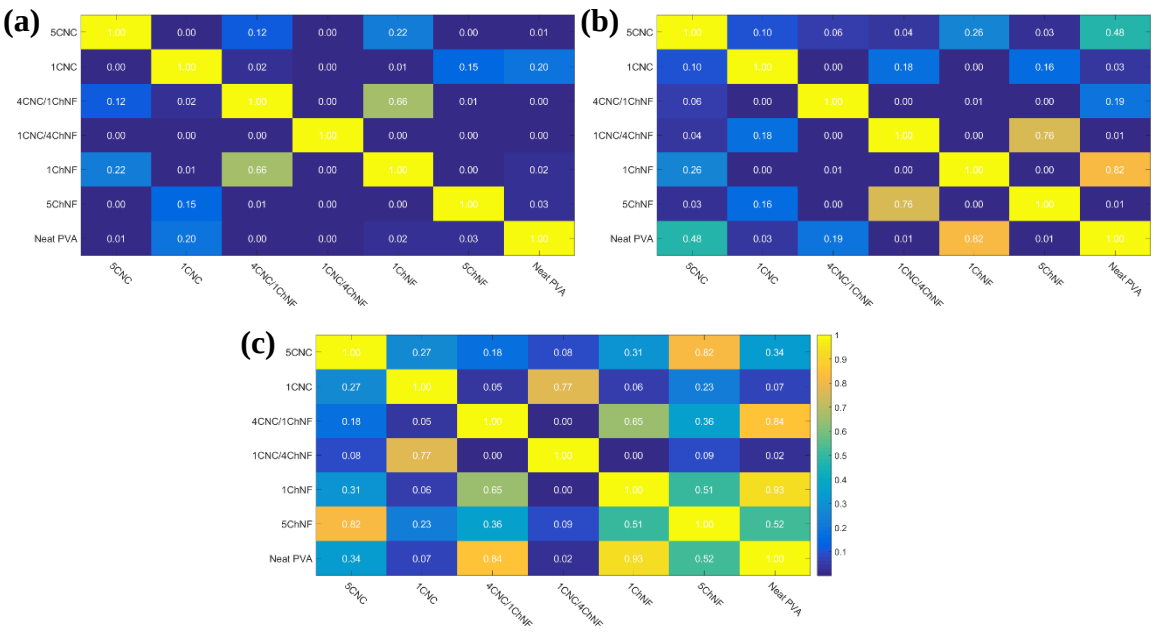

Figure A.14 Compression stress at 50% strain statistical map of (a) 1FT, (b) 3FT, and (c) 7FT PVA hydrogels showing comparisons of all data sets using a two-tailed Student's T-Test (alpha = 0.05).

Table A.1 Compressive modulus and stress at 50% strain statistical comparisons of 1FT, 3FT, and 7FT PVA hydrogels showing comparison p-values calculated using a two-tailed Student's T-Test (alpha = 0.05). Red coloration indicates no statistical difference, while green coloration indicates statistical difference between sets.

	1FT vs. 3FT		3FT vs. 7FT	
	Modulus	**Stress @ 50% Strain**	**Modulus**	**Stress @ 50% Strain**
Neat PVA	0.00	0.00	0.92	0.00
1CNC	0.00	0.00	0.26	0.00
5CNC	0.00	0.00	0.35	0.00
1ChNF	0.00	0.00	0.17	0.00
5ChNF	0.00	0.00	0.03	0.01
1CNC/4ChNF	0.00	0.00	0.00	0.00
4CNC/1ChNF	0.00	0.00	0.00	0.00

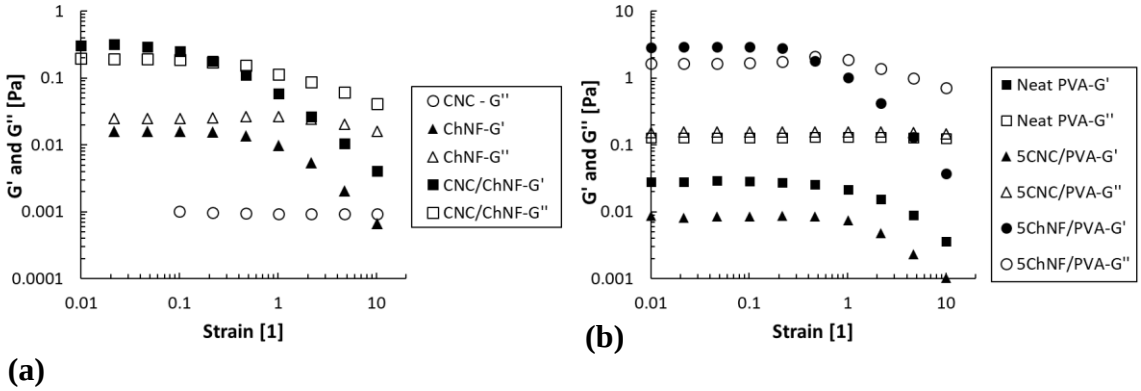

Figure A.15 Amplitude sweeps were performed on (a) nanofiller suspensions and (b) composite suspensions to determine the linear viscoelastic region.

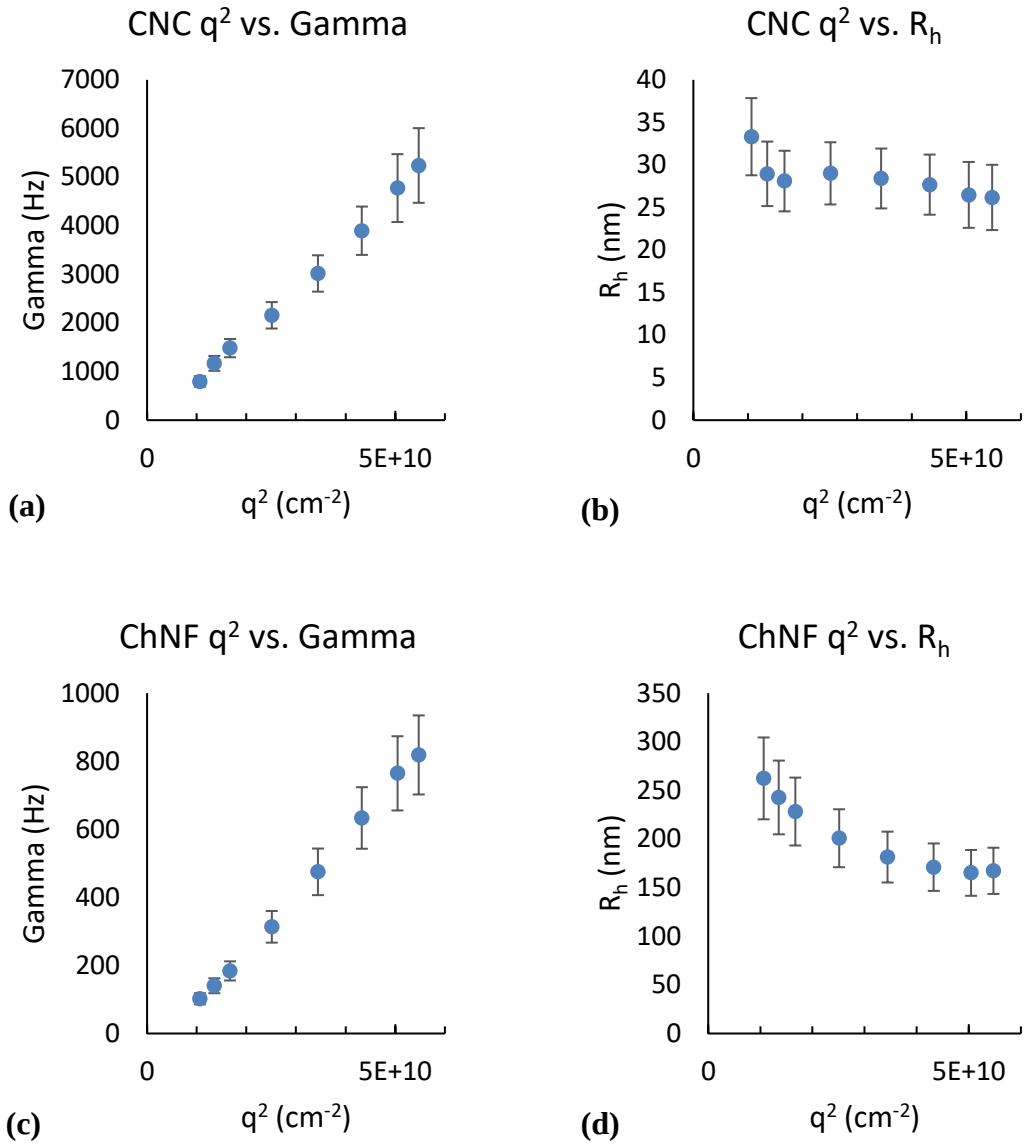

Figure A.16 Graphs showing q2 vs. Gamma values for (a) CNCs and (c) ChNFs, as well as q2 vs. Rh for (b) CNCs and (d) ChNFs.

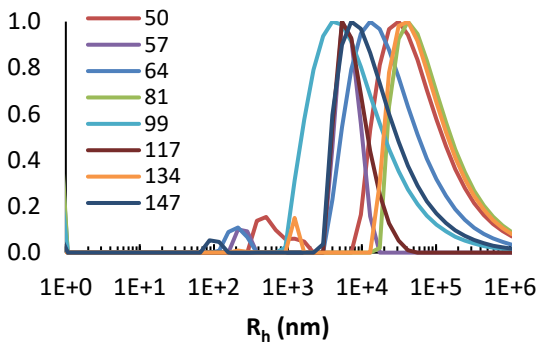

Figure A.17 Multiangle dynamic light scattering displaying hydrodynamic radius curves for suspension of 3CNC:1ChNF. Y-axis is a normalized intensity.

Percolation Threshold Measurements

In order to calculate the percolation threshold, the following equation was used:

$$V_c = \frac{0.7}{l/d}$$

In this equation, V_c is the volume fraction percolation threshold, l is the particle length, and d is the particle diameter, in which l/d represents the aspect ratio. The length of the CNCs are approximately 138 nm ± 22 nm with a width of 6.4 nm ± 0.6 nm as determined by a previous study,[58] for upper and lower aspect ratios of 28 and 17, respectively, and a resulting percolation threshold range of 2.5 – 4.1 vol.%. The width of the ChNFs produced through high-shear treatment is approximately 10 – 20 nm, while the literature reported lengths of ChNFs can vary from hundreds of nanometers to several microns.[81-82] Due to this, a length range of 200 nm to 2000 nm was chosen for the purpose of these calculations. These lengths and widths resulted in a wide range of aspect ratios of approximately 10 to

200 and a resulting percolation threshold range of 0.35 – 7 vol.%. In order to assess whether the prepared samples fell above or below this threshold, the following equation was used to convert their mass fractions to volume fractions:

$$V_f = \left(\frac{\rho_m}{\rho_f * \left(\frac{1}{m_f} - 1 \right) + \rho_m} \right)$$

In this equation, V_f is the volume fraction, ρ_m is the matrix density, ρ_f is the filler density, and m_f is the filler mass fraction. The densities used were 1.6 g/cm^3 for CNCs,[30] 1.425 g/cm^3 for ChNFs,[144] and 1.26 g/cm^3 for PVA.[176] The following were the mass to volume fraction values: 1CNC was 0.79 vol.%, 5CNC was 3.9 vol.%, 1ChNF was 0.88 vol.%, and 5ChNF was 3.5 vol.%. This resulted in 1CNC falling below the percolation threshold range, while 5CNC was within the range. This indicates that it was above a critical value where the CNCs were beginning to come in contact, which could explain the decrease in mechanical properties with the increase from 1CNC to 5CNC. However, given the wide variance in possible fiber lengths, 1ChNF and 5ChNF both fell within their wide percolation threshold range indicating they may be contacting each other within the hydrogel matrix.

0.2CNC/0.8ChNF Hydrogel Generation for Aerogel Comparison

Given the disparity between 1CNC:4ChNF ratio's improvement in properties in films and hydrogels and decrease in properties in aerogels, a 0.2CNC/0.8ChNF hydrogel sample was prepared and tested, then compared to 1CNC and 1ChNF hydrogels. The

results are displayed in Table A.2 below. For 1FT, 0.2CNC/0.8ChNF was shown to have a lower modulus value than both 1CNC and 1ChNF, which was also lower than any other hydrogel sample set from chapter 4. However, for 3FT, 5FT, and 7FT, 0.2CNC/0.8ChNF had a larger modulus than both 1CNC and 1ChNF, as well as the 3rd highest, highest, and 2nd highest modulus of the tested 3FT, 5FT, and 7FT hydrogel sets, respectively. For compressive stress at 50% strain, 0.2CNC/0.8ChNF never had a larger value than 1CNC, though it was higher than 1ChNF for 3FT, 5FT, and 7FT. The 1FT samples are closest to the methodology that produced the low-performance aerogel samples, so their 2nd lowest compressive stress (ahead of 5CNC) and lowest modulus for this FT cycle is consistent with these properties.

Table A.2 Mechanical properties of 0.2CNC/0.8ChNF hydrogel relative to 1CNC and 1ChNF. * indicates statistical difference from 1CNC, while ^ indicates statistical difference from 1ChNF.

		1CNC	**1ChNF**	**0.2CNC/0.8ChNF**
1FT	**Modulus (kPa)**	0.95 (± 0.52)	0.91 (± 0.28)	0.68 (± 0.28)
	Stress (kPa)	2.79 (± 0.44)	2.01 (± 0.30)	1.78 (± 0.24)*
3FT	**Modulus (kPa)**	5.36 (± 0.77)	6.57 (± 0.69)	6.91 (± 1.4)
	Stress (kPa)	28.3 (± 1.1)	22.7 (± 1.1)	24.1 (± 2.7)*
5FT	**Modulus (kPa)**	10.5 (± 5.0)	8.66 (± 2.4)	13.6 (± 3.7)^
	Stress (kPa)	63.8 (± 9.6)	41.2 (± 3.7)	51.1 (± 7.3)*^
7FT	**Modulus (kPa)**	9.37 (± 6.9)	9.91 (± 4.4)	15.1 (± 4.6)
	Stress (kPa)	69.5 (± 13.8)	53.6 (± 7.0)	64.6 (± 9.6)

REFERENCES

1. Zhang, Q.; Huang, J.-Q.; Qian, W.-Z.; Zhang, Y.-Y.; Wei, F., The Road for Nanomaterials Industry: A Review of Carbon Nanotube Production, Post-Treatment, and Bulk Applications for Composites and Energy Storage. *Small* **2013,** *9* (8), 1237-1265.

2. Irvin, C. W.; Satam, C. C.; Carson Meredith, J.; Shofner, M. L., Mechanical Reinforcement and Thermal Properties of PVA Tricomponent Nanocomposites with Chitin Nanofibers and Cellulose Nanocrystals. *Composites, Part A* **2019**.

3. Jonoobi, M.; Harun, J.; Mathew, A. P.; Oksman, K., Mechanical properties of cellulose nanofiber (CNF) reinforced polylactic acid (PLA) prepared by twin screw extrusion. *Compos. Sci. Technol.* **2010,** *70* (12), 1742-1747.

4. Koronis, G.; Silva, A.; Fontul, M., Green composites: A review of adequate materials for automotive applications. *Composites, Part B* **2013,** *44* (1), 120-127.

5. Fortunati, E.; Puglia, D.; Monti, M.; Santulli, C.; Maniruzzaman, M.; Kenny, J. M., Cellulose nanocrystals extracted from okra fibers in PVA nanocomposites. *J. Appl. Polym. Sci.* **2013,** *128* (5), 3220-3230.

6. Peng, Z.; Kong, L. X., A thermal degradation mechanism of polyvinyl alcohol/silica nanocomposites. *Polym. Degrad. Stab.* **2007,** *92* (6), 1061-1071.

7. Qian, D.; Dickey, E. C.; Andrews, R.; Rantell, T., Load transfer and deformation mechanisms in carbon nanotube-polystyrene composites. *Appl. Phys. Lett.* **2000,** *76* (20), 2868-2870.

8. Zhang, L.; Wang, Z.; Xu, C.; Li, Y.; Gao, J.; Wang, W.; Liu, Y., High strength graphene oxide/polyvinyl alcohol composite hydrogels. *Journal of Materials Chemistry* **2011,** *21* (28), 10399-10406.

9. Mittal, V.; Kim, S.; Neuhofer, S.; Paulik, C., Polyethylene/graphene nanocomposites: effect of molecular weight on mechanical, thermal, rheological and morphological properties. *Colloid and Polymer Science* **2016,** *294* (4), 691-704.

10. Can, V.; Abdurrahmanoglu, S.; Okay, O., Unusual swelling behavior of polymer–clay nanocomposite hydrogels. *Polymer* **2007,** *48* (17), 5016-5023.

11. Johnson, J. R.; Spikowski, J.; Schiraldi, D. A., Mineralization of Clay/Polymer Aerogels: A Bioinspired Approach to Composite Reinforcement. *ACS Applied Materials & Interfaces* **2009,** *1* (6), 1305-1309.

12. Kokabi, M.; Sirousazar, M.; Hassan, Z. M., PVA–clay nanocomposite hydrogels for wound dressing. *Eur. Polym. J.* **2007,** *43* (3), 773-781.

13. Mohanty, A. K.; Misra, M.; Drzal, L. T., Sustainable Bio-Composites from Renewable Resources: Opportunities and Challenges in the Green Materials World. *Journal of Polymers and the Environment* **2002,** *10* (1), 19-26.

14. Fortunati, E.; Peltzer, M.; Armentano, I.; Torre, L.; Jiménez, A.; Kenny, J. M., Effects of modified cellulose nanocrystals on the barrier and migration properties of PLA nano-biocomposites. *Carbohydr. Polym.* **2012,** *90* (2), 948-956.

15. Siracusa, V.; Rocculi, P.; Romani, S.; Rosa, M. D., Biodegradable polymers for food packaging: a review. *Trends Food Sci. Technol.* **2008,** *19* (12), 634-643.

16. Abdul Khalil, H. P. S.; Bhat, A. H.; Ireana Yusra, A. F., Green composites from sustainable cellulose nanofibrils: A review. *Carbohydr. Polym.* **2012,** *87* (2), 963-979.

17. Raquez, J. M.; Deléglise, M.; Lacrampe, M. F.; Krawczak, P., Thermosetting (bio)materials derived from renewable resources: A critical review. *Prog. Polym. Sci.* **2010,** *35* (4), 487-509.

18. Flieger, M.; Kantorová, M.; Prell, A.; Řezanka, T.; Votruba, J., Biodegradable plastics from renewable sources. *Folia Microbiol.* **2003,** *48* (1), 27.

19. Peng, J.; Cheng, Q., High-Performance Nanocomposites Inspired by Nature. *Adv Mater* **2017,** *29* (45), 1702959.

20. Srinivasa, P. C.; Tharanathan, R. N., Chitin/Chitosan — Safe, Ecofriendly Packaging Materials with Multiple Potential Uses. *Food Rev. Int.* **2007,** *23* (1), 53-72.

21. Yang, W.; Owczarek, J. S.; Fortunati, E.; Kozanecki, M.; Mazzaglia, A.; Balestra, G. M.; Kenny, J. M.; Torre, L.; Puglia, D., Antioxidant and antibacterial lignin nanoparticles in polyvinyl alcohol/chitosan films for active packaging. *Industrial Crops and Products* **2016,** *94*, 800-811.

22. Jayakumar, R.; Menon, D.; Manzoor, K.; Nair, S. V.; Tamura, H., Biomedical applications of chitin and chitosan based nanomaterials—A short review. *Carbohydr. Polym.* **2010,** *82* (2), 227-232.

23. Lin, N.; Dufresne, A., Nanocellulose in biomedicine: Current status and future prospect. *Eur. Polym. J.* **2014,** *59*, 302-325.

24. Jalal Uddin, A.; Araki, J.; Gotoh, Y., Toward "Strong" Green Nanocomposites: Polyvinyl Alcohol Reinforced with Extremely Oriented Cellulose Whiskers. *Biomacromolecules* **2011,** *12* (3), 617-624.

25. Baker, M. I.; Walsh, S. P.; Schwartz, Z.; Boyan, B. D., A review of polyvinyl alcohol and its uses in cartilage and orthopedic applications. *J. Biomed. Mater. Res., Part B* **2012,** *100B* (5), 1451-1457.

26. Ben Halima, N., Poly(vinyl alcohol): review of its promising applications and insights into biodegradation. *RSC Advances* **2016,** *6* (46), 39823-39832.

27. Xiao, Y.; Friis, E. A.; Gehrke, S. H.; Detamore, M. S., Mechanical Testing of Hydrogels in Cartilage Tissue Engineering: Beyond the Compressive Modulus. *Tissue Engineering. Part B, Reviews* **2013,** *19* (5), 403-412.

28. Ribeiro, M. V.; Moreira, M. R. V.; Ferreira, J. R., Optimization of titanium alloy (6Al–4V) machining. *Journal of Materials Processing Technology* **2003,** *143-144*, 458-463.

29. Evans, N. T.; Irvin, C. W.; Safranski, D. L.; Gall, K., Impact of surface porosity and topography on the mechanical behavior of high strength biomedical polymers. *Journal of the Mechanical Behavior of Biomedical Materials* **2016,** *59*, 459-473.

30. Moon, R. J.; Martini, A.; Nairn, J.; Simonsen, J.; Youngblood, J., Cellulose nanomaterials review: structure, properties and nanocomposites. *Chem. Soc. Rev.* **2011,** *40* (7), 3941-3994.

31. Dufresne, A., Nanocellulose: a new ageless bionanomaterial. *Materials Today* **2013,** *16* (6), 220-227.

32. Nechyporchuk, O.; Belgacem, M. N.; Bras, J., Production of cellulose nanofibrils: A review of recent advances. *Industrial Crops and Products* **2016,** *93*, 2-25.

33. Eichhorn, S. J., Cellulose nanowhiskers: promising materials for advanced applications. *Soft Matter* **2011,** *7* (2), 303-315.

34. Hubbe, M. A.; Rojas, O. J.; Lucia, L. A.; Sain, M., CELLULOSIC NANOCOMPOSITES: A REVIEW. *2008* **2008,** *3* (3), 52.

35. Mariano, M.; El Kissi, N.; Dufresne, A., Cellulose nanocrystals and related nanocomposites: Review of some properties and challenges. *J. Polym. Sci., Part B: Polym. Phys.* **2014,** *52* (12), 791-806.

36. Abitbol, T.; Kloser, E.; Gray, D. G., Estimation of the surface sulfur content of cellulose nanocrystals prepared by sulfuric acid hydrolysis. *Cellulose* **2013,** *20* (2), 785-794.

37. Boldizar, A., Prehydrolyzed Cellulose as Reinforcing Filler for Thermoplastics. *Int. J. Polym. Mater. Polym. Biomater.* **1987,** *11* (4), 229-262.

38. Roman, M.; Winter, W. T., Effect of Sulfate Groups from Sulfuric Acid Hydrolysis on the Thermal Degradation Behavior of Bacterial Cellulose. *Biomacromolecules* **2004,** *5* (5), 1671-1677.

39. Junior de Menezes, A.; Siqueira, G.; Curvelo, A. A. S.; Dufresne, A., Extrusion and characterization of functionalized cellulose whiskers reinforced polyethylene nanocomposites. *Polymer* **2009,** *50* (19), 4552-4563.

40. Maia, T. H. S.; Larocca, N. M.; Beatrice, C. A. G.; de Menezes, A. J.; de Freitas Siqueira, G.; Pessan, L. A.; Dufresne, A.; França, M. P.; de Almeida Lucas, A., Polyethylene cellulose nanofibrils nanocomposites. *Carbohydr. Polym.* **2017,** *173*, 50-56.

41. Chazeau, L.; Cavaillé, J. Y.; Canova, G.; Dendievel, R.; Boutherin, B., Viscoelastic Properties of Plasticized PVC Reinforced with Cellulose Whiskers. *J. Appl. Polym. Sci.* **1999,** *71* (11), 1797-1808.

42. Kaczmarek, H.; Bajer, K.; Podgórski, A., Properties of Poly(vinyl chloride) Modified by Cellulose. *Polymer Journal* **2005,** *37* (5), 340-349.

43. Pei, A.; Malho, J.-M.; Ruokolainen, J.; Zhou, Q.; Berglund, L. A., Strong Nanocomposite Reinforcement Effects in Polyurethane Elastomer with Low Volume Fraction of Cellulose Nanocrystals. *Macromolecules* **2011,** *44* (11), 4422-4427.

44. Kupka, V.; Zhou, Q.; Ansari, F.; Tang, H.; Šlouf, M.; Vojtová, L.; Berglund, L. A.; Jančář, J., Well-dispersed polyurethane/cellulose nanocrystal nanocomposites synthesized by a solvent-free procedure in bulk. *Polymer Composites* **2019,** *40* (S1), E456-E465.

45. Rueda, L.; Saralegui, A.; Fernández d'Arlas, B.; Zhou, Q.; Berglund, L. A.; Corcuera, M. A.; Mondragon, I.; Eceiza, A., Cellulose nanocrystals/polyurethane nanocomposites. Study from the viewpoint of microphase separated structure. *Carbohydr. Polym.* **2013,** *92* (1), 751-757.

46. Liu, H.; Liu, D.; Yao, F.; Wu, Q., Fabrication and properties of transparent polymethylmethacrylate/cellulose nanocrystals composites. *Bioresource Technology* **2010,** *101* (14), 5685-5692.

47. Erbas Kiziltas, E.; Kiziltas, A.; Bollin, S. C.; Gardner, D. J., Preparation and characterization of transparent PMMA–cellulose-based nanocomposites. *Carbohydr. Polym.* **2015,** *127*, 381-389.

48. Boujemaoui, A.; Ansari, F.; Berglund, L. A., Nanostructural Effects in High Cellulose Content Thermoplastic Nanocomposites with a Covalently Grafted Cellulose–Poly(methyl methacrylate) Interface. *Biomacromolecules* **2019,** *20* (2), 598-607.

49. Azizi Samir, M. A. S.; Alloin, F.; Dufresne, A., Review of Recent Research into Cellulosic Whiskers, Their Properties and Their Application in Nanocomposite Field. *Biomacromolecules* **2005,** *6* (2), 612-626.

50. Mi, H.-Y.; Jing, X.; Peng, J.; Salick, M. R.; Peng, X.-F.; Turng, L.-S., Poly(ε-caprolactone) (PCL)/cellulose nano-crystal (CNC) nanocomposites and foams. *Cellulose* **2014,** *21* (4), 2727-2741.

51. Kvien, I.; Oksman, K., Orientation of cellulose nanowhiskers in polyvinyl alcohol. *Applied Physics A* **2007,** *87* (4), 641-643.

52. Leitner, J.; Hinterstoisser, B.; Wastyn, M.; Keckes, J.; Gindl, W., Sugar beet cellulose nanofibril-reinforced composites. *Cellulose* **2007,** *14* (5), 419-425.

53. Millon, L. E.; Wan, W. K., The polyvinyl alcohol–bacterial cellulose system as a new nanocomposite for biomedical applications. *J. Biomed. Mater. Res., Part B* **2006,** *79B* (2), 245-253.

54. Paralikar, S. A.; Simonsen, J.; Lombardi, J., Poly(vinyl alcohol)/cellulose nanocrystal barrier membranes. *J. Membr. Sci.* **2008,** *320* (1), 248-258.

55. Satam, C. C.; Irvin, C. W.; Coffey, C. J.; Geran, R. K.; Ibarra-Rivera, R.; Shofner, M. L.; Meredith, J. C., Controlling Barrier and Mechanical Properties of Cellulose Nanocrystals by Blending with Chitin Nanofibers. *Biomacromolecules* **2019**.

56. Mokhena, T. C.; Sefadi, J. S.; Sadiku, E. R.; John, M. J.; Mochane, M. J.; Mtibe, A. Thermoplastic Processing of PLA/Cellulose Nanomaterials Composites *Polymers* [Online], 2018. PubMed. (accessed 2018/12//).

57. Orr, M. P.; Shofner, M. L., Processing strategies for cellulose nanocrystal/polyethylene-co-vinyl alcohol composites. *Polymer* **2017,** *126* (Supplement C), 211-223.

58. Girouard, N., Cellulose nanocrystal thermoset composites: A physical and chemical route to improving dispersion and mechanical properties. *Georgia Tech Theses and Dissertations* **2015**.

59. Nguyen, T.-D.; Sierra, E.; Eguiraun, H.; Lizundia, E., Iridescent cellulose nanocrystal films: the link between structural colour and Bragg's law. *European Journal of Physics* **2018,** *39* (4), 045803.

60. Petersson, L.; Oksman, K., Biopolymer based nanocomposites: Comparing layered silicates and microcrystalline cellulose as nanoreinforcement. *Compos. Sci. Technol.* **2006,** *66* (13), 2187-2196.

61. Li, F.; Biagioni, P.; Bollani, M.; Maccagnan, A.; Piergiovanni, L., Multi-functional coating of cellulose nanocrystals for flexible packaging applications. *Cellulose* **2013,** *20* (5), 2491-2504.

62. Heinze, T.; Liebert, T., Unconventional methods in cellulose functionalization. *Prog. Polym. Sci.* **2001,** *26* (9), 1689-1762.

63. Espino-Pérez, E.; Bras, J.; Almeida, G.; Relkin, P.; Belgacem, N.; Plessis, C.; Domenek, S., Cellulose nanocrystal surface functionalization for the controlled sorption of water and organic vapours. *Cellulose* **2016,** *23* (5), 2955-2970.

64. Jorfi, M.; Foster, E. J., Recent advances in nanocellulose for biomedical applications. *J. Appl. Polym. Sci.* **2015,** *132* (14), n/a-n/a.

65. Favier, V.; Canova, G. R.; Cavaillé, J. Y.; Chanzy, H.; Dufresne, A.; Gauthier, C., Nanocomposite materials from latex and cellulose whiskers. *Polym. Adv. Technol.* **1995,** *6* (5), 351-355.

66. Yeh, W. Y.; Young, R. J., Molecular deformation processes in aromatic high modulus polymer fibres. *Polymer* **1999,** *40* (4), 857-870.

67. Kim, J.-H.; Shim, B. S.; Kim, H. S.; Lee, Y.-J.; Min, S.-K.; Jang, D.; Abas, Z.; Kim, J., Review of nanocellulose for sustainable future materials. *International Journal of Precision Engineering and Manufacturing-Green Technology* **2015,** *2* (2), 197-213.

68. Jirawut, J.; Ratana, R.; Pitt, S., Fabrication of α-chitin whisker-reinforced poly(vinyl alcohol) nanocomposite nanofibres by electrospinning. *Nanotechnology* **2006,** *17* (17), 4519.

69. Ravi Kumar, M. N. V., A review of chitin and chitosan applications. *React. Funct. Polym.* **2000,** *46* (1), 1-27.

70. Hamed, I.; Özogul, F.; Regenstein, J. M., Industrial applications of crustacean by-products (chitin, chitosan, and chitooligosaccharides): A review. *Trends Food Sci. Technol.* **2016,** *48*, 40-50.

71. Raabe, D.; Sachs, C.; Romano, P., The crustacean exoskeleton as an example of a structurally and mechanically graded biological nanocomposite material. *Acta Materialia* **2005,** *53* (15), 4281-4292.

72. Lee, Y. M.; Kimt, S. H.; Kimt, S. J., Preparation and characteristics of β-chitin and poly(vinyl alcohol) blend. *Polymer* **1996,** *37* (26), 5897-5905.

73. Mok, C. F.; Ching, Y. C.; Muhamad, F.; Abu Osman, N. A.; Singh, R., Poly(vinyl alcohol)-α-chitin composites reinforced by oil palm empty fruit bunch fiber-derived nanocellulose. *Int. J. Polym. Anal. Charact.* **2017,** *22* (4), 294-304.

74. Rinaudo, M., Chitin and chitosan: Properties and applications. *Prog. Polym. Sci.* **2006,** *31* (7), 603-632.

75. Sriupayo, J.; Supaphol, P.; Blackwell, J.; Rujiravanit, R., Preparation and characterization of α-chitin whisker-reinforced poly(vinyl alcohol) nanocomposite films with or without heat treatment. *Polymer* **2005,** *46* (15), 5637-5644.

76. Cheng, M.; Deng, J.; Yang, F.; Gong, Y.; Zhao, N.; Zhang, X., Study on physical properties and nerve cell affinity of composite films from chitosan and gelatin solutions. *Biomaterials* **2003,** *24* (17), 2871-2880.

77. Nishino, T., Matsui, Ryousuke, Nakamae, Katsuhiko, Elastic modulus of the crystalline regions of chitin and chitosan. *J. Polym. Sci., Part B: Polym. Phys.* **1999,** *37* (11).

78. Gopalan Nair, K.; Dufresne, A., Crab Shell Chitin Whisker Reinforced Natural Rubber Nanocomposites. 1. Processing and Swelling Behavior. *Biomacromolecules* **2003,** *4* (3), 657-665.

79. Naseri, N.; Algan, C.; Jacobs, V.; John, M.; Oksman, K.; Mathew, A. P., Electrospun chitosan-based nanocomposite mats reinforced with chitin nanocrystals for wound dressing. *Carbohydr. Polym.* **2014,** *109*, 7-15.

80. Ifuku, S.; Saimoto, H., Chitin nanofibers: preparations, modifications, and applications. *Nanoscale* **2012,** *4* (11), 3308-3318.

81. Wu, J.; Zhang, K.; Girouard, N.; Meredith, J. C., Facile Route to Produce Chitin Nanofibers as Precursors for Flexible and Transparent Gas Barrier Materials. *Biomacromolecules* **2014,** *15* (12), 4614-4620.

82. Satam, C. C.; Irvin, C. W.; Lang, A. W.; Jallorina, J. C. R.; Shofner, M. L.; Reynolds, J. R.; Meredith, J. C., Spray-Coated Multilayer Cellulose Nanocrystal—Chitin Nanofiber Films for Barrier Applications. *ACS Sustainable Chem. Eng.* **2018,** *6* (8), 10637-10644.

83. Benhabiles, M. S.; Salah, R.; Lounici, H.; Drouiche, N.; Goosen, M. F. A.; Mameri, N., Antibacterial activity of chitin, chitosan and its oligomers prepared from shrimp shell waste. *Food Hydrocolloids* **2012,** *29* (1), 48-56.

84. Aslam, M.; Kalyar, M. A.; Raza, Z. A., Polyvinyl alcohol: A review of research status and use of polyvinyl alcohol based nanocomposites. *Polymer Engineering & Science* **2018,** *58* (12), 2119-2132.

85. Azizi, S.; Ahmad, M. B.; Ibrahim, N. A.; Hussein, M. Z.; Namvar, F., Preparation and properties of poly(vinyl alcohol)/chitosan blend bio-nanocomposites reinforced by cellulose nanocrystals. *Chin. J. Polym. Sci.* **2014,** *32* (12), 1620-1627.

86. Peresin, M. S.; Habibi, Y.; Zoppe, J. O.; Pawlak, J. J.; Rojas, O. J., Nanofiber Composites of Polyvinyl Alcohol and Cellulose Nanocrystals: Manufacture and Characterization. *Biomacromolecules* **2010,** *11* (3), 674-681.

87. Hietala, M.; Sain, S.; Oksman, K., Highly redispersible sugar beet nanofibers as reinforcement in bionanocomposites. *Cellulose* **2017,** *24* (5), 2177-2189.

88. DeMerlis, C. C.; Schoneker, D. R., Review of the oral toxicity of polyvinyl alcohol (PVA). *Food and Chemical Toxicology* **2003,** *41* (3), 319-326.

89. Nijenhuis, K. t., Poly(vinyl alcohol). In *Thermoreversible Networks: Viscoelastic Properties and Structure of Gels*, Springer Berlin Heidelberg: Berlin, Heidelberg, 1997; pp 37-66.

90. Hassan, C. M.; Peppas, N. A., Structure and applications of poly(vinyl alcohol) hydrogels produced by conventional crosslinking or by freezing/thawing methods. *Adv. Polym. Sci.* **2000,** *153*, 37-65.

91. Abitbol, T.; Johnstone, T.; Quinn, T. M.; Gray, D. G., Reinforcement with cellulose nanocrystals of poly(vinyl alcohol) hydrogels prepared by cyclic freezing and thawing. *Soft Matter* **2011,** *7* (6), 2373-2379.

92. Stauffer, S. R.; Peppas, N. A., Poly(vinyl alcohol) hydrogels prepared by freezing-thawing cyclic processing. *Polymer* **1992,** *33* (18), 3932-3936.

93. Allen, M. J.; Schoonmaker, J. E.; Bauer, T. W.; Williams, P. F.; Higham, P. A.; Yuan, H. A., Preclinical Evaluation of a Poly (Vinyl Alcohol) Hydrogel Implant as a Replacement for the Nucleus Pulposus. *Spine* **2004,** *29* (5), 515-523.

94. Baker, M. I.; Walsh, S. P.; Schwartz, Z.; Boyan, B. D., A review of polyvinyl alcohol and its uses in cartilage and orthopedic applications. *Journal of biomedical materials research. Part B, Applied biomaterials* **2012,** *100* (5), 1451-7.

95. Uddin, A. J.; Fujie, M.; Sembo, S.; Gotoh, Y., Outstanding reinforcing effect of highly oriented chitin whiskers in PVA nanocomposites. *Carbohydr. Polym.* **2012,** *87* (1), 799-805.

96. Roohani, M.; Habibi, Y.; Belgacem, N. M.; Ebrahim, G.; Karimi, A. N.; Dufresne, A., Cellulose whiskers reinforced polyvinyl alcohol copolymers nanocomposites. *Eur Polym J* **2008,** *44* (8), 2489-2498.

97. Araki, J.; Yamanaka, Y., Anionic and cationic nanocomposite hydrogels reinforced with cellulose and chitin nanowhiskers: effect of electrolyte concentration on mechanical properties and swelling behaviors. *Polym. Adv. Technol.* **2014,** *25* (10), 1108-1115.

98. Srinivasa, P. C.; Ramesh, M. N.; Kumar, K. R.; Tharanathan, R. N., Properties and sorption studies of chitosan–polyvinyl alcohol blend films. *Carbohydr. Polym.* **2003,** *53* (4), 431-438.

99. Siddaramaiah; Raj, B.; Somashekar, R., Structure–property relation in polyvinyl alcohol/starch composites. *J. Appl. Polym. Sci.* **2004,** *91* (1), 630-635.

100. Voronova, M. I.; Surov, O. V.; Guseinov, S. S.; Barannikov, V. P.; Zakharov, A. G., Thermal stability of polyvinyl alcohol/nanocrystalline cellulose composites. *Carbohydr. Polym.* **2015,** *130*, 440-447.

101. Shaffer, M. S. P.; Windle, A. H., Fabrication and characterization of carbon nanotube/poly(vinyl alcohol) composites. *Adv Mater* **1999,** *11* (11), 937-+.

102. Lee, J. S.; Choi, K. H.; Ghim, H. D.; Kim, S. S.; Chun, D. H.; Kim, H. Y.; Lyoo, W. S., Role of molecular weight of atactic poly(vinyl alcohol) (PVA) in the structure and properties of PVA nanofabric prepared by electrospinning. *J. Appl. Polym. Sci.* **2004,** *93* (4), 1638-1646.

103. Stammen, J. A.; Williams, S.; Ku, D. N.; Guldberg, R. E., Mechanical properties of a novel PVA hydrogel in shear and unconfined compression. *Biomaterials* **2001,** *22* (8), 799-806.

104. Hyon, S.-H.; Cha, W.-I.; Ikada, Y., Preparation of transparent poly(vinyl alcohol) hydrogel. *Polymer Bulletin* **1989,** *22* (2), 119-122.

105. Hassan, C. M.; Peppas, N. A., Structure and Morphology of Freeze/Thawed PVA Hydrogels. *Macromolecules* **2000,** *33* (7), 2472-2479.

106. Mansur, H. S.; Sadahira, C. M.; Souza, A. N.; Mansur, A. A. P., FTIR spectroscopy characterization of poly (vinyl alcohol) hydrogel with different hydrolysis degree and chemically crosslinked with glutaraldehyde. *Materials Science and Engineering: C* **2008,** *28* (4), 539-548.

107. Peppas, N. A., Turbidimetric studies of aqueous poly(vinyl alcohol) solutions. *Die Makromolekulare Chemie* **1975,** *176* (11), 3433-3440.

108. De France, K. J.; Hoare, T.; Cranston, E. D., Review of Hydrogels and Aerogels Containing Nanocellulose. *Chem. Mater.* **2017,** *29* (11), 4609-4631.

109. Yokoyama, F.; Masada, I.; Shimamura, K.; Ikawa, T.; Monobe, K., Morphology and structure of highly elastic poly(vinyl alcohol) hydrogel prepared by repeated freezing-and-melting. *Colloid and Polymer Science* **1986,** *264* (7), 595-601.

110. Samaddar, P.; Sen, K., Anion induced gelation in polyvinyl alcohol: a probe for metal ion speciation studies. *J. Sol-Gel Sci. Technol.* **2015,** *73* (2), 389-395.

111. Hyon, S.-H.; Cha, W.-I.; Ikada, Y.; Kita, M.; Ogura, Y.; Honda, Y., Poly(vinyl alcohol) hydrogels as soft contact lens material. *Journal of Biomaterials Science, Polymer Edition* **1994,** *5* (5), 397-406.

112. Zheng, Q.; Cai, Z.; Gong, S., Green synthesis of polyvinyl alcohol (PVA)–cellulose nanofibril (CNF) hybrid aerogels and their use as superabsorbents. *Journal of Materials Chemistry A* **2014,** *2* (9), 3110-3118.

113. Mueller, S.; Weder, C.; Foster, E. J., Water-insoluble aerogels made from cellulose nanocrystals and poly(vinyl alcohol). *Green Materials* **2014,** *2* (4), 169-182.

114. Yang, H.; Kershaw, S. V.; Wang, Y.; Gong, X.; Kalytchuk, S.; Rogach, A. L.; Teoh, W. Y., Shuttling Photoelectrochemical Electron Transport in Tricomponent CdS/rGO/TiO2 Nanocomposites. *The Journal of Physical Chemistry C* **2013,** *117* (40), 20406-20414.

115. Rajesh, R.; Ravichandran, Y. D., Development of a new carbon nanotube-alginate-hydroxyapatite tricomponent composite scaffold for application in bone tissue engineering. *Int J Nanomedicine* **2015,** *10 Suppl 1* (Suppl 1), 7-15.

116. Liu, A.; Medina, L.; Berglund, L. A., High-Strength Nanocomposite Aerogels of Ternary Composition: Poly(vinyl alcohol), Clay, and Cellulose Nanofibrils. *ACS Applied Materials & Interfaces* **2017,** *9* (7), 6453-6461.

117. Zheng, Q.; Javadi, A.; Sabo, R.; Cai, Z.; Gong, S., Polyvinyl alcohol (PVA)–cellulose nanofibril (CNF)–multiwalled carbon nanotube (MWCNT) hybrid organic aerogels with superior mechanical properties. *RSC Advances* **2013,** *3* (43), 20816-20823.

118. Bian, H.; Wei, L.; Lin, C.; Ma, Q.; Dai, H.; Zhu, J. Y., Lignin-Containing Cellulose Nanofibril-Reinforced Polyvinyl Alcohol Hydrogels. *ACS Sustainable Chem. Eng.* **2018,** *6* (4), 4821-4828.

119. Hasani, M.; Cranston, E. D.; Westman, G.; Gray, D. G., Cationic surface functionalization of cellulose nanocrystals. *Soft Matter* **2008,** *4* (11), 2238-2244.

120. Blocher, W. C.; Perry, S. L., Complex coacervate-based materials for biomedicine. *Wiley Interdisciplinary Reviews: Nanomedicine and Nanobiotechnology* **2017,** *9* (4), e1442.

121. Takegawa, A.; Murakami, M.-a.; Kaneko, Y.; Kadokawa, J.-i., Preparation of chitin/cellulose composite gels and films with ionic liquids. *Carbohydr. Polym.* **2010,** *79* (1), 85-90.

122. Duan, Y.; Freyburger, A.; Kunz, W.; Zollfrank, C., Cellulose and chitin composite materials from an ionic liquid and a green co-solvent. *Carbohydr. Polym.* **2018,** *192*, 159-165.

123. Zhang, L.; Guo, J.; Du, Y., Morphology and properties of cellulose/chitin blends membranes from NaOH/thiourea aqueous solution. *J. Appl. Polym. Sci.* **2002,** *86* (8), 2025-2032.

124. Robles, E.; Salaberria, A. M.; Herrera, R.; Fernandes, S. C. M.; Labidi, J., Self-bonded composite films based on cellulose nanofibers and chitin nanocrystals as antifungal materials. *Carbohydr. Polym.* **2016,** *144*, 41-49.

125. Khan, A.; Khan, R. A.; Salmieri, S.; Le Tien, C.; Riedl, B.; Bouchard, J.; Chauve, G.; Tan, V.; Kamal, M. R.; Lacroix, M., Mechanical and barrier properties of nanocrystalline cellulose reinforced chitosan based nanocomposite films. *Carbohydr. Polym.* **2012,** *90* (4), 1601-1608.

126. Nakagaito, A. N.; Kanzawa, S.; Takagi, H., Polylactic Acid Reinforced with Mixed Cellulose and Chitin Nanofibers—Effect of Mixture Ratio on the Mechanical Properties of Composites. *Journal of Composites Science* **2018,** *2* (2), 36.

127. Dong, X. M.; Revol, J.-F.; Gray, D. G., *Cellulose* **1998,** *5* (1), 19-32.

128. Mark, J. E., *Polymer Data Handbook*. Oxford University Press: 1999.

129. Socrates, G., *Infrared and Raman Characteristic Group Frequencies: Tables and Charts*. Wiley: 2001.

130. Sudhamani, S. R.; Prasad, M. S.; Udaya Sankar, K., DSC and FTIR studies on Gellan and Polyvinyl alcohol (PVA) blend films. *Food Hydrocolloids* **2003,** *17* (3), 245-250.

131. Gu, Q.; Trindle, C.; Knee, J. L., Communication: Frequency shifts of an intramolecular hydrogen bond as a measure of intermolecular hydrogen bond strengths. *J. Chem. Phys.* **2012,** *137* (9), 091101.

132. Petersson, L.; Kvien, I.; Oksman, K., Structure and thermal properties of poly(lactic acid)/cellulose whiskers nanocomposite materials. *Compos. Sci. Technol.* **2007,** *67* (11), 2535-2544.

133. Pracella, M.; Haque, M. M.-U.; Puglia, D., Morphology and properties tuning of PLA/cellulose nanocrystals bio-nanocomposites by means of reactive functionalization and blending with PVAc. *Polymer* **2014,** *55* (16), 3720-3728.

134. Marten, F. L., Vinyl Alcohol Polymers. In *Encycl. Polym. Sci. Technol.*, John Wiley & Sons, Inc.: 2002.

135. Schick, C., Differential scanning calorimetry (DSC) of semicrystalline polymers. *Anal. Bioanal. Chem.* **2009,** *395* (6), 1589.

136. Strawhecker, K. E.; Manias, E., Structure and Properties of Poly(vinyl alcohol)/Na+ Montmorillonite Nanocomposites. *Chem. Mater.* **2000,** *12* (10), 2943-2949.

137. Wang, L.-Y.; Wang, M.-J., Removal of Heavy Metal Ions by Poly(vinyl alcohol) and Carboxymethyl Cellulose Composite Hydrogels Prepared by a Freeze–Thaw Method. *ACS Sustainable Chem. Eng.* **2016,** *4* (5), 2830-2837.

138. Mahanta, N.; Teow, Y.; Valiyaveettil, S., Viscoelastic hydrogels from poly(vinyl alcohol)-Fe(iii) complex. *Biomater. Sci.* **2013,** *1* (5), 519-527.

139. Hojo, N.; Shirai, H.; Hayashi, S., Complex formation between poly(vinyl alcohol) and metallic ions in aqueous solution. *J. Polym. Sci., Polym. Symp.* **1974,** *47* (1), 299-307.

140. Xu, S.; Girouard, N.; Schueneman, G.; Shofner, M. L.; Meredith, J. C., Mechanical and thermal properties of waterborne epoxy composites containing cellulose nanocrystals. *Polymer* **2013,** *54* (24), 6589-6598.

141. Fornes, T. D.; Yoon, P. J.; Keskkula, H.; Paul, D. R., Nylon 6 nanocomposites: the effect of matrix molecular weight. *Polymer* **2001,** *42* (25), 09929-09940.

142. Wu, C. L.; Zhang, M. Q.; Rong, M. Z.; Friedrich, K., Tensile performance improvement of low nanoparticles filled-polypropylene composites. *Compos. Sci. Technol.* **2002,** *62* (10), 1327-1340.

143. Beck-Candanedo, S.; Roman, M.; Gray, D. G., Effect of Reaction Conditions on the Properties and Behavior of Wood Cellulose Nanocrystal Suspensions. *Biomacromolecules* **2005,** *6* (2), 1048-1054.

144. Ezekiel Mushi, N.; Butchosa, N.; Zhou, Q.; Berglund, L. A., Nanopaper membranes from chitin–protein composite nanofibers—structure and mechanical properties. *J. Appl. Polym. Sci.* **2014,** *131* (7).

145. ASTM D1621: Standard Test Method for Compressive Properties of Rigid Cellular Plastics. U.S. Department of Defense: 2016.

146. Nissilä, T.; Karhula, S. S.; Saarakkala, S.; Oksman, K., Cellulose nanofiber aerogels impregnated with bio-based epoxy using vacuum infusion: Structure, orientation and mechanical properties. *Compos. Sci. Technol.* **2018,** *155*, 64-71.

147. Jayaramudu, T.; Ko, H.-U.; Kim, H.; Kim, J.; Muthoka, R.; Kim, J., Electroactive Hydrogels Made with Polyvinyl Alcohol/Cellulose Nanocrystals. *Materials* **2018,** *11* (9), 1615.

148. Gonzalez, J. S.; Ludueña, L. N.; Ponce, A.; Alvarez, V. A., Poly(vinyl alcohol)/cellulose nanowhiskers nanocomposite hydrogels for potential wound dressings. *Materials Science and Engineering: C* **2014,** *34*, 54-61.

149. Mukherjee, A.; Hackley, V. A., Separation and characterization of cellulose nanocrystals by multi-detector asymmetrical-flow field-flow fractionation. *Analyst* **2018,** *143* (3), 731-740.

150. Guan, X.; Cueto, R.; Russo, P.; Qi, Y.; Wu, Q., Asymmetric Flow Field-Flow Fractionation with Multiangle Light Scattering Detection for Characterization of Cellulose Nanocrystals. *Biomacromolecules* **2012,** *13* (9), 2671-2679.

151. Mushi, N. E.; Nishino, T.; Berglund, L. A.; Zhou, Q., Strong and Tough Chitin Film from α-Chitin Nanofibers Prepared by High Pressure Homogenization and Chitosan Addition. *ACS Sustainable Chem. Eng.* **2019,** *7* (1), 1692-1697.

152. Gibson, I. J.; Ashby, M. F., The mechanics of three-dimensional cellular materials. *Proceedings of the Royal Society of London. A. Mathematical and Physical Sciences* **1982,** *382* (1782), 43-59.

153. Job, N.; Théry, A.; Pirard, R.; Marien, J.; Kocon, L.; Rouzaud, J.-N.; Béguin, F.; Pirard, J.-P., Carbon aerogels, cryogels and xerogels: Influence of the drying method on the textural properties of porous carbon materials. *Carbon* **2005,** *43* (12), 2481-2494.

154. Barrios, E.; Fox, D.; Li Sip, Y. Y.; Catarata, R.; Calderon, J. E.; Azim, N.; Afrin, S.; Zhang, Z.; Zhai, L., Nanomaterials in Advanced, High-Performance Aerogel Composites: A Review. *Polymers* **2019,** *11* (4), 726.

155. Mueller, S.; Sapkota, J.; Nicharat, A.; Zimmermann, T.; Tingaut, P.; Weder, C.; Foster, E. J., Influence of the nanofiber dimensions on the properties of nanocellulose/poly(vinyl alcohol) aerogels. *J. Appl. Polym. Sci.* **2015,** *132* (13).

156. Liu, D.; Ma, Z.; Wang, Z.; Tian, H.; Gu, M., Biodegradable Poly(vinyl alcohol) Foams Supported by Cellulose Nanofibrils: Processing, Structure, and Properties. *Langmuir* **2014,** *30* (31), 9544-9550.

157. Víctor-Román, S.; Simón-Herrero, C.; Romero, A.; Gracia, I.; Valverde, J. L.; Sánchez-Silva, L., CNF-reinforced polymer aerogels: Influence of the synthesis variables and economic evaluation. *Chemical Engineering Journal* **2015,** *262*, 691-701.

158. Simón-Herrero, C.; Gómez, L.; Romero, A.; Valverde, J. L.; Sánchez-Silva, L., Nanoclay-Based PVA Aerogels: Synthesis and Characterization. *Industrial & Engineering Chemistry Research* **2018,** *57* (18), 6218-6225.

159. Gawryla, M. D.; van den Berg, O.; Weder, C.; Schiraldi, D. A., Clay aerogel/cellulose whisker nanocomposites: a nanoscale wattle and daub. *Journal of Materials Chemistry* **2009,** *19* (15), 2118-2124.

160. Zhai, T.; Zheng, Q.; Cai, Z.; Xia, H.; Gong, S., Synthesis of polyvinyl alcohol/cellulose nanofibril hybrid aerogel microspheres and their use as oil/solvent superabsorbents. *Carbohydr. Polym.* **2016,** *148*, 300-308.

161. Simón-Herrero, C.; Caminero-Huertas, S.; Romero, A.; Valverde, J. L.; Sánchez-Silva, L., Effects of freeze-drying conditions on aerogel properties. *Journal of Materials Science* **2016,** *51* (19), 8977-8985.

162. Adapa, S.; Schmidt, K. A.; Jeon, I. J.; Herald, T. J.; Flores, R. A., MECHANISMS OF ICE CRYSTALLIZATION AND RECRYSTALLIZATION IN ICE CREAM: A REVIEW. *Food Rev. Int.* **2000,** *16* (3), 259-271.

163. Miller-Livney, T.; Hartel, R. W., Ice Recrystallization in Ice Cream: Interactions Between Sweeteners and Stabilizers. *Journal of Dairy Science* **1997,** *80* (3), 447-456.

164. Regand, A.; Goff, H. D., Ice Recrystallization Inhibition in Ice Cream as Affected by Ice Structuring Proteins from Winter Wheat Grass. *Journal of Dairy Science* **2006,** *89* (1), 49-57.

165. Tsouknidas, A.; Michailidis, N.; Savvakis, S.; Anagnostidis, K.; Bouzakis, K. D.; Kapetanos, G., A finite element model technique to determine the mechanical response of a lumbar spine segment under complex loads. *Journal of applied biomechanics* **2012,** *28* (4), 448-56.

166. Newell, N.; Little, J. P.; Christou, A.; Adams, M. A.; Adam, C. J.; Masouros, S. D., Biomechanics of the human intervertebral disc: A review of testing techniques and results. *Journal of the Mechanical Behavior of Biomedical Materials* **2017,** *69*, 420-434.

167. Wilke, H. J.; Neef, P.; Caimi, M.; Hoogland, T.; Claes, L. E., New In Vivo Measurements of Pressures in the Intervertebral Disc in Daily Life. *Spine* **1999,** *24* (8), 755-762.

168. Stemper, B. D.; Board, D.; Yoganandan, N.; Wolfla, C. E., Biomechanical properties of human thoracic spine disc segments. *J Craniovertebr Junction Spine* **2010,** *1* (1), 18-22.

169. Ha, S. K., Finite element modeling of multi-level cervical spinal segments (C3–C6) and biomechanical analysis of an elastomer-type prosthetic disc. *Medical Engineering & Physics* **2006,** *28* (6), 534-541.

170. Umehara, S.; Tadano, S.; Abumi, K.; Katagiri, K.; Kaneda, K.; Ukai, T., Effects of Degeneration on the Elastic Modulus Distribution in the Lumbar Intervertebral Disc. *Spine* **1996,** *21* (7), 811-819.

171. Schmedlen, R. H.; Masters, K. S.; West, J. L., Photocrosslinkable polyvinyl alcohol hydrogels that can be modified with cell adhesion peptides for use in tissue engineering. *Biomaterials* **2002,** *23* (22), 4325-4332.

172. Kobayashi, M.; Chang, Y.-S.; Oka, M., A two year in vivo study of polyvinyl alcohol-hydrogel (PVA-H) artificial meniscus. *Biomaterials* **2005,** *26* (16), 3243-3248.

173. Kobayashi, M.; Toguchida, J.; Oka, M., Preliminary study of polyvinyl alcohol-hydrogel (PVA-H) artificial meniscus. *Biomaterials* **2003,** *24* (4), 639-647.

174. Pal, K.; Banthia, A. K.; Majumdar, D. K., Preparation and characterization of polyvinyl alcohol-gelatin hydrogel membranes for biomedical applications. *AAPS PharmSciTech* **2007,** *8* (1), E142-E146.

175. Thomas, J.; Lowman, A.; Marcolongo, M., Novel associated hydrogels for nucleus pulposus replacement. *Journal of Biomedical Materials Research Part A* **2003,** *67A* (4), 1329-1337.

176. Ramaraj, B., Crosslinked poly(vinyl alcohol) and starch composite films. II. Physicomechanical, thermal properties and swelling studies. *J. Appl. Polym. Sci.* **2007,** *103* (2), 909-916.